

Development of a 3D myocardial damage analysis tool for the evaluation of multi-target cardioprotection strategies

Inaugural-Dissertation zur
Erlangung des Doktorgrades

Dr. rer. nat.

der Fakultät für Biologie
an der

Universität Duisburg-Essen

vorgelegt von

Sebastian Korste

Geboren in Velbert (NRW)

Dezember 2019

DuEPublico

Duisburg-Essen Publications online

UNIVERSITÄT
DUISBURG
ESSEN

Offen im Denken

ub | universitäts
bibliothek

Diese Dissertation wird über DuEPublico, dem Dokumenten- und Publikationsserver der Universität Duisburg-Essen, zur Verfügung gestellt und liegt auch als Print-Version vor.

DOI: 10.17185/duepublico/71581

URN: urn:nbn:de:hbz:464-20200513-073410-9

Alle Rechte vorbehalten.

Die der vorliegenden Arbeit zugrundeliegenden Experimente wurden in den CardioScienceLabs der Klinik für Kardiologie und Angiologie am Westdeutschen Herz- und Gefäßzentrum des Universitätsklinikums Essen der Universität Duisburg-Essen durchgeführt.

1. Gutachter: Prof. Dr. Peter Bayer

2. Gutachter: PD Dr. Ulrike Hendgen-Cotta

Vorsitzender des Prüfungsausschusses: Prof. Dr. Joachim Fandrey

Tag der mündlichen Prüfung: 19.03.2020

Für meine Eltern

Research is what I am doing,
when I don't know what I am doing.

Wernher von Braun

Content

| | |
|---|-----------|
| List of publications | I |
| Abbreviations and Acronyms | III |
| List of figures | VII |
| List of tables | IX |
| 1 Zusammenfassung | 1 |
| 2 Summary | 2 |
| 3 Background | 3 |
| 3.1 Acute myocardial infarction | 3 |
| 3.2 The acute myocardial ischemia/reperfusion (I/R) injury | 4 |
| 3.3 Vascular damage in the course of ischemia/reperfusion | 8 |
| 3.4 The role of the immune system in I/R injury and cardiac repair | 9 |
| 3.5 The current state of I/R injury assessment techniques | 13 |
| 3.6 Aims | 15 |
| 4 Publications | 16 |
| 4.1 S-nitrosation of calpains is associated with cardioprotection in myocardial I/R injury | 16 |
| 4.1.1 Abstract | 17 |
| 4.1.2 Background | 18 |
| 4.1.3 Methods | 19 |
| 4.1.4 Results and discussion | 24 |
| 4.1.5 Conclusion | 29 |
| 4.1.6 References | 30 |
| 4.1.7 Supplementary data | 35 |
| 4.2 Contemporaneous 3D characterization of acute and chronic myocardial I/R injury and response | 36 |
| 4.2.1 Abstract | 37 |
| 4.2.2 Introduction | 37 |
| 4.2.3 Results | 38 |

| | | |
|----------|---|-----------|
| 4.2.4 | Discussion | 48 |
| 4.2.5 | Methods | 51 |
| 4.2.6 | References | 60 |
| 4.2.7 | Supplementary material | 65 |
| 5 | Discussion | 78 |
| 5.1 | Calpains as mediators of nitric oxide derived cardioprotection | 79 |
| 5.2 | Simultaneous measurement of I/R injury and response for multi-target strategies | 81 |
| 5.3 | Conclusion and outlook | 85 |
| 6 | References | 86 |
| 7 | Appendix | 97 |
| 7.1 | Author publication contributions | 97 |
| 7.2 | Acknowledgement | 99 |
| 7.3 | Curriculum vitae | 100 |
| 7.4 | Eidesstattliche Erklärung | 101 |

List of publications

Original articles

Totzeck Matthias, Korste Sebastian, Miinalainen Ilkka, Hendgen-Cotta Ulrike, Rassaf Tienush. S-nitrosation of calpains is associated with cardioprotection in myocardial I/R injury. *Nitric Oxide* 2017;67;68-74. DOI: 10.1016/j.niox.2017.04.003.

Merz Simon F*, Korste Sebastian*, Bornemann Lea*, Michel Lars, Stock Pia, Squire Anthony, Soun Camille, Engel Daniel R, Detzer Julia, Lörchner Holger, Hermann Dirk M, Kamler Markus, Klode Joachim, Hendgen-Cotta Ulrike, Rassaf Tienush, Gunzer Matthias#, Totzeck Matthias#. Contemporaneous 3D characterization of acute and chronic myocardial I/R injury and response. *Nat Commun* 2019;10;2312. DOI: 10.1038/s41467-019-10338-2.

*these authors contributed equally

#these authors jointly supervised the work

Published abstracts

Korste Sebastian, Hendgen-Cotta Ulrike, Stock Pia, Rassaf Tienush, Totzeck Matthias (2016). Cardiac calpains in mitochondria following acute myocardial ischemia/reperfusion injury. 82. Jahrestagung der Deutschen Gesellschaft für Kardiologie, 31.03.2016, Mannheim, poster presentation. *Clin. Res. Cardiol.* 2016;105. DOI: 10.1007/s00392-016-0967-z

Korste Sebastian, Hendgen-Cotta Ulrike, Stock Pia, Rassaf Tienush, Totzeck Matthias (2016). Cardiac calpains in mitochondria following acute myocardial ischemia/reperfusion injury. Congress of the European Society of Cardiology 2016, 29.08.2016, Rome, Italy, oral presentation. *Eur. Heart J.* 2016;37;629-630. DOI: 10.1093/eurheartj/ehw433

Korste Sebastian, Merz Simon, Stock Pia, Hendgen-Cotta Ulrike, Rassaf Tienush, Gunzer Matthias, Totzeck Matthias (2018). 3D-model for quantification of infarct size and immune cell invasion following myocardial ischemia/reperfusion using light sheet fluorescence microscopy. 84. Jahrestagung der Deutschen Gesellschaft für Kardiologie, 05.04.2018, Mannheim, poster presentation. *Clin. Res. Cardiol.* 2018;107. DOI: 10.1007/s00392-018-1216-4

Korste Sebastian, Merz Simon, Bornemann Lea, Michel Lars, Stock Pia, Hendgen-Cotta Ulrike, Kamler Markus, Rassaf Tienush, Gunzer Matthias, Totzeck Matthias (2019). Light sheet-guided analysis of human cardiac samples for disease diagnosis. 85. Jahrestagung der Deutschen Gesellschaft für Kardiologie, 25.04.2019, Mannheim, poster presentation. *Clin. Res. Cardiol.* 2019;108. DOI: 10.1007/s00392-019-1435-9

Korste Sebastian, Merz Simon F, Bornemann Lea, Michel Lars, Stock Pia, Hendgen-Cotta Ulrike, Rassaf Tienush, Gunzer Matthias, Totzeck Matthias (2019). A novel tool for light sheet-guided analysis of myocardial injury in murine and human samples. Congress of the European Society of Cardiology 2019, 01.09.2019, Paris, France, poster presentation. *Eur. Heart J.* 2019;40:1519. DOI: 10.1093/eurheartj/ehz748.0885

Other contributions

Korste Sebastian (2018). Novel aspects of myocardial I/R injury and cardioprotection. Nitric Oxide Meeting 2018, 18.09.2018, Oxford, England, oral presentation

Korste Sebastian, Stock Pia, Hendgen-Cotta Ulrike, French Brent, Rassaf Tienush, Totzeck Matthias (2017). Blocking CD47-Signaling reduces infarct size, but increases response after acute myocardial infarction. 16. Tag der Forschung der Medizinischen Fakultät, 17.11.2017, Essen, poster presentation

Korste Sebastian, Merz Simon, Bornemann Lea, Stock Pia, Squire Anthony, Soun Camille, Engel Daniel, Detzer Julia, Lörchner Holger, Klode Joachim, Hendgen-Cotta Ulrike, Rassaf Tienush, Gunzer Matthias, Totzeck Matthias (2018). A cleared path to new insights: light sheet-guided myocardial ischemia/reperfusion analysis. 17. Tag der Forschung der Medizinischen Fakultät, 07.12.2018, Essen, poster presentation

Abbreviations and Acronyms

| | |
|-----------|---|
| % | percent |
| °C | degrees Celsius |
| μl | microliters |
| μm | micrometers |
| μM | micromolar |
| μmol | micromol |
| 2D | two dimensional |
| 3D | three dimensional |
| 4D | four dimensional |
| a.u. | arbitrary units |
| AAR | area at risk |
| Ab | antibody |
| AF | AlexaFluor |
| AMI | acute myocardial infarction |
| ANOVA | Analysis of Variance |
| APC | antigen-presenting cell |
| ATP | adenosine triphosphate |
| BALANCE | Bleaching-Augmented solvent-based Non-toxic Clearing |
| Capn | Calpain(s) |
| CatNo | catalogue number |
| CLARITY | Clear Lipid-exchanged Acrylamide-hybridized Rigid Imaging/Immunostaining/In situ hybridization-compatible Tissue-hydrogel |
| CM | cardiomyocyte |
| cm | centimeter |
| cTNI | cardiac troponin I |
| CTRL/Ctrl | control |
| CUBIC | Clear, Unobstructed Brain/Body Imaging Cocktails and Computational analysis |
| CVD | cardiovascular disease |
| d | day(s) |
| DAMPs | danger-associated molecular patterns |
| DMSO | dimethyl sulfoxide |

| | |
|-------------|---|
| DNA | deoxyribonucleic acid |
| DPBS | Dulbeccos phosphate buffered saline |
| EB | Evan's blue |
| EC | endothelial cell |
| ECi | ethyl cinnamate |
| ECM | extracellular matrix |
| EF | ejection fraction |
| e.g. / z.B. | exempli gratia / zum Beispiel |
| EtOH | ethanol |
| FITC | fluorescein isothiocyanate |
| FMO | fluorescence minus one |
| FSC | forward scatter |
| g | g forces |
| h | hours |
| H&E | hematoxylin & eosin staining |
| i.p. | intraperitoneal(ly) |
| i.v. | intravenous(ly) |
| I/R | ischemia/reperfusion |
| IBD | interbranch distance |
| iDISCO | immunolabeling-enabled three-dimensional imaging of solvent-cleared organs |
| IHD | ischemic heart disease |
| IL-1 | interleukin-1 |
| Inhib | inhibitor |
| IPC | ischemic pre-conditioning |
| IPost | ischemic post-conditioning |
| IVS | interventricular septum |
| kg | kilogram |
| l or L | liter |
| LAA | left atrial appendage |
| LCA | left coronary artery |
| LSFM | light sheet fluorescence microscopy |
| LV | left ventricle |
| LVW | left ventricle wall |

| | |
|---------|--|
| M | molar |
| Mb | myoglobin |
| MCU | mitochondrial calcium uniporter |
| mg | milligram |
| MHC | major histocompatibility complex |
| min | minute(s) |
| MIP | maximum intensity projection |
| ml | milliliter |
| mM | millimolar |
| mm | millimeter |
| mmol | millimol |
| MPTP | mitochondrial permeability transition pore |
| ms | milliseconds |
| MULNV | Ministry for Environment, Agriculture, Conservation and Consumer Protection of the State of North Rhine-Westphalia |
| MVO | microvascular obstruction |
| n | group size |
| NADPH | nicotinamide adenine dinucleotide phosphate |
| neg | negative |
| NET | neutrophil extracellular trap |
| NK cell | natural killer cell |
| nm | nanometer |
| NO | nitric oxide |
| p | p value |
| PAMPs | pathogen-associated molecular patterns |
| PBS | phosphate buffered saline |
| PCD | programmed cell death |
| PCI | percutaneous coronary intervention |
| PFA | paraformaldehyde |
| pH | potentia hydrogenii |
| PKC | protein kinase C |
| pos | positive |
| r | Pearson's r |

| | |
|--------------|---|
| RIC | remote ischemic conditioning |
| ROI | region of interest |
| ROS | reactive oxygen species |
| RT | room temperature |
| RV | right ventricle |
| RVW | right ventricle wall |
| RyR | ryanodine receptor |
| s | seconds |
| s.c. | subcutaneous(ly) |
| s.d. | standard deviation |
| SERCA | sarco/endoplasmic reticulum Ca^{2+} -ATPase |
| SH-group | sulfhydryl-group |
| SNAP | S-Nitroso-N-acetyl- DL-penicillamine |
| SR | sarcoplasmic reticulum |
| SSC | side scatter |
| SWITCH | System-Wide control of Interaction Time and kinetics of Chemicals |
| TLR | toll-like receptor |
| TNF α | tumor necrosis factor alpha |
| TTC | triphenyl tetrazolium chloride |
| U | units |
| v/v | volume per volume |
| VAR | volumes at risk |
| VEGF | vascular endothelial growth factor |
| VEGFR | vascular endothelial growth factor receptor |
| VLD | vessel length density |
| w/v | weight per volume |
| w/w | weight per weight |

List of figures

| | | |
|--------------|--|----|
| Figure 3-1: | Intracellular cardiomyocyte signaling during ischemia and early reperfusion. | 5 |
| Figure 3-2: | Domain structure of calpains. | 6 |
| Figure 3-3: | Nitrite mediated cardioprotection via posttranslational modification of calpains (Capn). | 7 |
| Figure 3-4: | Occlusion and constriction of the capillary network. | 9 |
| Figure 3-5: | Immune cell classification. | 11 |
| Figure 3-6: | Phases of immune cell response after AMI. | 12 |
| Figure 4-1: | <i>Fig. 1</i> Nitrite supplementation is associated with increased calpain S-nitrosation, decreased calpain activity and higher cell viability in an in vitro hypoxia/reoxygenation model. | 25 |
| Figure 4-2: | <i>Fig. 2</i> Nitrite supplementation is also accompanied in vivo by increased calpain S-nitrosation, decreased calpain activity and smaller infarct size after I/R. | 27 |
| Figure 4-3: | <i>Fig. 3</i> Mitochondrial structure and calpain localization at mitochondria following nitrite supplementation in in vivo I/R. | 28 |
| Figure 4-4: | <i>Supplemental Fig. 1</i> Calpain activity in vitro following supplementation with nitrite, SNAP or calpain inhibitor. | 35 |
| Figure 4-5: | <i>Supplemental Fig. 2</i> Calcium measurement following nitrite treatment in HL-1 cells. | 35 |
| Figure 4-6: | <i>Fig. 1</i> Fluorophore compatible bleaching enables homogenous light-sheet fluorescence microscopy (LSFM) in whole murine hearts. | 41 |
| Figure 4-7: | <i>Fig. 2</i> High resolution light-sheet fluorescence microscopy (LSFM) of murine and human tissue. | 42 |
| Figure 4-8: | <i>Fig. 3</i> 3D quantification and characterization of ischemia/reperfusion (I/R) injury size using light sheet fluorescence microscopy (LSFM). | 43 |
| Figure 4-9: | <i>Fig. 4</i> Correlation of echocardiography, cardiac troponin I (cTNI) plasma levels, triphenyl tetrazolium chloride negative (TTC ^{neg}) areas and CD31 negative (CD31 ^{neg}) volumes after 24 h of reperfusion in the same 5 mice. | 44 |
| Figure 4-10: | <i>Fig. 5</i> 4D analysis of vascular meshwork in basal and infarcted hearts. | 46 |

| | |
|--|----|
| Figure 4-11: <i>Fig. 6</i> Quantifying I/R injury, AAR and CD31 curly localization in mice with the left ventricular 17 segment model. | 47 |
| Figure 4-12: <i>Fig. 7</i> Characterization of immune cell infiltrates into I/R injury. | 50 |
| Figure 4-13: <i>Supplementary Figure 1</i> Tissue autofluorescence homogenization using different bleaching protocols. | 69 |
| Figure 4-14: <i>Supplementary Figure 2</i> Endogenous fluorescence and i.v.-mediated staining in organic- and water-based clearing. | 70 |
| Figure 4-15: <i>Supplementary Figure 3</i> CD31 imaging in the heart. | 71 |
| Figure 4-16: <i>Supplementary Figure 4</i> TTC-planimetry and subsequent LSFM of murine hearts in a myocardial ischemia/reperfusion (I/R) model. | 72 |
| Figure 4-17: <i>Supplementary Figure 5</i> Ischemia/reperfusion (I/R) injury parameters in 3D – triphenyl tetrazolium chloride (TTC)- and light sheet fluorescence microscopy (LSFM)-based analysis in comparison. | 73 |
| Figure 4-18: <i>Supplementary Figure 6</i> 2D and 3D cardiac vessel measurements. | 74 |
| Figure 4-19: <i>Supplementary Figure 7</i> Quantifying ischemia/reperfusion (I/R) injury, area at risk (AAR) and CD31 curly localization. | 75 |
| Figure 4-20: <i>Supplementary Figure 8</i> Co-localization of ischemia/reperfusion (I/R) injury with Ly-6G positive (Ly-6G ^{pos}) neutrophils. | 75 |
| Figure 4-21: <i>Supplementary Figure 9</i> Immune cell identification in LSFM and flow cytometry analysis. | 76 |

List of tables

| | | |
|------------|---|----|
| Table 4-1: | <i>Supplementary Table 1</i> Comparison of alternative bleaching approaches with the BALANCE protocol. | 67 |
| Table 4-2: | <i>Supplementary Table 2</i> Comparison of established clearing methods with the BALANCE protocol (shrinkage is mean \pm s.d.). | 67 |
| Table 4-3: | <i>Supplementary Table 3</i> Comparison of assessed parameters, shortcomings, time-expense and difficulty of available techniques to evaluate myocardial ischemia/reperfusion (I/R) injury and associated parameters. | 68 |

1 Zusammenfassung

Der gegenwärtige klinische Standard zur Therapie des akuten Myokardinfarktes (AMI) beinhaltet eine zeitige Reperfusion des ischämischen Myokards. Diese erfolgreiche Reperfusion kann jedoch einen weiteren Zelltod und Gewebeschaden verursachen, der sogenannte Ischämie/Reperusions- (I/R) Schaden. Verschiedene Möglichkeiten der Kardioprotektion zur Minimierung der Infarktgröße wurden in vorklinischen und klinischen Studien untersucht. Bisher hat jedoch kein Ansatz die Translation in die Klinik geschafft. Dies wurde zurückgeführt auf die Limitierung der Untersuchung einzelner Wirkmechanismen, genauer entweder vermehrtes Überleben der Kardiomyozyten, Bewahrung der Endothelintegrität oder Modulation der Immunantwort. Daher werden multi-target Strategien, die zwei oder alle drei zelluläre Entitäten behandeln, als vielversprechende Herangehensweise betrachtet.

In verschiedenen experimentellen Studien konnten die protektiven Effekte von Stickstoffmonoxid (NO) auf das geschädigte Myokard nachgewiesen werden. NO hat sowohl einen Einfluss auf das Immunsystem, als auch die Möglichkeit Proteine mittels S-Nitrosierung posttranslational zu modifizieren und wirkt so als multi-target Strategie. In dieser Arbeit wurde die durch Myoglobin vermittelte Produktion von NO aus Nitrit dazu genutzt die Aktivität von Calpainen zu hemmen, welche Apoptosesignalwege z.B. am Mitochondrium anstoßen. Die untersuchten Calpaine 1, 2 und 10 zeigten einen erhöhten S-Nitrosierungsspiegel und es konnte eine verringerte Calpainaktivität, sowie ein vermehrtes Überleben der Zellen gemessen werden. Auch die Lokalisation der Calpaine am Mitochondrium war beeinflusst.

Weiterhin wurde in dieser Arbeit ein Verfahren zur Analyse des I/R-Schadens mittels Lichtblattfluoreszenzmikroskopie (LSFM) etabliert, welches die gleichzeitige Messung verschiedener Parameter des I/R-Schadens in der gleichen Probe ermöglicht. Der hier benutzte endotheliale Marker CD31 zeigte dabei gleiche Infarktgrößen an wie traditionelle Methoden. Kombiniert mit der Markierung von Immunzellen (Ly-6G für Neutrophile und F4/80 für Makrophagen) war eine Korrelation und Ko-Lokalisation von I/R Schaden und Antwort im selben Herzen möglich. Auch ermöglichte die abnormale CD31 Expression nach 5 d Reperfusion (CD31^{curly}) eine Quantifizierung und Lokalisation des ursprünglichen Schadengebietes nach 24 h.

Zusammengefasst zeigt diese Arbeit eine neue Möglichkeit der Kardioprotektion nach AMI basierend auf Inhibierung von Calpainen, sowie eine vielversprechende Methode zur I/R-Schadensanalyse mittels LSFM.

2 Summary

Current clinical practice for acute myocardial infarction (AMI) involves the timely reperfusion of the ischemic myocardium, which causes further cell death and tissue damage, the so-called myocardial ischemia/reperfusion (I/R) injury. While various means of cardioprotection to minimize infarct size have been investigated in pre-clinical and clinical studies, none have translated into treatment options that improve patient outcomes. This has been attributed to the limited focus on singular mechanisms of action, whether it is increasing cardiomyocyte survival, preserving endothelial integrity, or modulating the immune system response. As such, multi-target strategies dealing with two or all three cellular entities have been proposed as promising approaches.

In several experimental setups, the protective effects of nitric oxide (NO) on the injured myocardium have been investigated. Since NO influences the immune system but can also posttranslationally modify proteins via S-nitrosation, it acts in a multi-targeting way. In the work presented herein, myoglobin-facilitated production of NO from nitrite was used to inhibit calpain activity, which mediates apoptosis-inducing pathways, e.g., those at the mitochondria. Indeed, investigated calpains 1, 2 and 10 showed higher S-nitrosation levels after nitrite supplementation, combined with less overall calpain activity and improved cell survival/tissue preservation. Similarly, the localization of calpains at the mitochondria was altered.

Furthermore, this work presents the development of a novel approach for I/R injury analysis using light sheet fluorescence microscopy to enable simultaneous measurement of several I/R injury parameters in the same specimen. The endothelial marker CD31 was used to determine the I/R injury size, which was equal to that measured by traditional methods. In combination with labeling of immune cells (Ly-6G for neutrophils and F4/80 for macrophages) it was possible to correlate and co-localize the I/R injury size and response inside the same heart. In addition, abnormal CD31 expression after 5 d of reperfusion (termed CD31^{curly}) was similar in size and localization as the damage found at 24 h and could be established as a proxy for analysis of the original injury days after the incident.

Taken together, this work presents a novel approach for cardioprotection after AMI based on calpain inhibition, as well as a promising technique for I/R injury investigation using light sheet-guided analysis.

3 Background

Cardiovascular disease (CVD) remains the most relevant cause of mortality and morbidity in western, industrialized countries. In 2017, nearly 45% of all deaths in Europe resulted from CVDs¹ and data from Germany showed that ischemic heart disease (IHD) and acute myocardial infarction (AMI) were the two leading causes of death in 2015.² Most patients today receive optimal guideline-based treatment when hospitalized due to a CVD.³ Given the persistently increased mortality rates in patients after an AMI, there is still an urgent medical need for novel therapeutic options. Moreover, our understanding of the underlying biomolecular mechanisms ensuing a cardiovascular event remains incomplete. This work aims to elucidate the early detrimental effectors of myocardial ischemia/reperfusion (I/R) injury with a focus on intracellular pathways including in particular calcium-dependent proteases, called calpains, as well as to simultaneously investigate the immunological and structural response to I/R injury in the murine heart using light sheet fluorescence microscopy (LSFM).

3.1 Acute myocardial infarction

A prototypical AMI results from arteriosclerotic plaque rupture and coronary artery thrombus formation.⁴ When the innermost, endothelial layer of the coronary arteries, the tunica intima, is damaged and platelets come into contact with a necrotic core situated between the intima and the tunica media, platelets become activated.⁵ These activated platelets lead to the formation of a thrombus, which then occludes the artery on site or, if it is embolized with the blood stream, at a location further downstream in smaller vessels. This occlusion induces a cessation of blood flow (ischemia) to the distal myocardium, which causes a shortage of oxygen and nutrition supply of the cardiac cells. The ischemic region defines the area at risk (AAR).⁶ Prolonged ischemia results in cellular damage and cell death, which is the fundamental definition of an AMI.⁴ The therapy of choice is a timely restoration of blood flow (reperfusion) to the injured myocardium. Advances in reperfusion therapy and co-medication in recent years have led to a decrease in mortality following AMI.⁷ Reperfusion itself surprisingly causes additional tissue damage, which can account for up to 50% of the resulting infarct size, a phenomenon that has been termed ischemia/reperfusion (I/R) injury.⁸ I/R also affects the vasculature and provokes an immune response, with both factors potentially compounding the damage already inflicted.⁹

3.2 The acute myocardial ischemia/reperfusion (I/R) injury

Myocardial I/R injury is characterized by the death of cardiac myocytes that survived an ischemic episode and were viable immediately before reperfusion. When oxygen concentration in the myocardium drops rapidly¹⁰, oxidative phosphorylation is terminated within seconds, resulting in depletion of adenosine triphosphate (ATP) supply, depolarization of the mitochondrial membrane and loss of contractile function.⁶ Further ATP is hydrolyzed by the mitochondrial ATPase to retain mitochondrial membrane potential, generating more inorganic phosphate.⁶ To generate energy, ischemic cardiomyocytes (CMs) switch to anaerobic glycolysis, which then accumulates lactic acid thus reducing the intracellular pH to about 6.0.¹¹ The surplus of protons inside the cell activates the $\text{Na}^+\text{-H}^+$ ion exchanger to exchange protons for sodium ions from the extracellular compartment.¹² The resulting excess of sodium ions cannot be reduced by the $3\text{Na}^+\text{-2K}^+$ ATPase, as it is ATP dependent and as such sodium ions are exchanged for calcium ions via the $2\text{Na}^+\text{-Ca}^{2+}$ exchanger.¹² Thus, although intracellular calcium concentration is increased, CM contraction is dysfunctional due to low pH (see Figure 3-1).^{6,12}

With the restoration of blood flow, delivery of oxygen leads to the generation of reactive oxygen species (ROS).⁶ These ROS stem from reverse electron transport mediated by complex I of the respiratory chain inside the mitochondria.¹³ Uncompensated ROS levels lead to membrane integrity loss by means of lipid oxidation, oxidative modification of proteins and damage to the deoxyribonucleic acid (DNA).^{8,14} Furthermore, instability of the sarcoplasmic reticulum (SR) caused by ROS affects cytoplasmic calcium levels, which adds to the calcium overload during ischemia.⁶ Calcium is imported into the mitochondria by the mitochondrial calcium uniporter (MCU) as pH levels are rapidly normalized by the wash-out of lactic acid and mitochondrial membrane potential is reinstalled.¹⁵ High calcium levels inside the mitochondria, combined with phosphate accumulated during ischemia and ROS, trigger mitochondria-associated programmed cell death (PCD) pathways and calcium-dependent proteolysis.¹⁶ Preservation of mitochondrial integrity is thus considered beneficial to the outcome of I/R injury.¹³

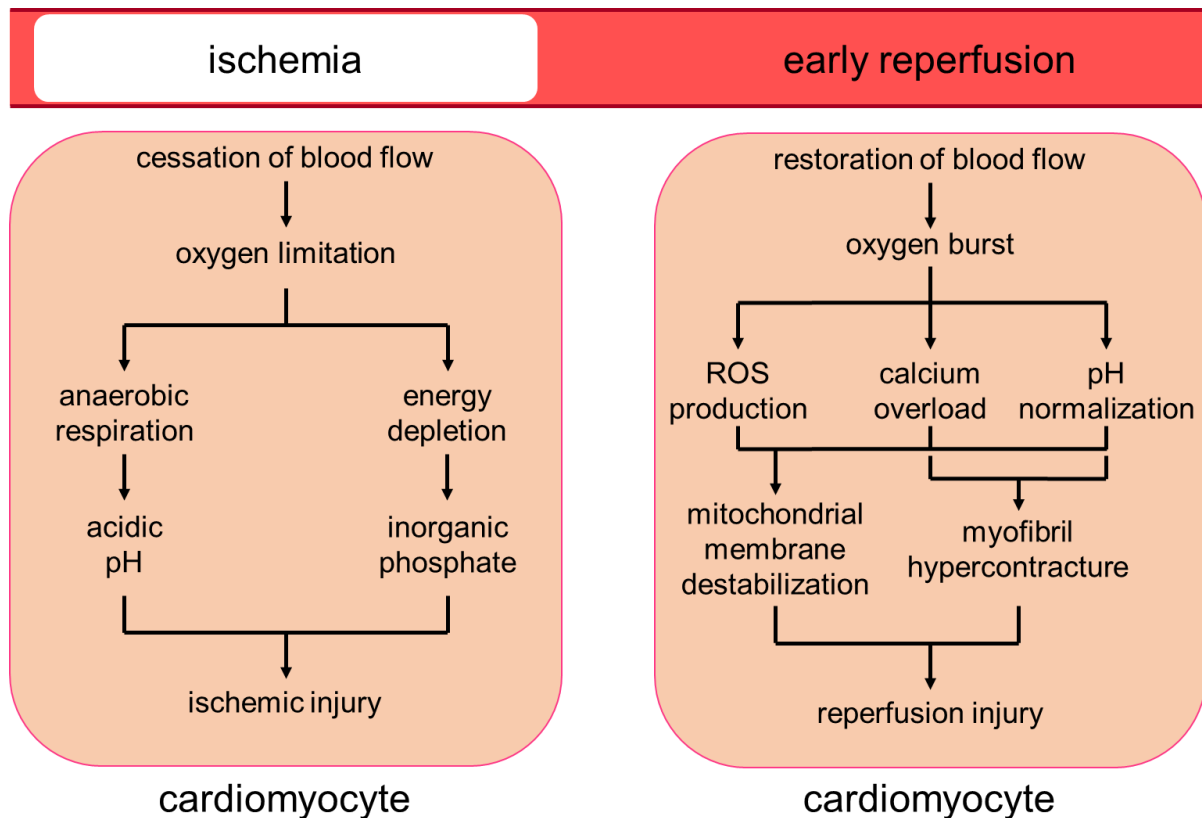


Figure 3-1: Intracellular cardiomyocyte signaling during ischemia and early reperfusion. Ischemia leads to a limitation of oxygen supply. Energy is depleted from the cells and anaerobic glycolysis is preferred, which produces lactate and thus lowers intracellular pH. Prolonged ischemia results in cell death and is termed ischemic injury. Upon reperfusion, rapid reoxygenation leads to the production of reactive oxygen species (ROS), calcium influx and pH normalization. These lead to destabilization of the mitochondrial membrane and cardiomyocyte hypercontracture, which in turn lead to more cell death. This is termed reperfusion injury (modified from Hausenloy and Yellon, J Clin Invest 2013⁶).

One harmful pathway that also affects mitochondria during reperfusion involves the calcium-dependent group of proteases called calpains. To date, 14 calpain isoforms have been found, along with two additional variants of small regulatory subunits, which bind via a C-terminal EF-hand motif (a 3D helix-loop-helix structure facilitating Ca^{2+} binding). Four additional EF-hand motifs at the C-terminus regulate calpain activity via calcium binding (see Figure 3-2).¹⁷ Calpain expression among different tissues varies according to specific isoforms. Inside the heart, calpain 1, 2 and 10 are highly expressed.¹⁸ In homeostasis, calpains are bound by their endogenous inhibitor calpastatin, which maintains them in an inactive status. Upon I/R, intracellular Ca^{2+} levels rise and calpains translocate to plasma membranes, be it the cell membrane or at the mitochondria.¹⁹

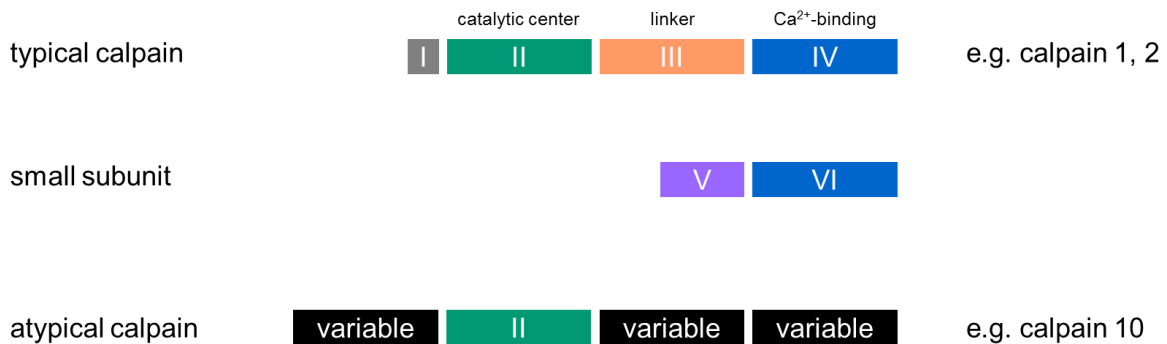


Figure 3-2: Domain structure of calpains. Typical calpains such as calpain 1 and 2 have a four domain layout, where domain II contains the catalytic center, which is conserved in all calpains and domain IV contains five EF-hand motifs, four for Ca²⁺-binding and the 5th for interaction with domain VI of the small regulatory subunit. Atypical calpains such as calpain 10 vary greatly in structure and even presence of domains besides domain II (modified from Suzuki et. al., Diabetes 2004¹⁷).

There, they dissociate from their inhibitor and are placed near calcium channels for further regulation of their activity.²⁰ The auto-proteolysis of domain I seems to be necessary for calpain activity. In contrast, calpain isoforms have been found that are not regulated by binding to calpastatin or one of the small regulatory subunits, which have therefore been named atypical calpains (see Figure 3-2).²¹ One such atypical calpain, calpain 10, seems to be exclusively localized at the mitochondria and mediates proteolysis in a number of pathways upon reperfusion.²² Among these are truncation of apoptosis inducing factor (AIF)²³ into its active form, lysis of respiratory chain proteins (complex I)²² and induction of cytochrome C release.²⁴ Typical calpains (e.g. calpain 1 and 2) have been associated with the cleavage of ryanodine receptor (RyR) and sarco/endoplasmic reticulum Ca²⁺-ATPase (SERCA) at the SR²⁵, α -fodrin fibers of the plasma membrane cytoskeleton²⁶, degradation of myofibrillar proteins (e.g. cardiac troponins)²⁷ and lysis of regulatory proteins such as protein kinase C (PKC)^{28,29} due to their localization inside the cytoplasm (see Figure 3-3).

Activity of calpains is conferred via their catalytic center (domain II), which was identified as a cysteine protease (see Figure 3-2).³¹ Within domain II, the catalytic triad consists of a cysteine, a histidine and an asparagine. In the inactive form, the distance between cysteine and histidine is too large, therefore, conformational changes upon calcium binding are believed to trigger catalytic activity.¹⁸

Inhibition of calpain activity was proposed to reduce myocardial I/R injury. Indeed many calpain inhibitors were shown to be cardioprotective in an experimental setup, though

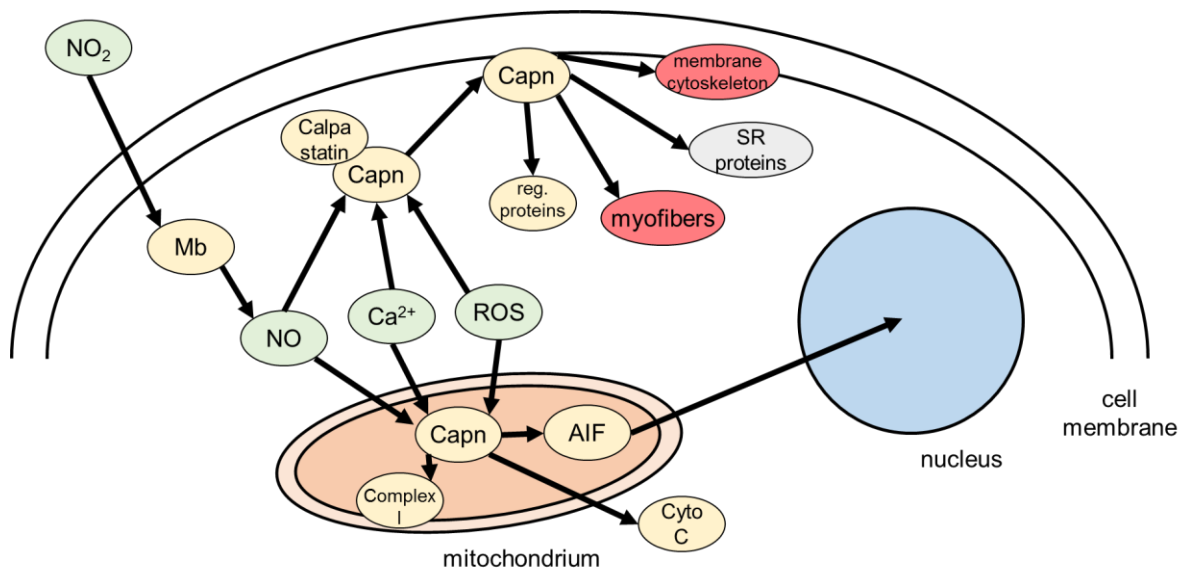


Figure 3-3: Nitrite mediated cardioprotection via posttranslational modification of calpains (Capn). Nitrite is reduced to nitric oxide (NO) by myoglobin (Mb) under ischemic conditions, which elevates NO levels during reperfusion. Rising calcium and ROS levels mediate calpain activity, which could be attenuated by calpain S-nitrosation. Calpains themselves have deleterious effects on apoptotic and necrotic pathways inside the mitochondria as well as in the cytoplasm (modified from Insette et. al., *Cardiovasc Res* 2012³⁰).

this failed to translate favorably into clinical practice. This may be partly due to the detrimental effects of prolonged inhibition, thus making the reversible, short-term reduction of calpain activity a desired target³⁰, which could be achieved via posttranslational modification using nitric oxide (NO). NO has been extensively investigated as a mediator of cardioprotection.³² In low O₂ scenarios, supplementation with inorganic nitrite was shown to be cardioprotective and to convey beneficial signaling via NO.³³ In the heart during ischemia, it was shown that myoglobin was able to produce NO from nitrite³⁴ and that this process was necessary for the reduction of infarct size via nitrite.³⁵ NO modifies proteins posttranslationally to regulate their activity in a process called S-nitrosation. S-nitrosation describes the reaction of the NO[•] radical with a free sulfhydryl- (SH-) group, usually inhibiting the formation of a disulfide bond at cysteines with the subsequent breakdown of 3D structure and protein activity modulation. This was shown to be the case for several proteins involved in both deleterious and beneficial pathways after I/R.^{36–38}

In vitro and *in vivo* studies have shown that S-nitrosation can reversible inhibit calpain activity.^{39,40} Whether the posttranslational modification of calpains is a possible target for cardioprotection has remained unknown and nitrite supplementation was used as a tool to investigate this question in the present work.

3.3 Vascular damage in the course of ischemia/reperfusion

In addition to cardiomyocytes, endothelial cells (ECs) are also subject to detrimental effects of I/R injury. Although they survive hypoxia for some days *in vitro*⁴¹, lack of blood flow and shear stress *in vivo* lead to cell swelling and blebbing.⁴²

Ischemia induces intracellular edema in both CMs and ECs as a result of energy-lacking ion pumps.⁴³ Edema development inside the interstitium is caused by increased ion concentrations and endothelial barrier breakdown, which is composed of the glycocalyx (a lumen-facing protein/lipid covering of the ECs), the endothelial cells themselves and pericytes.⁴⁴ Glycocalyx degradation is mediated by tumor necrosis factor α (TNF α)⁴⁵, and it promotes edema development⁴⁶ and leukocyte/platelet adherence to the endothelial layer.^{47,48} Endothelial intercellular junctions are loosened by EC hypercontracture from increased intracellular calcium concentrations and cytoskeletal disruption.^{49,50} An important component of the endothelial layer is vascular endothelial growth factor (VEGF), which is released in low oxygen conditions. Binding to VEGF receptor 2 (VEGFR2) also induces the destabilization of endothelial intercellular junctions via diffusion of the complex composed of VEGFR2 and vascular endothelial cadherin (VE-cadherin) with subsequent integrity loss.⁵¹ Upon reperfusion, intracellular and interstitial edema are further increased due to the washout of ions. Swelling of ECs can result in rupture of the endothelial layer and hemorrhage into the surrounding tissue.⁵² Excessive edema and/or hemorrhage may restrict blood flow in the microvasculature even after reperfusion by tissue expansion (see Figure 3-4).⁵³

Percutaneous coronary intervention (PCI), as a means to achieve reperfusion, can cause an embolization of debris from the thrombus into the circulation that occludes vessels further downstream in the microcirculation.⁵⁴ This can lead to microinfarction and subsequent immune responses.⁵⁵ Further clogging of small blood vessels can occur due to expression of adherence molecules on ECs and blood cells with subsequent aggregation of erythrocytes, platelets and leukocytes (see Figure 3-4).^{56–58} During I/R, constriction inducing agents such as thromboxane, serotonin and endothelin are released from the primary occlusion site.^{59–61} Thus, distal blood vessels show dysfunctional vasodilation, further exacerbating the blood flow impairment.

In areas with cessation of blood flow in the microcirculation by either occlusion or constriction the no-reflow phenomenon (also known as microvascular obstruction [MVO]) occurs, where despite reopening of the major vessel ischemia persists and

leads to tissue damage.⁶² MVO localizes only at sites of infarction (meaning dead, formerly ischemic tissue) and not in viable tissue within the AAR, and infarction can also occur without MVO. More importantly, I/R injury and MVO sizes can be separately investigated and earlier studies found ways to reduce one without the other.^{63,64} Whether MVO is a consequence of I/R or (transient) MVO is the cause of dead tissue remains to be investigated.

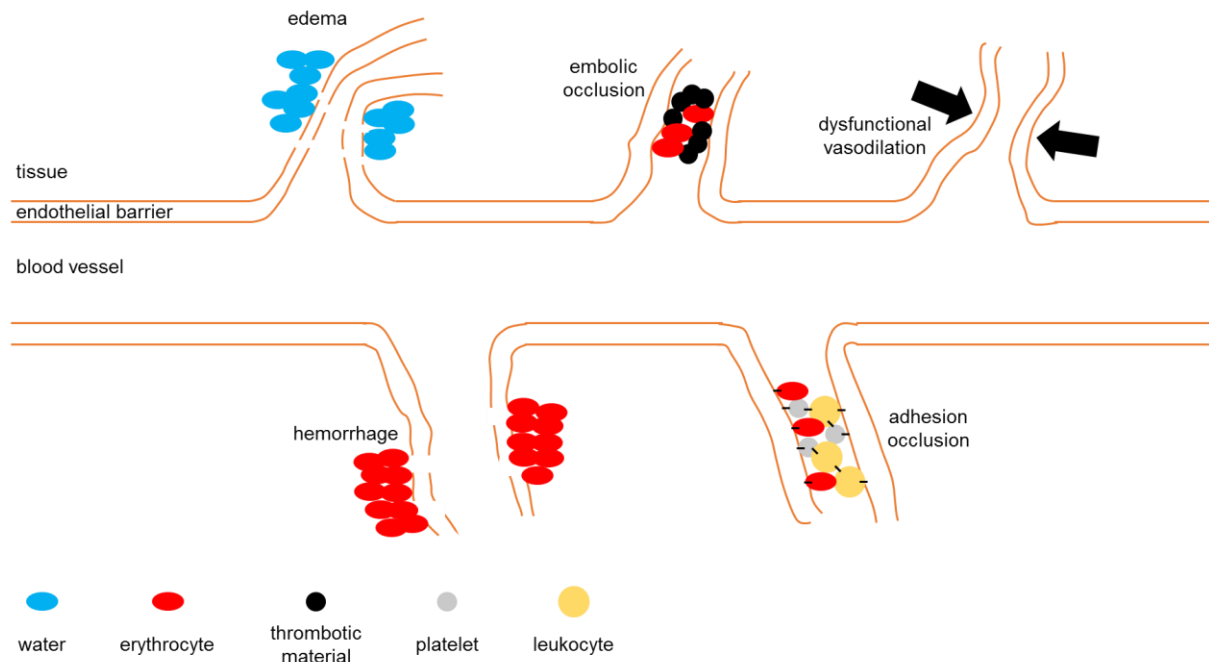


Figure 3-4: Occlusion and constriction of the capillary network. After I/R, small blood vessels are prone to further dysfunctionality by either occlusion, embolic or adhesion mediated and/or constriction via edema/hemorrhage induced tissue swelling or insufficient vasodilation (modified from Heusch *Circ. Res.* 2016⁶⁵).

Previous studies on MVO have used fluorescent dyes to localize the sites of endothelial barrier perforation in thick histological samples. This method combines well with the assessment of infarct size in the same sample, but fails to allow for spatial analysis and combination with other I/R injury parameters. In this context, 3 dimensional (3D) LSM of the vascular network has shown great potential in recent years for the investigation of various diseases^{66–68}, as it allows for both spatial and simultaneous analysis. This work attempts to elucidate the configuration of the vascular network and other I/R injury parameters after myocardial I/R injury using LSM.

3.4 The role of the immune system in I/R injury and cardiac repair

I/R has a significant impact on circulating blood cells. During ischemia, terminated blood flow allows cells to adhere to the endothelial layer, e.g. neutrophils.⁶⁹ These cells are activated upon binding and/or during reperfusion and stimulate an immune

response.⁷⁰ Most important for the activation of the immune system is the secretion of danger-associated molecular patterns (DAMPs) from dead and dying cells inside the heart.⁷⁰

After an AMI, cardiac function is impaired as dead CMs no longer contribute to heart muscle contractility. Since the heart itself lacks sufficient cell renewal, dead cells are replaced with fibrotic tissue via an immune system-mediated process⁷¹ in which different cells play vital roles either individually or cooperatively.

The cells of the immune system can be distinguished by either their lineage from myeloid or lymphoid predecessors after their differentiation from hematopoietic stem cells or their association with the innate and adaptive immune system. Cells of myeloid lineage include monocytes, which develop into macrophages *in situ*, and granulocytes, which are further classified by their histological staining behavior as eosinophils, basophils, neutrophils and mast cells. Lymphoid cells are B cells, T cells and natural killer (NK) cells. Uniquely, dendritic cells can be either of myeloid (derived from monocytes) or lymphoid origin (see Figure 3-5).⁷²

Innate immune cells are activated non-specifically by pathogen cell surface structures called pathogen-associated molecular patterns (PAMPs) or DAMPs and are therefore characterized by a fast reaction. Upon activation they release chemokines and cytokines to attract more immune cells and coordinate their behavior. Furthermore, innate immune cells digest pathogens, via either phagocytation or the release of digestive enzymes into extracellular space. After digestion some cells (namely macrophages and dendritic cells) can present antigens via major histocompatibility complex (MHC) class II molecules to the adaptive immune system to trigger a specific immune response via T and B cells (see Figure 3-5).⁷³

Adaptive immune response is either humoral or cell mediated, with the former being conducted by B cells and the latter by T cells.⁷⁴ B cells reside within lymphoid tissue and recognize antigen-MHC class II complexes present on antigen-presenting cells (APCs), that have migrated into said tissue. They are primed for the antigen presented and develop either into plasma cells, which leave the lymphoid tissue and produce antibodies, or memory B cells, which maintain their specificity to the antigen presented and thus allow for a faster adaptive immune response at a later stage (see Figure 3-5).⁷⁴ T cells recognize both MHC class II molecules on APCs and MHC class I molecules, which are expressed by all nucleated cells and allow for the presentation of endogenous materials like tumor or viral proteins. Primed T cells circulate

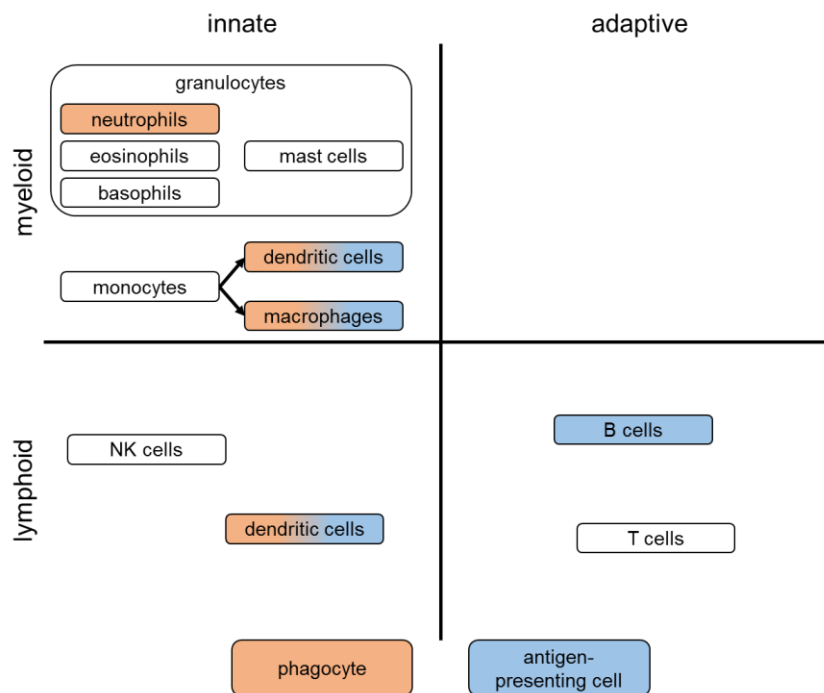


Figure 3-5: Immune cell classification. After differentiation from common hematopoietic precursors, immune cells can be either of myeloid or lymphoid origin. Further classification regards their manner of interaction with pathogens/dangers that can be either unspecific (innate) or selective based on antigen recognition (adaptive). Some cells are able to phagocytose foreign or damaged material to exclude them from the system. Presentation of antigens via MHC class II molecules for activation of an adaptive immune response is mediated by dendritic cells, macrophages and B cells.

throughout the body in search of their specific antigen. Upon binding, T cell subpopulations can either induce PCD of the presenting cell (mediated by CD8^{pos}, cytotoxic T cells via MHC class I) or regulate other immune cells by releasing cytokines (mediated by CD4^{pos}, helper T cells via MHC class II).⁷⁴

The immune cell response after AMI can be roughly divided into the inflammatory, reparative and remodeling phase.⁷⁵ Following the necrotic death of CMs after I/R, DAMPs are released from the cellular remains and initiate an innate immune response.⁷⁰ Intracellular molecules such as ATP and heat shock proteins, as well as fragments from the damaged extracellular matrix (ECM) and ROS can act as DAMPs.^{76,77} Furthermore specific signal proteins termed alarmins can mediate innate immune cell activation e.g. via toll-like receptors (TLR).⁷⁸ The starting point in this cascade are resident cells (macrophages, mast cells, dendritic cells) within the heart, which then release more pro-inflammatory cytokines.

Neutrophils are believed to be the first to migrate into the myocardium and further degrade extracellular matrix by secretion of matrix metalloproteinases (MMP) and ROS, as well as attracting other immune cells via cytokine production. Their numbers grow rapidly with a peak at approximately 24 h after AMI and neutrophil amount has been correlated with infarct size.^{79,80} Additionally, the inhibition of adhesion, activation,

as well as neutrophil extracellular trap (NET) formation have been linked with reduced infarct size and improved cardiac function.^{81–83} Pro-inflammatory monocytes migrate into cardiac tissue shortly after neutrophils following a chemokine gradient of monocyte chemoattractant protein-1 (MCP-1). These cells express high levels of Lymphocyte Antigen 6 Complex (Locus C) (Ly-6C^{high}) and differentiate into pro-inflammatory macrophages and dendritic cells. At a later time point, Ly-6C^{low} monocytes migrate into the myocardium, where they are believed to play a more reparative role. However, Ly-6C^{low} macrophages seem to develop from Ly-6C^{high} monocytes, prompting further questions about the role of Ly-6C^{low} monocytes during AMI.⁸⁴ During the inflammatory phase, macrophages phagocytize the remains of dead cells and ECM to enable cardiac repair. Although lymphocytes are mainly associated with later time points of infarction, studies have revealed their impact even during the acute phase. B cells can be found in the infarcted myocardium from day 1 on, with a peak at day 3 and were shown to negatively affect cardiac function via the recruitment of pro-inflammatory monocytes.⁸⁵ On the other hand, the absence of an early population of T cells has been linked with worse outcomes in a clinical setting.⁸⁶

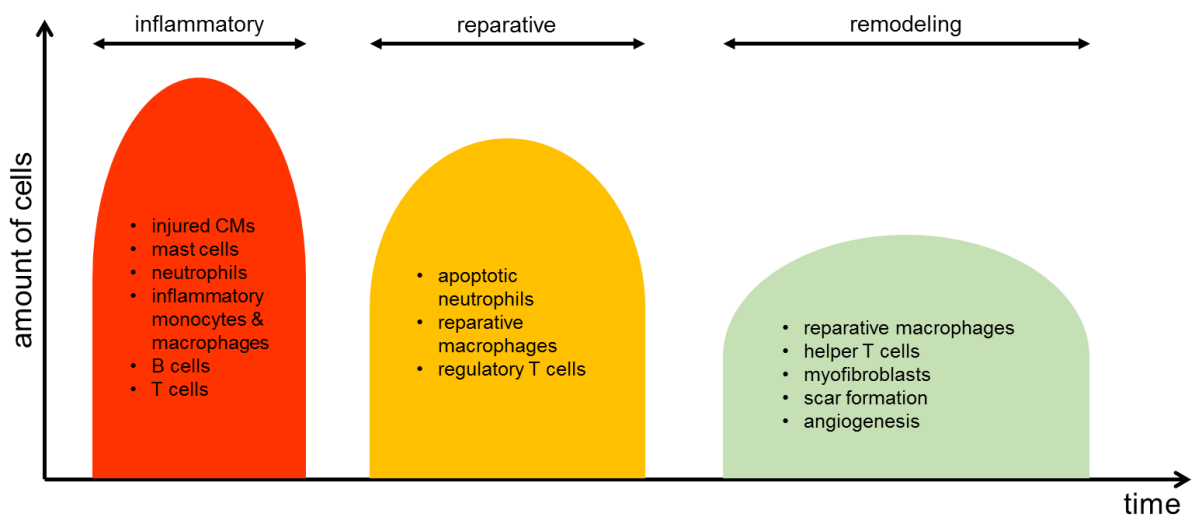


Figure 3-6: Phases of immune cell response after AMI. In the first days, neutrophils and inflammatory monocytes/macrophages clear the heart of debris and path the way for restructuring. Later inflammation is stopped by apoptotic neutrophils, reparative macrophages and regulatory T cells. Remodeling takes place with the invasion of myofibroblasts forming the scar (modified from Prabhu and Frangogiannis Circ Res 2016⁸⁷).

Following the sudden increase in immune cell concentration, anti-inflammatory signals are secreted within the myocardium, both to resolve inflammation to a more reparative state and to restrict it to the infarcted area.⁸⁸ Among these signals, most are produced by innate immune cells themselves e.g. neutrophils release lactoferrin and

macrophages (after the phagocytosis of apoptotic neutrophils) interleukin-10 and transforming growth factor β .⁸⁹ Missing phagocytosis (by depletion of neutrophils) has been shown to increase fibrosis and thereby worsen cardiac function.⁹⁰ In addition, several intracellular pathways within macrophages impact the change to an anti-inflammatory milieu.^{91–93} CD4^{pos} regulatory T cells (Tregs) seem to play a beneficial role in inflammation resolution, as the depletion of Tregs impairs the transition of macrophages to an anti-inflammatory phenotype.⁹⁴ Furthermore, Tregs influence pro-inflammatory/pro-fibrotic signal molecules such as ATP and the deletion of that pathway worsens the outcome.⁹⁵ Healing of the infarcted area involves activation of (myo-) fibroblasts that produce large amounts of ECM proteins to preserve heart wall integrity and express contractile proteins to maintain cardiac function. In addition, new blood vessels are formed via angiogenesis to supply the scar tissue. Reparative macrophages play a central role as they modulate both processes.⁹⁶ CD4^{pos}, helper T cells influence (myo-) fibroblast activity directly with the release of cytokines and growth factors and indirectly by affecting macrophages.⁹⁷ Following scar formation, the inflammatory response after AMI ends with the PCD of reparative cells. Due to the replacement of dead CMs with (myo-) fibroblasts and scar tissue, the heart loses much of its former contractile strength. This results in decreased cardiac function and, in the worst case scenario, further remodeling of the heart muscle until compensation is no longer possible.⁹⁸ This is termed heart failure, a deadly disease requiring replacement of the heart with either a donor or synthetic heart.

Despite the monumental work of research done on immune cell mediated processes after AMI, several aspects remain poorly understood. Depletion of neutrophils has been shown to be beneficial either in the early reperfusion stages via reduction of tissue damage⁹⁹ or at later time point by modulation of macrophages⁹⁰, though the exact pathway remains elusive. Moreover, localization of neutrophils inside the heart after AMI was only vaguely investigated previously and whether modulation of their position relative to the damaged tissue can be therapeutically targeted is an open question. Furthermore, clinical trials on neutrophil treatment were non-conclusive¹⁰⁰, adding to the controversy surrounding immune cell processes.

3.5 The current state of I/R injury assessment techniques

Previous research on cardiac I/R injury treatment has been persistently focused on either salvaging CMs, preserving vascular integrity, or modulating the immune

response. A multitude of therapeutic options have been proposed from experimental studies.¹⁰¹ However, while these single-target strategies may have yielded beneficial results in preclinical models, they failed to translate to the real-life human context. Debate continues as to why clinical trials for novel cardioprotective agents have been unsuccessful thus far. Some potential targets failed due to their time of administration, as beneficial pathways are redundant if their required modulation is prior to ischemia. Similarly, most suggested therapies focused on one cellular entity, which may be too narrow a view for the multi-component orchestra that is AMI. Consensus has been reached that treatment of only one I/R injury entity is not sufficient to achieve better outcomes in heterogeneous human patient cohorts. Therefore the development of multi-target therapies to simultaneously protect cardiac vasculature and CMs, while modulating immune response has been proposed as the most promising approach.^{102,103} To this end, simultaneous measurement of different infarct parameters in the same sample is a necessary step for the accurate evaluation of these multi-target therapies during pre-clinical studies. Currently, applied techniques lack the capability for simultaneous analysis, especially when measuring tissue damage. Early measurements of infarct size were performed in large animals (e.g. dogs) using histological techniques like hematoxylin and eosin (H&E) staining on chemically fixed samples.¹⁰⁴ These can be similarly applied to the mouse models more commonly used today. Moreover, a huge variance of staining techniques is available to test for several cellular conditions, making the histological approach quite versatile. To better estimate the extent of damage, live tissue methods were established whereby the status can be assessed immediately after organ extraction based on intracellular redox potentials.¹⁰⁵ The gold standard method currently in practice is based on the reduction of triphenyl tetrazolium chloride (TTC) via dehydrogenase activity in live cardiac cells. To do this, the heart is cut into thick slices (~1-2mm) that are incubated in a TTC solution and then photographed. Delineation of the AAR is done by prior injection of a colored dye (in most cases Evan's Blue), and inside the AAR viable myocardium stains red where TTC is reduced.¹⁰⁶ Both methods represent an endpoint measurement approach, which restricts complementary analysis due to a lack of leftover cardiac tissue material. To this end, non-invasive or indirect methods to determine infarct size were established. Echocardiographic and magnetic resonance imaging were both found to correlate well with infarct size measured via TTC staining, though the exact size of the infarcted tissue varied.^{107,108} However, these methods require the use of contrast agents, which

can complicate protocol execution and hamper subsequent analysis. Indirect evaluation of infarct size was conducted by correlation with proteins released from the damaged tissue, most notably cardiac troponins and creatine kinase. This represents the most gentle approach in terms of heart tissue preservation, and it is routinely used in clinical practice.¹⁰⁹ However, even in the clinical setting, linear correlation is seldom possible and therefore precise determination of infarct size remains challenging.⁴ Currently established methods for I/R injury analysis have limitations that restrict the investigation of multiple parameters in the same specimen, including I/R injury size and damage response, in terms of both quantity and spatial localization. To this end, LSFM may provide an accurately 3D reconstructed picture of the heart, and its use in combination with fluorescent markers provides greater detail on the parameters of interest. With LSFM, simultaneous measurement of multiple infarct parameters is feasible, which may represent a critical step in the assessment of multi-target cardioprotection strategies.

3.6 Aims

Many experimentally-tested therapeutic applications to reduce infarct size and facilitate better outcomes after AMI have not translated into clinical practice.^{110,111} In recent years, this has been attributed to the fact that most pre-clinical studies focused on either increasing CM survival, preserving vascular integrity, or modulating the immune response. Therefore it has been proposed that a successfully translatable cardioprotection strategy should address all three of these entities.^{102,103}

As such, the following questions shall be addressed in this work:

1. Does S-nitrosation via nitrite reduction influence intracellular, apoptotic pathways by modifying calpain function as a potential multitarget in the heart during I/R?
2. Can a LSFM-based approach provide simultaneous measurements of the precise I/R injury to the tissue and vasculature in volumes?
3. How do volumes of I/R injury co-localize with mediators of I/R injury including distinct immune cell populations in the course of healing?

4 Publications

4.1 S-nitrosation of calpains is associated with cardioprotection in myocardial I/R injury

Matthias Totzeck^{a,*}, Sebastian Korste^a, Ilkka Miinalainen^b, Ulrike B. Hendgen-Cotta^a, Tienush Rassaf^a

*Corresponding author

^aUniversity Hospital Essen, Medical Faculty, West German Heart and Vascular Center, Department of Cardiology and Angiology, Hufelandstr. 55, 45147 Essen, Germany

^bBiocenter Oulu Electron Microscopy Core Facility, University of Oulu, Finland

Nitric Oxide 2017;67;68-74. doi: 10.1016/j.niox.2017.04.003

4.1.1 Abstract

Background: Myocardial infarction remains the single leading cause of death worldwide. Upon reperfusion of occluded arteries, deleterious cellular mediators particularly located at the mitochondria level can be activated, thus limiting the outcome in patients. This may lead to the so-called ischemia/reperfusion (I/R) injury. Calpains are cysteine proteases and mediators of caspase-independent cell death. Recently, they have emerged as central transmitters of cellular injury in several cardiac pathologies e.g. hypertrophy and acute I/R injury.

Methods: Here we investigated the role of cardiac calpains in acute I/R in relation to mitochondrial integrity and whether calpains can be effectively inhibited by posttranslational modification by S-nitrosation. Taking advantage of the a cardiomyocyte cell line (HL1), we determined S-nitrosation by the Biotin-switch approach, cell viability and intracellular calcium concentration after simulated ischemia and reoxygenation - all in dependence of supplementation with nitrite, which is known as an 'hypoxic nitric oxide (NO) donor'. Likewise, using an *in vivo* I/R model, calpain S-nitrosation, calpain activity and myocardial I/R injury were characterized *in vivo*.

Results: Nitrite administration resulted in an increased S-nitrosation of calpains, and this was associated with an improved cell-survival. No impact was detected on calcium levels. In line with these *in vitro* experiments, nitrite initiated calpain S-nitrosation *in vivo* and caused an infarct sparing effect in an *in vivo* myocardial I/R model. Using electron microscopy in combination with immuno-gold labeling we determined that calpain 10 increased, while calpain 2 decreased in the course of I/R. Nitrite, in turn, prevented an I/R induced increase of calpains 10 at mitochondria and reduced levels of calpain 1.

Conclusion: Lethal myocardial injury remains a key aspect of myocardial I/R. We show that calpains, as key players in caspase-independent apoptosis, increasingly locate at mitochondria following I/R. Inhibitory post-translational modification by S-nitrosation of calpains reduces deleterious calpain activity in murine cardiomyocytes and *in vivo*.

Keywords: calpains, S-nitrosation, myocardial I/R injury, nitrite

4.1.2 Background

Acute coronary syndromes represent one of the leading single causes of death worldwide. The foremost therapeutic goal is a timely restoration of perfusion and concomitant reoxygenation. This has, however, been associated with an exacerbation of tissue injury, the so-called I/R injury^{1, 2}. Emerging evidence points to a central yet incompletely defined role for the first few minutes of reperfusion of the acute I/R event³. On a cellular level, I/R associated damage has largely been related to increased cytosolic and subsequently mitochondrial calcium levels, deterioration and rapid normalization of pH levels, and excess generation of reactive oxygen species (ROS)^{4, 5}. These patho-mechanisms may finally target and deteriorate cardiac mitochondria⁶. The exact events leading to mitochondria-driven cell death by mechanisms of necrosis, apoptosis, or autophagy are incompletely understood. Dysregulated calcium signaling and normalized pH values, as found in early reperfusion, provide excellent circumstances under which cardiac neutral cysteine proteases are activated with subsequent cellular devastation¹.

Calpains are a group of highly conserved non-lysosomal calcium-dependent cysteine proteases⁷⁻¹¹. Sequencing has revealed 14 subunit members and one endogenous inhibitor (calpastatin) with some of these expressed in a tissue specific manner. Calpains can also be subdivided into typical (e.g., calpain 1 and 2) and atypical calpains (e.g. calpain 10)¹². This relates to a potential binding and inhibition via calpastatin, a missing characteristic of atypical calpains (e.g. calpain 10)¹³. In mammalian hearts, calpains 1, 2 and 10 are highly expressed¹⁴. It is generally acknowledged that calpains are present in the cytosol and remain silent under normal physiological conditions. Recently, they have also been detected in mitochondria^{15, 16}. Upon activation in the environment of myocardial reperfusion, calpains are found to be localized more closely to cellular membranes. It has been speculated that this enhances their activity¹⁷. However, it is not known whether calpains are translocated to mitochondria or even enter mitochondria in the course of myocardial I/R. Calpains are activated by and in response to specific calcium signals^{13, 18}. In myocardial I/R, this occurs as a burst during early reperfusion also affecting mitochondrial calcium concentration^{19, 20}. Upon activation, calpains hydrolyze target proteins in the cytosol and at membranes and direct cells into cell death^{15, 16, 21}.

Apart from deteriorated calcium signaling, ROS contribute significantly to myocardial I/R injury³. Rapid recovery of cellular oxygen (O₂) levels after ischemia triggers an

inadequate respiration with mitochondria-derived release of superoxide anion radicals. Furthermore, aconitase is a protein highly susceptible to oxidative stress and we demonstrated that this sensor was significantly damaged in the first few minutes of reperfusion^{22, 23}. The deleterious respiratory chain-derived oxidative stress can be improved by cardioprotective measures. A posttranslational modification of complex I can be therapeutically achieved to reduce its activity and ROS generation^{22, 23}. Endogenous as well as exogenously supplied NO is generally believed to be protective for myocardial functions arguably with exemption of excessive levels during, e.g., inflammation²⁴⁻²⁸. The induction of nitroso species formation from NO is largely capable of reducing myocardial I/R injury²⁹. This is achieved by chemical nitrite reduction to bioactive NO via cardiac myoglobin (Mb)^{22, 23, 30}, a mechanism, which is also biologically active under physiological conditions^{23, 31, 32} regulating hypoxic vasodilation by nitrite reduction to NO via Mb in the vascular bed^{23, 31}. In humans, Mb's nitrite reductase activity is even enhanced³³. Following NO formation from nitrite and induction of S-nitrosation, specific cardiomyocyte targets may be posttranslationally modified and regulated²⁹. Particularly, S-nitrosation of macrophage migration inhibitory factor as well as complex I may lead to an increase in ROS decomposition²⁹. However, the complete NO signaling and the targets of NO in the reperfused myocardium are incompletely characterized.

Given their remarkable contribution to the initiation and progression of myocardial I/R injury, an inhibition of calpains is a desirable therapeutic approach^{17, 21, 34}. However, pharmacological inhibitors have not been proven yet to exert enough specificity (e.g. without affecting cathepsin activity) to be implemented in clinical practice. Interestingly, *in vitro* studies have assessed calpain activity in dependence of posttranslational modification via targeted S-nitrosation³⁵. This modification has led to a much reduced calpain activity and subsequent cellular functions – as determined for cultured immune cells³⁶. It is unclear whether an *in vivo* posttranslational modification of calpains by S-nitrosation can be achieved to initiate their temporal inhibition with reduced damage of mitochondria and with resulting cardioprotection during acute myocardial infarction.

4.1.3 Methods

Chemicals

All chemicals were obtained from Sigma, Germany, unless stated otherwise.

Animals

Ethics approval for mouse studies was obtained from the responsible government agency (LANUV). Male C57BL/6JRJ mice (12 ± 3 weeks of age; Janvier) were held at the local animal house on 12 h/12 h light and dark cycle with water and food ad libitum. As no human experiments were performed, no written consent from participants was required.

HL-1 cell culture

HL-1 mouse cells were a kind gift of Dr. William Claycomb (New Orleans, LA, USA) and cultured as described by Claycomb et al.³⁷. Cells were cultured in Claycomb medium, incubated at 37 °C and 5% carbon dioxide (CO₂) and passaged when they reached 80-90% confluence, unless stated differently. Cells between passage 33 and 40 were used in these experiments and cultures were reestablished from frozen stocks every 3 months.

In vitro hypoxia/reoxygenation model

HL-1 cells were seeded into 6-well-plates at 3 x 10⁵ cells/cm² and incubated as described before for 3-4 days, until they reached close to 100% confluence while starting to contract spontaneously. The medium was then changed to Claycomb medium without fetal serum to simulate ischemia. Cells were transferred to an incubator, set at 37 °C, 5% CO₂ and 1% O₂ and cultured under these conditions for 22 h. Hereafter, media was changed to complete Claycomb medium. Finally, the cells were incubated at 37 °C, 5% CO₂, 21% O₂ for 1 h to simulate reperfusion. The cells were then subjected to different bioassays. For controls, cells remained in complete Claycomb medium and were incubated at 37 °C, 5% CO₂, 21% O₂. For nitrite supplementation, 30 mM sodium nitrite (Merck, Darmstadt, Germany) in Dulbecco's Phosphate-Buffered Saline (DPBS, v/v) was added 1:100 to the culture media prior to hypoxia induction, resulting in a final concentration of 300 mM sodium nitrite³⁸. DPBS alone served as control for nitrite supplementation.

In vivo I/R model and infarct size measurement

Male C57BL/6JRJ mice (12 ± 3 weeks of age) were subjected to a myocardial I/R *in vivo* protocol as described previously^{22,31}. Briefly, mice were anesthetized by intraperitoneal (i.p.) injection of ketamine (100 mg/kg) and xylazin (Rompun 10 mg/kg).

They were orally intubated and ventilated throughout the operation procedure, with 0.8 l/min air and 0.2 l/min O₂ at a tidal volume of 250 ml/ stroke and a breathing frequency of 140 strokes/min. Anesthesia was maintained during the operation by supplementing 2% isoflurane. The chest was opened through a left lateral thoracotomy and the left coronary artery was ligated. The application of 1.67 mmol/kg sodium nitrite (in 50 ml 0.9% sodium chloride) into the left ventricular cavity was carried out 5 min before reperfusion. After 30 min of ischemia, reperfusion was allowed for either 5 min or 24 h. In the former case, mice did not regain consciousness and were killed by heart excision while still anesthetized. For experiments requiring 24 h of reperfusion, mice were allowed to wake up in a warmed cage and received pain treatment every 8 h (buprenorphine, 0.05-0.1 mg/kg, s.c.). At the end of the 24 h reperfusion time, mice received 1000 IE heparin i.p. 10 min before the experimental protocol and were killed by cervical dislocation. Hearts were excised, perfused free of blood with phosphate buffered saline and subjected to the respective bioassays (5 min reperfusion) or infarct size measurement (24 h reperfusion). Computer-assisted planimetry was done to measure infarct size in a double blinded fashion using ImageJ software²². In all, 28 mice were used in these experiments, with a total of 3 animals excluded due to either atypical behavioral syndromes, >20% weight loss, signs of excessive burden, movement disorders, secondary injuries, infections or open wounds.

Biotin switch assay and immunoblotting

In order to determine and quantify the extent of the S-nitrosation of calpains, the S nitrosylated Protein Detection Assay Kit (Cayman Chemicals, Michigan, USA) was used according to the manufacturer's instructions. In brief, HL-1 cells were subjected to the hypoxia/reoxygenation model or were cultured under control conditions with and without nitrite supplementation. Cell suspensions were centrifuged at 500 x g for 5 min, the supernatant was aspirated and the cell pellet subjected to the kit protocol. When investigating S-nitrosation *in vivo*, mouse hearts were perfused free of blood after 5 min of reperfusion, excised, snap-frozen in liquid nitrogen and stored at -80 °C for a maximum of 7 days. Hearts were homogenized at 4 °C in 1 ml buffer A using a glass on glass homogenizer. Lysates were centrifuged at 4000xg, 4 °C for 15 min, the supernatant was transferred to a new tube and subjected to the kit's protocol. For each sample a control was generated, which was non-biotinylated to account for endogenous biotinylation. Protein concentration was determined using a DC protein

assay (Bio Rad, Hercules, CA, USA) with bovine serum albumin (Thermo Fisher, Waltham, MA, USA) as standard. Proteins were separated on a Bolt 4-12% BIS-TRIS Plus gel (Thermo Fisher, Waltham, MA, USA) and transferred to nitrocellulose membranes using a dry blotting procedure on an iBlot2 device (Thermo Fisher, Waltham, MA, USA). Blotting was performed at room temperature for 7 min total. The membrane was blocked, followed by 3 times washing. The primary antibody was diluted (Calpain 1, mouse, 1:2000; Calpain 2, mouse, 1:500; Calpain 10, rabbit, 1:5000, all from Abcam, Cambridge, UK) and incubated at 4 °C overnight. The membrane was washed 3 times followed by incubation with the matching secondary antibody (Calpain 1 and 2, anti-mouse; Calpain 10, anti-rabbit; both Abcam, Cambridge, UK, 1:4000) for 1 h at room temperature. Specific protein bands were visualized using the SuperSignal West Femto Maximum Sensitivity Substrate Kit (Thermo Fisher, Waltham MA, USA) and an Amersham 600 Imager (GE Healthcare, Buckinghamshire, UK). Biotinylation was shown by incubating the membrane with the S-nitrosylation Detection Reagent I (HRP) provided by the kit for 1 h at room temperature, followed by 3 washing steps and subsequent visualization of biotin bands using the SuperSignal West Pico Chemiluminescent Substrate (Thermo Fisher, Waltham, MA, USA) and an Amersham 600 Imager (GE Healthcare, Buckinghamshire, UK). Non-biotinylated samples were used as endogenous controls. Quantification of bands was done by ImageJ software and relative biotinylation was determined by intensity biotin/intensity protein of interest.

Calpain activity assay

Calpain activity was measured using the Calpain Activity Assay Kit (Abcam, Cambridge, UK) following manufacturer's instructions. In brief, HL-1 cells were subjected to the hypoxia/reoxygenation model or were cultured under control conditions. Afterwards wells were washed twice with ice-cold DPBS and then scraped from the wells in 200 µl aliquots. Cell suspensions were centrifuged at 500 x g, 4 °C for 5 min. The supernatant was discarded and the cell pellet was re-suspended in 100 µl extraction buffer. The cell suspensions were then snap-frozen in liquid nitrogen and thawed four times to lyse the cells. Lysates were centrifuged at 20817 x g, 4 °C for 5 min. Supernatants were transferred to new tubes and either used directly or snap frozen in liquid nitrogen and stored at -80 °C for a maximum of 7 days. Hearts from *in vivo* experiments were perfused free of blood after 5 min of reperfusion, excised, snap-

frozen in liquid nitrogen and stored at -80 °C for a maximum of 7 days. Hearts were homogenized at 4 °C in 1 ml extraction buffer. Lysates were centrifuged at 20817 x g, 4 °C for 5 min. Supernatants were transferred to new tubes and used directly. Protein concentration was measured using a DC protein assay (BioRad, Hercules, CA, USA) with bovine serum albumin (Thermo Fisher, Waltham, MA, USA) as standard. 100 mg of protein was used to determine calpain activity as described by the manufacturer. Active calpain 1 (provided from the kit) was used as positive control on every plate and active calpain 1 in conjunction with calpain inhibitor (provided from the kit) as well as one control sample in conjunction with calpain inhibitor served as negative control. Samples and controls were measured in duplicates. Fluorometric signal was quantified using a BMG FLUOStar (BMG Labtech, Ortenberg, Germany) at Ex/Em = 400/505 nm

Cell viability assay

Neutral red uptake assay was carried out with modifications as described previously³⁸. Briefly, cells underwent the hypoxia/ reoxygenation model or were cultured under control conditions, reperfusion-medium was aspirated and wells were washed twice. Pre-warmed, sterile-filtered Claycomb medium without serum and in conjunction with 0.8% neutral red solution was added and cells were incubated for 75 min at 37 °C, 5% CO₂. Staining solution was then aspirated; wells were washed twice and then dried for 1 h. Remaining neutral red dye was extracted from the cells using 1 M hydrogen chloride 1:100 in ice-cold isopropyl alcohol (Roth, Karlsruhe, Germany) and intensity of staining was determined with a BMG FLUOStar (BMG Labtech, Ortenberg, Germany) by measuring absorbance at 540 nm. Extraction solution was used as blank.

Electron microscopy

The hearts were fixed in 4% paraformaldehyde in 0.1 M phosphatebuffer (pH 7.4) supplemented with 2.5% sucrose for 2 h. Hereafter, hearts were immersed in 2.3 M sucrose solved in phosphate-buffered saline and rotated at 4 °C for 4 h. Specimens were frozen in liquid nitrogen and thin cryosections were cut using a Leica EM UC7 cryo-ultramicrotome (Leica Microsystems, Vienna, Austria). The sections were picked on nickel grids. The grids were first incubated in 2% gelatine and then in 0.1% glycine phosphate buffered saline for 10 min followed by incubation in a blocking serum containing 1% bovine serum albumin for 5 min. Sections were exposed to the primary antibodies to calpain 1, calpain 2 and calpain 10 (Abcam, Cambridge, UK) for 45min.

For monoclonal antibodies (calpain 1 and 2) rabbit-anti-mouse IgG (Jackson ImmunoResearch Laboratories Inc. Baltimore, PA, USA) was used as a bridging antibody for 30 min followed by incubation with protein A-gold (10 nm) for 30 min³⁹. Polyclonal antibody (calpain 10) was directly detected by incubation with protein A-gold conjugate. The controls were prepared by replacing the primary antibody with phosphate buffered saline. The grids were stained with neutral uranyl acetate (UA) and embedded in 2% methyl cellulose and examined with a Tecnai Spirit transmission electron microscope (FEI, Eindhoven, The Netherlands). Images were captured by a Quemesa CCD camera (Olympus Soft Imaging Solutions GMBH, Munster, Germany). Mitochondria were labelled as regions of interest (ROI). Area of ROIs was calculated as well as protein A-gold particles counted using ImageJ software and particle density per area was calculated, averaged and normalized to basal samples. A total of 8 images per sample were quantified, with mitochondria count ranging between 33 and 78 per image.

Statistical analysis

Values shown are means \pm standard error of the mean (sem). Statistical differences between samples were tested by analysis of variance using ANOVA with Bonferroni's post hoc test or by Student's t-test. P-values are given for each test at the respective place.

4.1.4 Results and discussion

S-nitrosation of calpains is associated with a decrease in calpain activity and an increase in cell viability during simulated I/R in vitro

HL-1 cardiac cells were subjected to hypoxia (1% O₂), followed by 1 h reoxygenation period. Prior to hypoxia induction, media was changed to Claycomb medium without fetal bovine serum to deprive cells. Normoxic controls were cultured in fully supplemented Claycomb medium. S-nitrosation was induced using a co-incubation of nitrite (300 μ M final concentration) at levels previously determined to be optimal for NO formation in cell cultures³⁸. Fig. 1A shows the experimental schema. We first analyzed the relative S-nitrosation as induced by nitrite supplementation after hypoxia/reoxygenation. Fig. 1B shows that nitrite causes a significant increase in S-nitrosation of calpain 1 and 2 *in vitro* under these conditions (calpain 1 CTRL vs. nitrite: 100% \pm 9.5 vs. 224.7% \pm 45.3, p = 0.0273, n = 5; calpain 2 CTRL vs. nitrite: 100% \pm

16 vs. $207.3\% \pm 28.9$, $p = 0.0118$, $n = 5$). No significant S-nitrosation was determined for calpain 10 (calpain 10 CTRL vs. nitrite: $100\% \pm 25.6$ vs. $152.5\% \pm 46.5$, $p = 0.3524$, $n = 5$). Normoxic controls showed less calpain S-nitrosation than hypoxia/reoxygenation samples, but did not reach statistic significance (calpain 1 CTRL vs. normoxia: $100\% \pm 62.9$ vs. $66.4\% \pm 48.2$, $p = 0.534$; calpain 2 CTRL vs. normoxia: $100\% \pm 63.9$ vs. $46.3\% \pm 11.4$, $p = 0.228$; calpain 10 CTRL vs. normoxia: $100\% \pm 94.6$ vs. $45.3\% \pm 5.9$, $p = 0.375$). The posttranslational modification of calpain by S-nitrosation has previously been associated with a decrease in calpain activity *in vitro* using the purified protein³⁵. Fig.1C shows a significantly reduced overall calpain activity in those cells treated with nitrite and previously assessed to have higher S-nitrosated calpains (CTRL vs. nitrite: $100\% \pm 8.9$ vs. $72.6\% \pm 7.9$, $p = 0.0438$, $n = 6$). We could also show a similar decrease of calpain activity when incubating pure calpain 1 protein with either calpain inhibitor or S-Nitroso-N-acetyl- DL-penicillamine (SNAP) as a NO donor (Supplemental Fig.1). In contrast, nitrite supplementation did not decrease calpain activity under these conditions. Arguably, nitrite supplementation was without acute effect on calcium levels in these cells, a known mediator of calpain activity (Supplemental Fig. 2). Finally, this nitrite-co-incubation could be related to an enhanced cellular viability following our *in vitro* simulated I/R model (Fig. 1D, CTRL vs. nitrite: $17.12\% \pm 3.2$ vs. 43.1 ± 5.2 , $p = 0.0017$, $n = 6$).

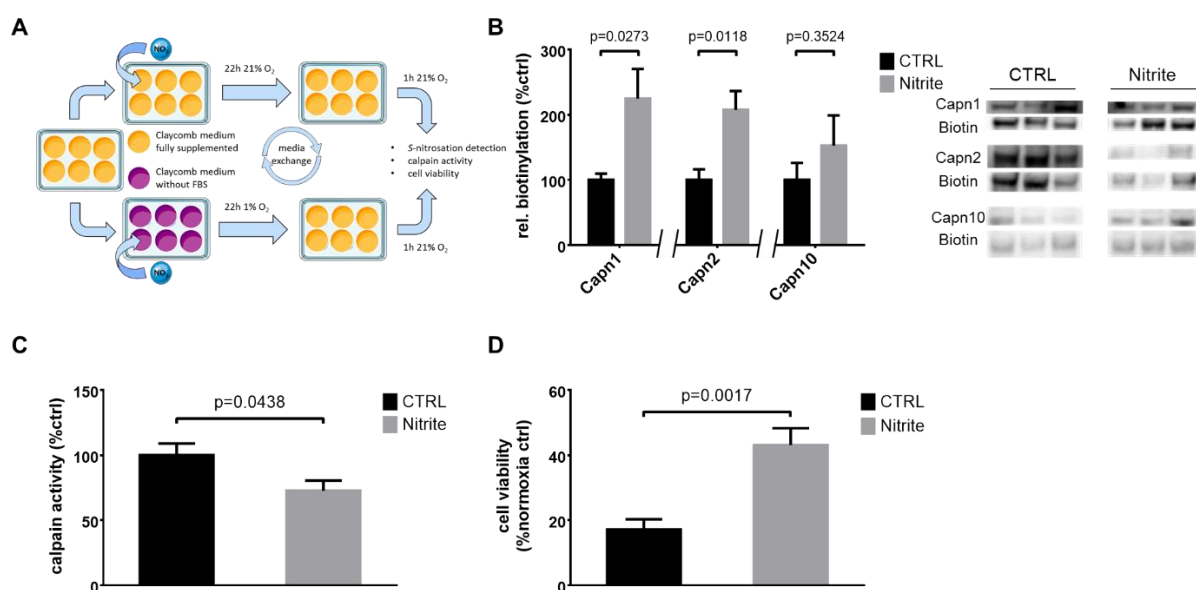


Figure 4-1: Fig. 1 Nitrite supplementation is associated with increased calpain S-nitrosation, decreased calpain activity and higher cell viability in an *in vitro* hypoxia/reoxygenation model. (A) Experimental scheme - HL-1 cells were subjected to 22 h of hypoxia (1%O₂), followed by 1 h at atmospheric O₂ for simulation of reperfusion. Nitrite was supplemented to the cell culture media to induce S-nitrosation in the course of simulated I/R. (B) Biotin switch assay and subsequent western blotting was used to determine relative biotinylation. Left Calpains 1 and 2 revealed

a significant increase in S-nitrosation, while for calpain 10 a trend was noted ($n = 5$; unpaired, two-tailed Student's t -test). Right exemplary original micrographs. (C) This was accompanied by a significant decrease in overall calpain activity for those cells treated with nitrite ($n = 6$; two-tailed Student's t -test). (D) After reoxygenation, cells were stained with neutral red to assess viability. Apart from increased S-nitrosation levels and calpain activity, administration of the hypoxic NO donor nitrite increased the viability of HL 1 cells significantly after simulated I/R ($n = 6$; unpaired, two-tailed Student's t -test).

S-nitrosation of calpains is associated with a decrease in calpain activity and decrease in infarct size during in vivo I/R

We next set out to relate our *in vitro* findings to cardioprotection *in vivo*. Mice were subjected to *in vivo* I/R consisting of 30 min of regional ischemia by reversible coronary ligation followed by reperfusion. We assessed S-nitrosation and calpain activity in the reperfused myocardium using a very short reperfusion regimen of 5 min (experimental scheme in Fig. 2A)²². Fig. 2B shows – in analogous to our *in vitro* results – a significantly increased S-nitrosation of calpain 1 and 2 (calpain 1 CTRL vs. nitrite: $100\% \pm 13.4$ vs. $157\% \pm 18$, $p = 0.0346$, $n = 5$; calpain 2 CTRL vs. nitrite: $100\% \pm 13.6$ vs. $145.7\% \pm 8.9$, $p = 0.0228$, $n = 5$), while no difference was detectable in calpain 10 S nitrosation (CTRL vs. nitrite: $100\% \pm 17.5$ vs. $119.7\% \pm 27.8$, $p = 0.5659$, $n = 5$). Basal controls showed comparable levels of calpain S-nitrosation to CTRL samples (calpain 1 CTRL vs. basal: $100\% \pm 7.43$ vs. $79.3\% \pm 14.7$, $p = 0.139$; calpain 2 CTRL vs. basal: $100\% \pm 10.47$ vs. $122\% \pm 50.1$, $p = 0.573$; calpain 10 CTRL vs. basal: $100\% \pm 1.88$ vs. $137.0\% \pm 74.4$, $p = 0.521$). Calpain S-nitrosation was again paralleled by a reduction of overall calpain activity in the reperfused myocardium (Fig. 2C, CTRL vs. nitrite: $100\% \pm 12.6$ vs. $54.2\% \pm 10.5$, $p = 0.0193$, $n = 6$) and a significantly reduced infarct size (Fig. 2D, CTRL vs. nitrite: $36.4\% \pm 1.2$ vs. $24.4\% \pm 1$, $p < 0.0001$, $n = 6$).

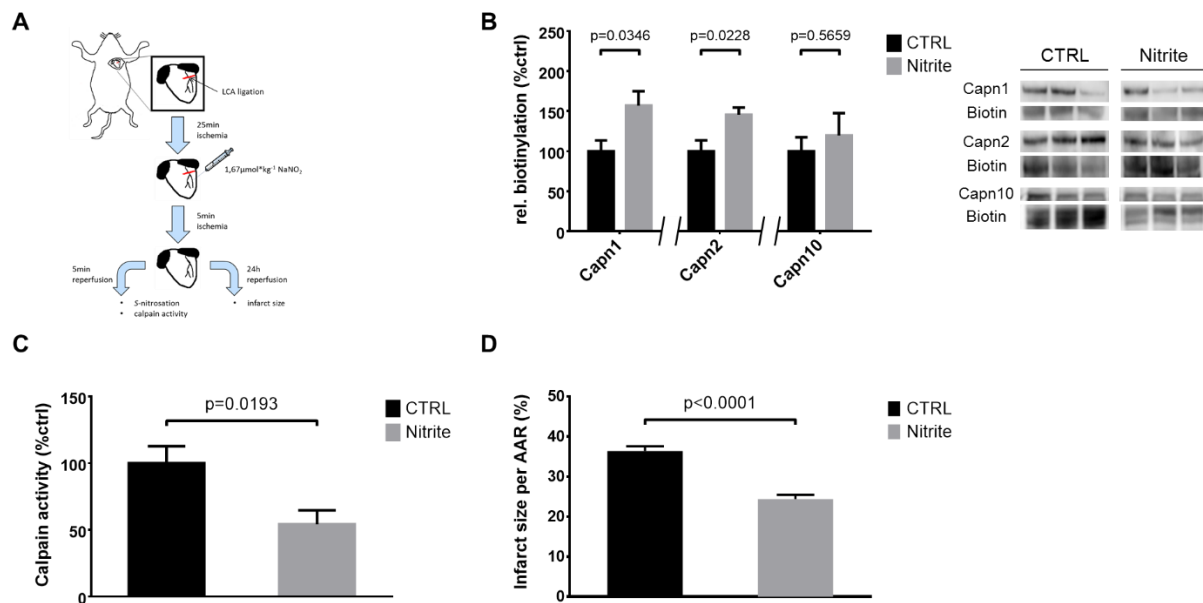


Figure 4-2: Fig. 2 Nitrite supplementation is also accompanied in vivo by increased calpain S-nitrosation, decreased calpain activity and smaller infarct size after I/R. (A) Experimental scheme - Male C57BL/6 mice (12 ± 3 weeks old) were subjected to in vivo I/R, with 30min of ischemia and either 5min (S-nitrosation detection and calpain activity assays) or 24 h (infarct size measurement) of reperfusion. Nitrite supplementation was supplied directly to the left ventricular myocardium 5min before reperfusion. (B) S-nitrosation was analyzed as for the in vitro samples by biotin switch assay, followed by western blotting. Left Quantitative analysis shows a significant increase in in vivo S-nitrosation of calpain 1 and 2, while this was not statistically significant in calpain10 (n = 5; unpaired Student's t-test). Right exemplary original micrographs. (C) In vivo nitrite administration also caused an overall decrease in calpain activity (n = 6; unpaired, two-tailed Student's t-test) and (D) and significant reduction in infarct sizes (n = 6; unpaired, two-tailed Student's t-test).

Mitochondrial structure and calpain localization at mitochondria following nitrite supplementation in in vivo I/R

Distribution of calpains in the myocardium is currently a matter of investigation. The exact subcellular levels of calpains 1, 2 and 10 and particularly in mitochondria are not known. However, recent evidence points a disease-driven translocation of calpains to certain subcellular structures^{15,40-43}. Taking advantage of the described *in vivo* I/R mouse model, we performed electron microscopy studies in conjunction with immuno gold labeling to determine the localization of calpains with and without nitrite supplementation (original micrographs in Fig. 3A). The quantitative analysis (Fig. 3B-D) revealed that I/R did not affect calpain 1 levels at mitochondrial membranes (Basal vs. I/R: 100% ± 69 vs. 115% ± 85, p = 0.618, n = 3), while calpain 2 levels decreased (calpain 2 Basal vs. I/R: 100% ± 44 vs. 62% ± 30, p < 0.0001, n = 3) and calpain 10 levels increased during I/R (calpain 10 Basal vs. I/R: 100% ± 71 vs. 151% ± 83, p = 0.0021, n = 3). Nitrite, in turn, significantly reduced mitochondrial levels in calpains 1 and 10 (calpain 1 I/R vs. I/R + nitrite: 115% ± 85 vs. 67% ± 45, p = 0.0003, n = 3; calpain 10 I/R vs. I/R + nitrite: 151% ± 83 vs. 107% ± 50, p = 0.0016, n = 3), while no

impact was observed on calpain 2 levels (I/R vs. I/R + nitrite: 62% \pm 30 vs. 50% \pm 23, $p = 0.226$, $n = 3$).

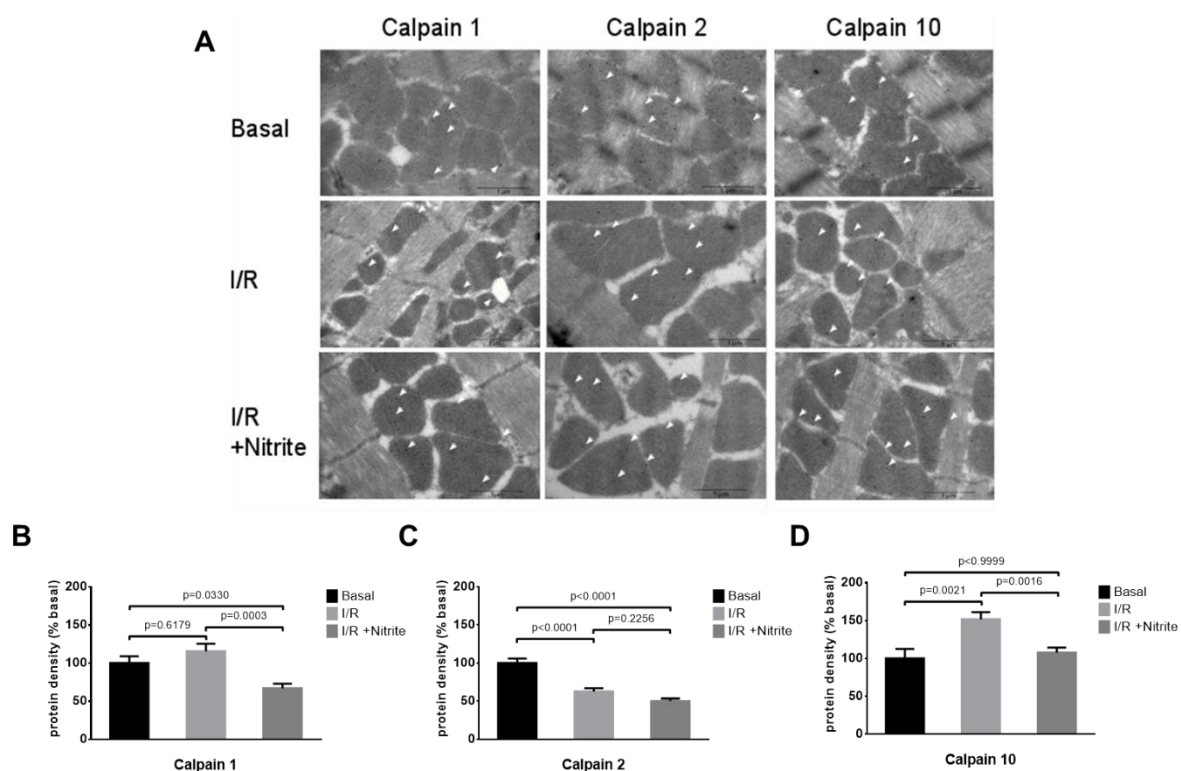


Figure 4-3: Fig. 3 Mitochondrial structure and calpain localization at mitochondria following nitrite supplementation in vivo I/R. (A) Calpain signal at mitochondria was quantified by defining mitochondria as regions of interest (ROI) and measuring gold labeling signals. Panel shows original micrographs from electron microscopy. Black lines indicate scale and white arrows exemplary gold labeled calpains. (B-D) Values were normalized to mean of basal calpain density and compared using 1-way ANOVA with Bonferroni correction ($n = 3$). For calpain 1 a significantly lower association at the mitochondrial level was denoted (B), which was not the case for calpain 2 (C) but for calpain 10 (D).

Arguably, our current results warrant more investigations relating to the exact contribution of each calpain to I/R injury and how this can be prevented by nitrite-related S-nitrosation. Interestingly, calcium - the canonical trigger of calpain activation²¹ - was unaffected by nitrite supplementation. However, one limitation of current *in vivo* research during I/R is the determination of the exact calcium levels at which calpain are activated and whether current bioassays can determine these presumably very distinct differences in concentrations²¹. While calcium levels appear unaffected, supplementation of nitrite is generally acknowledged to initiate a beneficial hypoxic NO signaling. We and others have recently shown that this burst of NO causes a decrease in ROS formation by blockade of deteriorated mitochondrial respiration⁴⁴. Furthermore, this was associated with a posttranslational modification, e.g. of

chemokines such as macrophage migration inhibitory factor to enhance its functional properties. The current studies shows that S-nitrosation of calpains is a result of nitrite administration and that this is associated with an overall reduction in calpain activity. One limitation of the current approach is the lack of specific calpain mutants that prevent an S-nitrosation. This must be studied in future trials to attribute the reduction of overall calpain activity to the specific calpain subtypes. However, both *in vitro* and *in vivo* assays demonstrate that S- nitrosation is particularly relevant in calpain 1 and 2. On the other hand, calpain 10 is affected by nitrite-dependent S-nitrosation to a lesser extent, but is, as well as calpain 1, significantly less found at mitochondrial membranes in nitrite-treated hearts after I/R. It is tempting to speculate that nitrite exerts a divergent cardioprotective effect by direct inhibition of calpain 1 and 2 (S-nitrosation) and by indirect prevention of mitochondrial translocation (calpain 10). In sum, the effects of calpains and their respective targets must be further studied. This relates to the deleterious calpain-related cleavage of mitochondrial structures and the initiation of an apoptosis related program^{15,40,41,45-50}. Characterization of this particular signaling, in turn, may further elucidate the yet incompletely defined apoptosis- and infarct sparing effect of nitrite in the I/R challenged heart.

4.1.5 Conclusion

Taken together, the current combined cell culture and *in vivo* approaches demonstrate that nitrite administration causes an S-nitrosation of cardiac calpains, which is associated with a decrease in deleterious calpain activity. This, in turn, could be related to an increase in cell survival in both *in vitro* and *in vivo* experiments. Future studies must identify the exact contribution of each calpain and the relevant downstream cellular targets.

Ethics

The animal experiments were approved by responsible government agency (LANUV, Recklinghausen, Germany).

Availability of data and material

All respective data is presented within the manuscript file.

Authors' contributions

MT conceived the study, analyzed data and wrote the manuscript. SK performed experiments and contributed to writing of the manuscript. IM performed experiments and contributed to writing. UHC conceived the study and contributed to writing of the manuscript. TR conceived the study, analyzed data and wrote the manuscript.

Consent to publish

Not applicable.

Competing interests

The authors declare no competing interest.

Acknowledgments

TR was supported by a grant from the Deutsche Forschungsgemeinschaft (RA 969/4-2). The funding body was not involved in either the conception of the study, the experiments, data analysis or the writing or submission of the manuscript.

4.1.6 References

- 1 D.M. Yellon, D.J. Hausenloy, Myocardial reperfusion injury, *N. Engl. J. Med.* 357 (11) (2007) 1121-1135.
- 2 H.K. Eltzschig, T. Eckle, Ischemia and reperfusion from mechanism to translation, *Nat. Med.* 17 (11) (2011) 1391-1401.
- 3 J.L. Zweier, M.A. Talukder, The role of oxidants and free radicals in reperfusion injury, *Cardiovasc. Res.* 70 (2) (2006) 181-190.
- 4 G. Heusch, Cardioprotection: chances and challenges of its translation to the clinic, *Lancet* 381 (9861) (2013) 166-175.
- 5 G. Heusch, Molecular basis of cardioprotection: signal transduction in ischemic pre-, post-, and remote conditioning, *Circ. Res.* 116 (4) (2015) 674-699.
- 6 G.W. Dorn, 2nd: mitochondrial dynamics in heart disease, *Biochimica et biophysica acta* 1833 (1) (2013) 233-241.
- 7 D.E. Croall, G.N. DeMartino, Comparison of two calcium-dependent proteinases from bovine heart, *Biochimica et biophysica acta* 788 (3) (1984) 348-355.

- 8 U.P. Zimmerman, W.W. Schlaepfer, Multiple forms of Ca-activated protease from rat brain and muscle, *J. Biol. Chem.* 259 (5) (1984) 3210-3218.
- 9 S. Pontremoli, E. Melloni, F. Salamino, B. Sparatore, M. Michetti, B.L. Horecker, Cytosolic Ca²⁺-dependent neutral proteinases from rabbit liver: activation of the proenzymes by Ca²⁺ and substrate, *Proc. Natl. Acad. Sci. U. S. A.* 81 (1) (1984) 53-56.
- 10 D.E. Croall, G.N. DeMartino, Purification and characterization of calcium-dependent proteases from rat heart, *J. Biol. Chem.* 258 (9) (1983) 5660-5665.
- 11 N. Kajikawa, A. Kishimoto, M. Shiota, Y. Nishizuka, Ca²⁺-dependent neutral protease and proteolytic activation of Ca²⁺-activated, phospholipid-dependent protein kinase, *Methods Enzym.* 102 (1983) 279-290.
- 12 A.C. Shore, J.C. Evans, T.M. Frayling, P.M. Clark, B.C. Lee, Y. Horikawa, A.T. Hattersley, J.E. Tooke, Association of calpain-10 gene with microvascular function, *Diabetologia* 45 (6) (2002) 899-904.
- 13 R.A. Hanna, R.L. Campbell, P.L. Davies, Calcium-bound structure of calpain and its mechanism of inhibition by calpastatin, *Nature* 456 (7220) (2008) 409-412.
- 14 D.D. Arrington, T.R. Van Vleet, R.G. Schnellmann, Calpain 10: a mitochondrial calpain and its role in calcium-induced mitochondrial dysfunction, *Am. J. Physiol. Cell Physiol.* 291 (6) (2006) C1159-C1171.
- 15 M.A. Smith, R.G. Schnellmann, Calpains, mitochondria, and apoptosis, *Cardiovasc. Res.* 96 (1) (2012) 32-37.
- 16 J. Inserte, V. Hernando, D. Garcia-Dorado, Contribution of calpains to myocardial ischaemia/reperfusion injury, *Cardiovasc. Res.* 96 (1) (2012) 23-31.
- 17 J. Inserte, Calpains in the cardiovascular system, *Cardiovasc. Res.* 96 (1) (2012) 9-10.
- 18 S. Ohno, Y. Emori, S. Imajoh, H. Kawasaki, M. Kisaragi, K. Suzuki, Evolutionary origin of a calcium-dependent protease by fusion of genes for a thiol protease and a calcium-binding protein? *Nature* 312 (5994) (1984) 566-570.
- 19 Y. Kirichok, G. Krapivinsky, D.E. Clapham, The mitochondrial calcium uniporter is a highly selective ion channel, *Nature* 427 (6972) (2004) 360-364.

- 20 M.L. Joiner, O.M. Koval, J. Li, B.J. He, C. Allamargot, Z. Gao, E.D. Luczak, D.D. Hall, B.D. Fink, B. Chen, et al., CaMKII determines mitochondrial stress responses in heart, *Nature* 491 (7423) (2012) 269-273.
- 21 C. Neuhof, H. Neuhof, Calpain system and its involvement in myocardial ischemia and reperfusion injury, *World J. Cardiol.* 6 (7) (2014) 638-652.
- 22 T. Rassaf, M. Totzeck, U.B. Hendgen-Cotta, S. Shiva, G. Heusch, M. Kelm, Circulating nitrite contributes to cardioprotection by remote ischemic preconditioning, *Circ. Res.* 114 (10) (2014) 1601-1610.
- 23 M. Totzeck, U.B. Hendgen-Cotta, P. Luedike, M. Berenbrink, J.P. Klare, H.J. Steinhoff, D. Semmler, S. Shiva, D. Williams, A. Kipar, et al., Nitrite regulates hypoxic vasodilation via myoglobin-dependent nitric oxide generation, *Circulation* 126 (3) (2012) 325-334.
- 24 S.A. Hamid, M. Totzeck, C. Drexhage, I. Thompson, R.C. Fowkes, T. Rassaf, G.F. Baxter, Nitric oxide/cGMP signalling mediates the cardioprotective action of adrenomedullin in reperfused myocardium, *Basic Res. Cardiol.* 105 (2) (2010) 257-266.
- 25 T. Rassaf, L.W. Poll, P. Brouzos, T. Lauer, M. Totzeck, P. Kleinbongard, P. Gharini, K. Andersen, R. Schulz, G. Heusch, et al., Positive effects of nitric oxide on left ventricular function in humans, *Eur. heart J.* 27 (2006) 1699-1705.
- 26 C. Heiss, C. Meyer, M. Totzeck, U.B. Hendgen-Cotta, Y. Heinen, P. Luedike, S. Keymel, N. Ayoub, J.O. Lundberg, E. Weitzberg, et al., Dietary inorganic nitrate mobilizes circulating angiogenic cells, *Free Radic. Biol. Med.* 52 (9) (2012) 1767-1772.
- 27 F.R. Heinzel, P. Gres, K. Boengler, A. Duschin, I. Konietzka, T. Rassaf, J. Snedovskaya, S. Meyer, A. Skyschally, M. Kelm, et al., Inducible nitric oxide synthase expression and cardiomyocyte dysfunction during sustained moderate ischemia in pigs, *Circ. Res.* 103 (10) (2008) 1120-1127.
- 28 A. Dejam, P. Kleinbongard, T. Rassaf, S. Hamada, P. Gharini, J. Rodriguez, M. Feelisch, M. Kelm, Thiols enhance NO formation from nitrate photolysis, *Free Radic. Biol. Med.* 35 (12) (2003) 1551-1559.
- 29 P. Luedike, U.B. Hendgen-Cotta, J. Sobierajski, M. Totzeck, M. Reeh, M. Dewor, H. Lue, C. Krisp, D. Wolters, M. Kelm, et al., Cardioprotection through Snitros(yl)ation of macrophage migration inhibitory factor, *Circulation* 125 (15) (2012) 1880-1889.

- 30 U.B. Hendgen-Cotta, P. Luedike, M. Totzeck, M. Kropp, A. Schicho, P. Stock, C. Rammos, M. Niessen, C. Heiss, J.O. Lundberg, et al., Dietary nitrate supplementation improves revascularization in chronic ischemia, *Circulation* 126 (16) (2012) 1983-1992.
- 31 M. Totzeck, U.B. Hendgen-Cotta, M. Kelm, T. Rassaf, Crosstalk between nitrite, myoglobin and reactive oxygen species to regulate vasodilation under hypoxia, *PloS one* 9 (8) (2014) e105951.
- 32 M. Totzeck, A. Schicho, P. Stock, M. Kelm, T. Rassaf, U.B. Hendgen-Cotta, Nitrite circumvents canonical cGMP signaling to enhance proliferation of myocyte precursor cells, *Mol. Cell. Biochem.* 401 (1-2) (2015) 175-183.
- 33 M. Totzeck, U.B. Hendgen-Cotta, C. Rammos, A.M. Petrescu, C. Meyer, J. Balzer, M. Kelm, T. Rassaf, Assessment of the functional diversity of human myoglobin, *Nitric oxide Biol. Chem./official J. Nitric Oxide Soc.* 26 (2012) 211-216.
- 34 A.L. Muller, N.S. Dhalla, Role of various proteases in cardiac remodeling and progression of heart failure, *Heart Fail. Rev.* 17 (3) (2012) 395-409.
- 35 M. Michetti, F. Salamino, E. Melloni, S. Pontremoli, Reversible inactivation of calpain isoforms by nitric oxide, *Biochem. biophys. Res. Commun.* 207 (3) (1995) 1009-1014.
- 36 P. Forsythe, A.D. Befus, Inhibition of calpain is a component of nitric oxide-induced down-regulation of human mast cell adhesion, *J. Immunol.* 170 (1) (2003) 287-293.
- 37 W.C. Claycomb, N.A. Lanson Jr., B.S. Stallworth, D.B. Egeland, J.B. Delcarpio, A. Bahinski, N.J. Izzo Jr., HL-1 cells: a cardiac muscle cell line that contracts and retains phenotypic characteristics of the adult cardiomyocyte, *Proc. Natl. Acad. Sci. U. S. A.* 95 (6) (1998) 2979-2984.
- 38 M. Totzeck, A. Schicho, P. Stock, M. Kelm, T. Rassaf, U.B. Hendgen-Cotta, Nitrite circumvents canonical cGMP signaling to enhance proliferation of myocyte precursor cells, *Mol. Cell. Biochem.* 401 (1e2) (2015) 175-183.
- 39 J.W. Slot, H.J. Geuze, A new method of preparing gold probes for multiple labeling cytochemistry, *Eur. J. cell Biol.* 38 (1) (1985) 87-93.
- 40 J.J. Sheng, H. Chang, Z.B. Yu, Nuclear translocation of Calpain-2 mediates apoptosis of hypertrophied cardiomyocytes in transverse Aortic constriction rat, *J. Cell. Physiol.* 230 (11) (2015) 2743-2754.

- 41 P.K. Sobhan, M. Seervi, L. Deb, S. Varghese, A. Soman, J. Joseph, K.A. Mathew, G. Raghu, G. Thomas, E S, et al., Calpain and reactive oxygen species targets Bax for mitochondrial permeabilisation and caspase activation in zerumbone induced apoptosis, *PloS one* 8 (4) (2013) e59350.
- 42 M.A. Perez-Pinzon, R.A. Stetler, G. Fiskum, Novel mitochondrial targets for neuroprotection, *J. Cereb. blood flow metabolism official J. Int. Soc. Cereb. Blood Flow Metabolism* 32 (7) (2012) 1362-1376.
- 43 M.A. Smith, M.D. Covington, R.G. Schnellmann, Loss of calpain 10 causes mitochondrial dysfunction during chronic hyperglycemia, *Archives Biochem. Biophys.* 523 (2) (2012) 161-168.
- 44 U.B. Hendgen-Cotta, M.W. Merx, S. Shiva, J. Schmitz, S. Becher, J.P. Klare, H.J. Steinhoff, A. Goedecke, J. Schrader, M.T. Gladwin, et al., Nitrite reductase activity of myoglobin regulates respiration and cellular viability in myocardial ischemia-reperfusion injury, *Proc. Natl. Acad. Sci. U. S. A.* 105 (29) (2008) 10256-10261.
- 45 A. Comitato, D. Sanges, A. Rossi, M.M. Humphries, V. Marigo, Activation of Bax in three models of retinitis pigmentosa, *Investigative Ophthalmol. Vis. Sci.* 55 (6) (2014) 3555-3562.
- 46 D.L. Douglas, C.P. Baines, PARP1-mediated necrosis is dependent on parallel JNK and Ca²⁺/calpain pathways, *J. cell Sci.* 127 (19) (2014) 4134-4145.
- 47 H. Kim, A.Y. Kang, A.R. Ko, H.C. Park, I. So, J.H. Park, H.I. Cheong, Y.H. Hwang, C. Ahn, Calpain-mediated proteolysis of polycystin-1 C-terminus induces JAK2 and ERK signal alterations, *Exp. cell Res.* 320 (1) (2014) 62-68.
- 48 H. Weber, L. Muller, L. Jonas, C. Schult, G. Sparmann, P. Schuff-Werner, Calpain mediates caspase-dependent apoptosis initiated by hydrogen peroxide in pancreatic acinar AR42J cells, *Free Radic. Res.* 47 (5) (2013) 432-446.
- 49 M. Xu, X. Li, S.W. Walsh, Y. Zhang, J.M. Abais, K.M. Boini, P.L. Li, Intracellular two-phase Ca²⁺ release and apoptosis controlled by TRP-ML1 channel activity in coronary arterial myocytes, *Am. J. Physiol. Cell Physiol.* 304 (5) (2013) C458-C466.
- 50 M. Shi, T. Zhang, L. Sun, Y. Luo, D.H. Liu, S.T. Xie, X.Y. Song, G.F. Wang, X.L. Chen, B.C. Zhou, et al., Calpain, Atg5 and Bak play important roles in the crosstalk between apoptosis and autophagy induced by influx of extracellular calcium, *Apoptosis Int. J. Program. cell death* 18 (4) (2013) 435-451.

4.1.7 Supplementary data

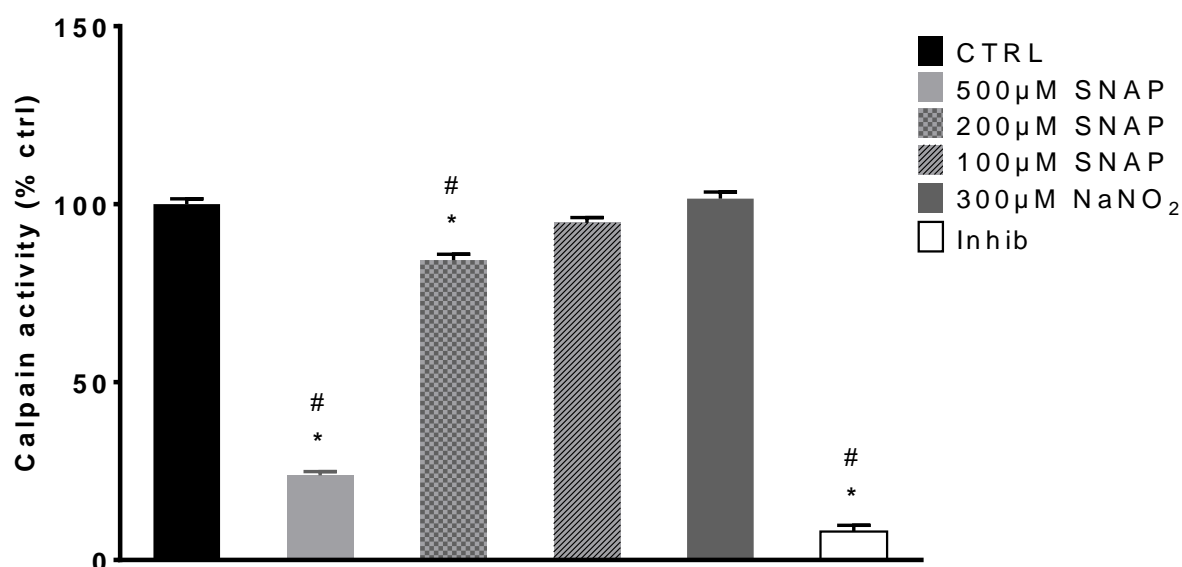


Figure 4-4: Supplemental Fig. 1 Calpain activity in vitro following supplementation with nitrite, SNAP or calpain inhibitor. 3.06 units of active human calpain 1 were incubated at 37°C in the dark for 30min with either increasing concentrations of S-Nitroso-N-acetyl-DL-penicillamine (SNAP), 300µM sodium nitrite or calpain inhibitor before being subjected to the calpain activity assay kit protocol following manufacturer's instructions as described (calpain 1 and calpain inhibitor were taken from the calpain activity assay kit, Abcam, Cambridge, UK). SNAP supplementation decreased calpain activity significantly at concentrations of 200µM and higher, while nitrite did not decrease calpain activity under these normoxic conditions (n=6; #: $p < 0.05$ compared to 300µM NaNO₂, *: $p < 0.05$ compared to CTRL; 1-way ANOVA with Bonferroni correction).

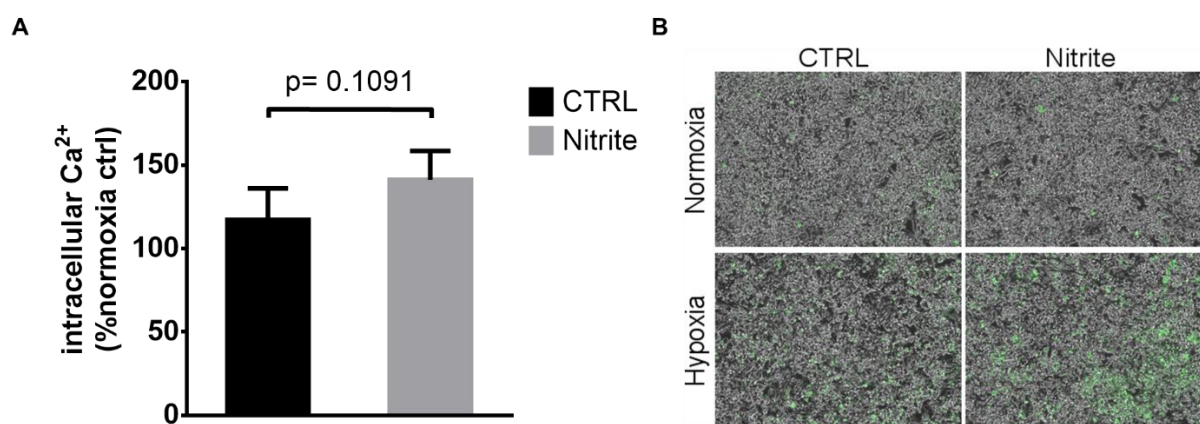


Figure 4-5: Supplemental Fig. 2 Calcium measurement following nitrite treatment in HL-1 cells. (A) Upon hypoxia and reoxygenation no significant differences in calcium levels were noted in HL-1 cells (nitrite vs. CTRL; n=4; two-tailed, unpaired Student's t-test). (B) Original micrographs.

4.2 Contemporaneous 3D characterization of acute and chronic myocardial I/R injury and response

Simon F. Merz^{*1,2}, Sebastian Korste^{*3}, Lea Bornemann^{*1}, Lars Michel³, Pia Stock³, Anthony Squire¹, Camille Soun¹, Daniel R. Engel¹, Julia Detzer⁴, Holger Lörchner^{4,5}, Dirk M. Hermann⁶, Markus Kamler⁷, Joachim Klode², Ulrike Hendgen-Cotta³, Tienush Rassaf³, Matthias Gunzer^{#1} and Matthias Totzeck^{#3}

**These authors contributed equally*

#These authors jointly supervised this work

¹Institute for Experimental Immunology and Imaging, University Hospital Essen, 45147, Essen, Germany

²Department of Dermatology, Venerology and Allergology, University Hospital Essen, 45147, Essen, Germany

³Department of Cardiology and Vascular Medicine, University Hospital Essen, 45147, Essen, Germany

⁴Max Planck Institute for Heart and Lung Research, Dept. of Cardiac Development and Remodelling, 61231, Bad Nauheim, Germany

⁵German Centre for Cardiovascular Research (DZHK), Partner site Rhine-Main, Frankfurt am Main, Germany

⁶Department of Neurology, University Hospital Essen, 45147, Essen, Germany

⁷Department of Thoracic and Cardiovascular Surgery, University Hospital Essen, 45147, Essen, Germany

Nat Commun. 2019;10(1):2312. doi:10.1038/s41467-019-10338-2

4.2.1 Abstract

Cardioprotection by salvage of the infarct-affected myocardium is an unmet yet highly desired therapeutic goal. To develop new dedicated therapies, experimental myocardial ischemia/reperfusion (I/R) injury would require methods to simultaneously characterize extent and localization of the damage and the ensuing inflammatory responses in whole hearts over time. Here we present a three-dimensional (3D), simultaneous quantitative investigation of key I/R injury components by combining bleaching-augmented solvent-based non-toxic clearing (BALANCE) using ethyl cinnamate (ECi) with light sheet fluorescence microscopy. This allows structural analyses of fluorescence-labeled I/R hearts with exceptional detail. We discover and 3D-quantify distinguishable acute and late vascular I/R damage zones. These contain highly localized and spatially structured neutrophil infiltrates that are modulated upon cardiac healing. Our model demonstrates that these characteristic I/R injury patterns can detect the extent of damage even days after the ischemic index event hence allowing the investigation of long-term recovery and remodeling processes.

4.2.2 Introduction

Restoration of perfusion after acute myocardial infarction is the most frequent and effective medical treatment, but the process may inflict massive ischemia/reperfusion (I/R) injury¹. A hallmark of I/R injury is the major loss of the vasculature² accompanied by impairment of the endothelium. In parallel, I/R results in an extensive inflammatory response³. Within minutes, circulating neutrophils are attracted to the affected vasculature where they transmigrate into the damaged tissue with incompletely defined roles in injury progression or protection^{4,5}. Macrophages, in turn, exhibit complex functions in cardiac inflammation and injury site repair peaking days after the onset of I/R⁶. A precise spatial identification and characterization of the cellular composition of the injured region reflecting the complex interplay between I/R-signaling and repair mechanisms, therefore, is essential for their breakdown into tractable therapeutic targets⁷.

The established tools for the characterization of I/R injury and response assessment have several limitations. This particularly relates to the co-localization of pathophysiological events including inflammation and (re-) vascularization. The mainstay for cardiac injury analysis in animal models is measurement of metabolic activity of cardiomyocytes in serial thick sections using triphenyl tetrazolium chloride

(TTC)⁸. However, this does typically not include advanced histological and immuno-histochemical co-assessments and fails to provide an accurate 3D reconstruction of the affected tissue. To precisely localize and quantify the extent of cardiac damage, a global 3D-structural analysis of the heart is mandatory. Light sheet fluorescence microscopy (LSFM) has been particularly effective to perform similar analyses and was previously used to image large tissue specimens^{9,10}, including the heart¹¹. Therefore, we hypothesized that LSFM was capable of characterizing myocardial ischemia/reperfusion (I/R) injury in conjunction with significant I/R injury response mechanisms, particularly immune cell infiltration. However, the technique requires high tissue transparency. In murine organs, this can be achieved by complex, often toxic chemical pretreatments, collectively termed clearing^{12,13}.

We have recently introduced a non-toxic clearing method using ethyl cinnamate (ECi) as the refractive index-matching component⁹. While ECi performed well for murine organs, such as kidney and bone, it suffered, like other approaches, from extremely high tissue autofluorescence of the heart muscle. Until now, this made quantitative LSFM of whole hearts challenging.

Hence, we wished to (i) develop a readily applicable, non-toxic workflow with chemicals and tools that are commercially available, (ii) benchmark this work flow against standard I/R histology techniques in compliance with recent guideline recommendations¹⁴, (iii) quantify I/R injury parameters in 3D, (iv) assess the long-term impact of I/R injury following days after reperfusion and (v) relate the I/R injury zones to immune response mechanisms.

Here we introduce an ECi-based 3D myocardial I/R injury assessment workflow, termed BALANCE (Bleaching-Augmented soLvent-bAsed Non-toxic CLEaring), to overcome the limitations of the current analysis tools.

4.2.3 Results

BALANCE enables 3D whole heart imaging and analysis

Central to BALANCE is a peroxide-based bleaching step compatible with antibody-mediated fluorescence labeling *in vivo*. Bleaching was key to unlock lower wavelength channels for homogenous imaging (Fig. 1 and Supplementary Figure 1a and d). We tested other established protocols¹⁵ for tissue autofluorescence reduction and found BALANCE to be the most suitable for homogenizing tissue autofluorescence fast and throughout the whole heart using our I/R injury protocol workflow (Supplementary

Figure 1, Supplementary Table 1 and Supplementary Note 1). Applying BALANCE to our samples, tissue autofluorescence itself could be used to visualize the overall heart muscle structure allowing clear detection of cardiomyocytes and their nuclei (Fig. 2a, b) at much higher optical resolution than previously possible^{16,17}.

CD31, a surface molecule on endothelial cells, is a potential marker for vascular integrity¹⁸. Intravital staining with fluorescent anti-CD31 antibodies⁹ revealed homogenously labeled vasculature- and heart-structures as shown before^{19,20} (Fig. 2a). BALANCE now allowed to combine autofluorescence and CD31 signals to precisely reconstruct prominent but delicate structures such as the aortic valve (Fig. 2c and Supplementary Movie 1). Additionally, we could demonstrate the applicability of our clearing protocol to other murine tissues (e.g. liver, Fig. 2d)^{9,21,22} and the human heart (left atrial appendage biopsy, Fig. 2e). Note that BALANCE was designed to maximize the signal quality of intravenous (i.v.)-mediated staining using synthetic fluorophores, allowing cell identification with high precision against a highly autofluorescent background. However, homogenizing tissue autofluorescence with peroxide may quench endogenously expressed fluorophores (Supplementary Figure 2, Supplementary Note 2).

Generating infarct and area at risk volumes for I/R analysis

Next, we identified the 3D-extent of I/R injury in a model of left coronary artery (LCA) I/R. This induced an area of terminated blood supply, which could be restored upon reperfusion (area at risk [AAR])²³. To precisely define and quantify the AAR, we injected a fluorescein isothiocyanate (FITC)-conjugated albumin solution into the aorta following re-occlusion of the LCA in the excised heart. This led to a clearly detectable AAR as FITC negative (FITC^{neg}), hence non-perfused zone (Fig. 3a, b). I/R generated an AAR that comprised around 29% (21-35, median and interquartile range, n=6) of the whole heart (Fig. 3b, Supplementary Movie 2, Supplementary Figure 5e).

The onset of I/R injury causes not only a deterioration of cardiomyocytes but also neighboring endothelial cells¹⁸. Therefore, this I/R injury could be identified by complete loss of CD31 signals, termed CD31^{neg}, in LSM images (Fig. 3c). 3D tracing of CD31^{neg} areas allowed to generate volumetric and quantifiable 3D infarct-bodies (Figure 3 c, Supplementary Movie 3). These were clearly distinguishable from autofluorescent artifacts showing reduced CD31 signal (CD31^{dim}) which were seen in all hearts (Supplementary Figure 3). Figure 3b, c shows a CD31^{neg} to AAR injury of

10%, but the spectrum of small to larger infarction of this model can be visualized as outlined below. Furthermore, 3D vessel tracing allowed to reconstruct the relation between vessels affected by I/R, the ensuing AAR and the respective size and localization of infarct-bodies (Fig. 3d). This analysis also demonstrated that vessels occluded during I/R matched the AAR defined by FITC-absence (Supplementary Movie 4).

Benchmarking of CD31-based I/R injury analysis

Histological 2D approaches using triphenyl tetrazolium chloride (TTC) have been the mainstay for quantifying the degree of I/R injury²⁴. Cardiomyocytes with intact mitochondria convert TTC to a red dye, while I/R-affected cells remain unstained (TTC^{neg}). By classical TTC staining of sequential 2-mm slices, we assessed the I/R injury. When we analyzed the same slices by LSM, we indeed observed CD31^{neg} regions that overlapped with TTC^{neg} areas (Fig. 4 and Supplementary Figure 4). While larger vessels appeared to retain CD31 inside the infarcted area, smaller capillaries had completely lost their CD31 signal. The 3D analysis also demonstrated that TTC overshadowed the fine structural details of I/R damage. In contrast, LSM of CD31 faithfully reconstructed the complex 3D structure of the I/R injury-site after 24 h without destroying the tissue (Supplementary Figure 4). We correlated CD31^{neg} volumes to standard markers of myocardial damage, such as TTC staining, ejection fraction (EF) reduction and cardiac troponin I (cTNI) release, as recommended tools in experimental studies¹⁴. We found a highly linear relationship between TTC^{neg} areas, CD31^{neg} volumes (both normalized to single slices as well as total hearts) and EF reduction (Fig. 4a, e). Regions of abnormal left ventricular wall movement were located mostly in mid anterior, mid lateral and mid inferolateral zones, where TTC^{neg} and CD31^{neg} co-localized (Fig. 4c, d). Plasma cTNI levels indicated establishment of infarction, but linearity was not statistically significant for the assessed infarction sizes (Fig. 4f). Of note, infarct size determination by troponin assessment has been rather difficult in both, clinical and experimental environments^{14,25}. Finally, a comparison of 3 operators regarding CD31^{neg} volume quantification yielded <15% difference of average values (Fig. 4b). Interestingly, we observed a wide spread of infarct-body sizes relative to the AAR (Supplementary Figure 5). Notably, several zones low on TTC (TTC^{low}), which might be considered I/R injury, were not co-localized with CD31 negativity (Fig. 4 and Supplementary Figures 4 and 5).

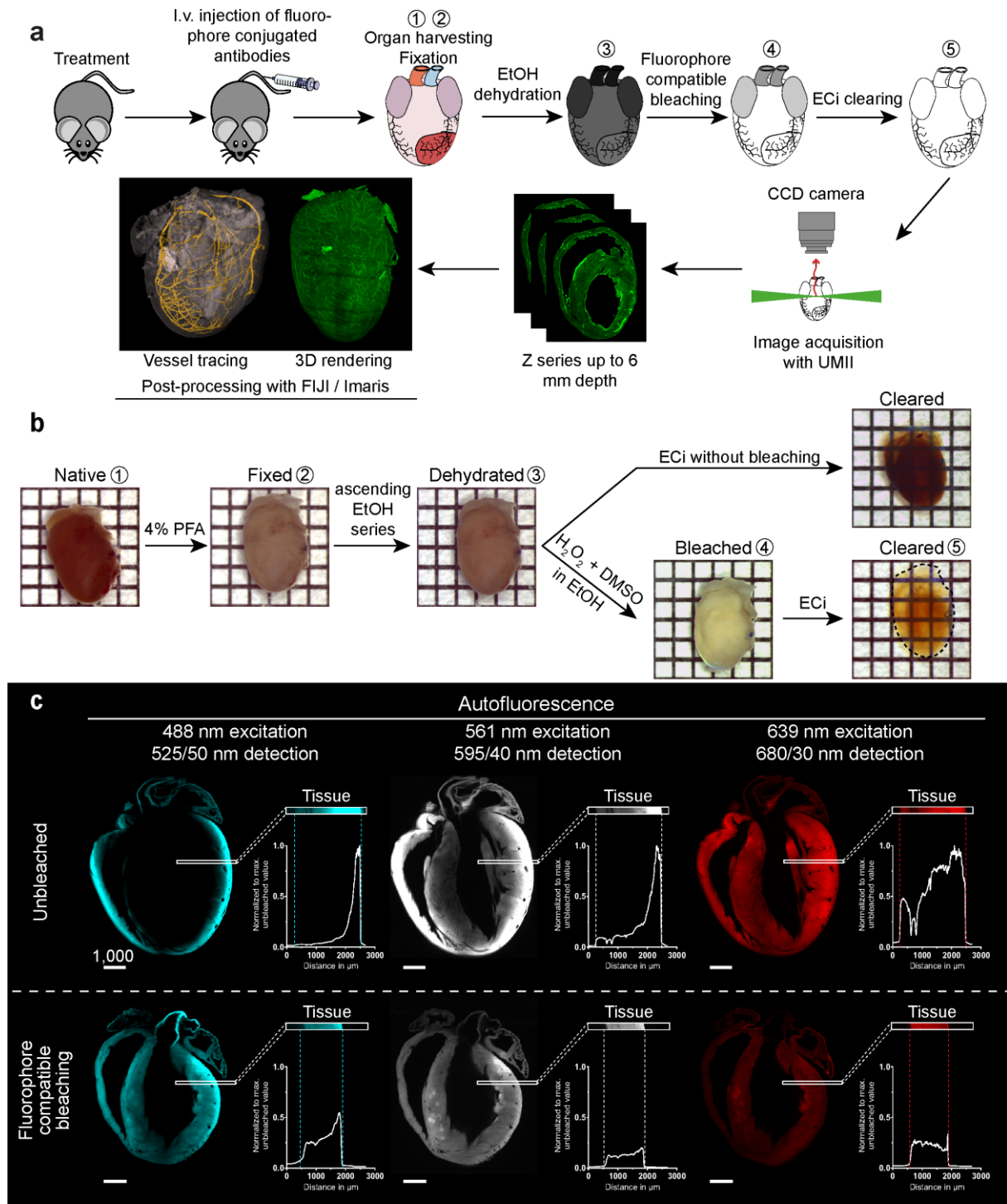


Figure 4-6: Fig.1 Fluorophore compatible bleaching enables homogenous light-sheet fluorescence microscopy (LSFM) in whole murine hearts. (a) Graphical abstract of light-sheet guided heart analysis procedure. (b) Macroscopic images of murine hearts during protocol steps. In comparison to the non-bleached sample, fluorophore compatible bleaching enhances the clarity of the sample. One square equals 2x2 mm. (c) Signal distribution of ethyl cinnamate (ECi)-cleared, unbleached or bleached hearts in LSM in different channels, single wavelength excitation and filtered detection range given in wavelength/range, detecting autofluorescence. The region of interest (ROI) in the left ventricular wall (LVW) shows high autofluorescence at the edge of unbleached hearts. This peak is lowered, together with an overall lower autofluorescence intensity in bleached hearts. The homogenization of autofluorescence is most prominent in the short wavelength channels, unlocking those for quantitative imaging and general thresholding. Scale bar values in μm . Source data are provided as a Source Data file.

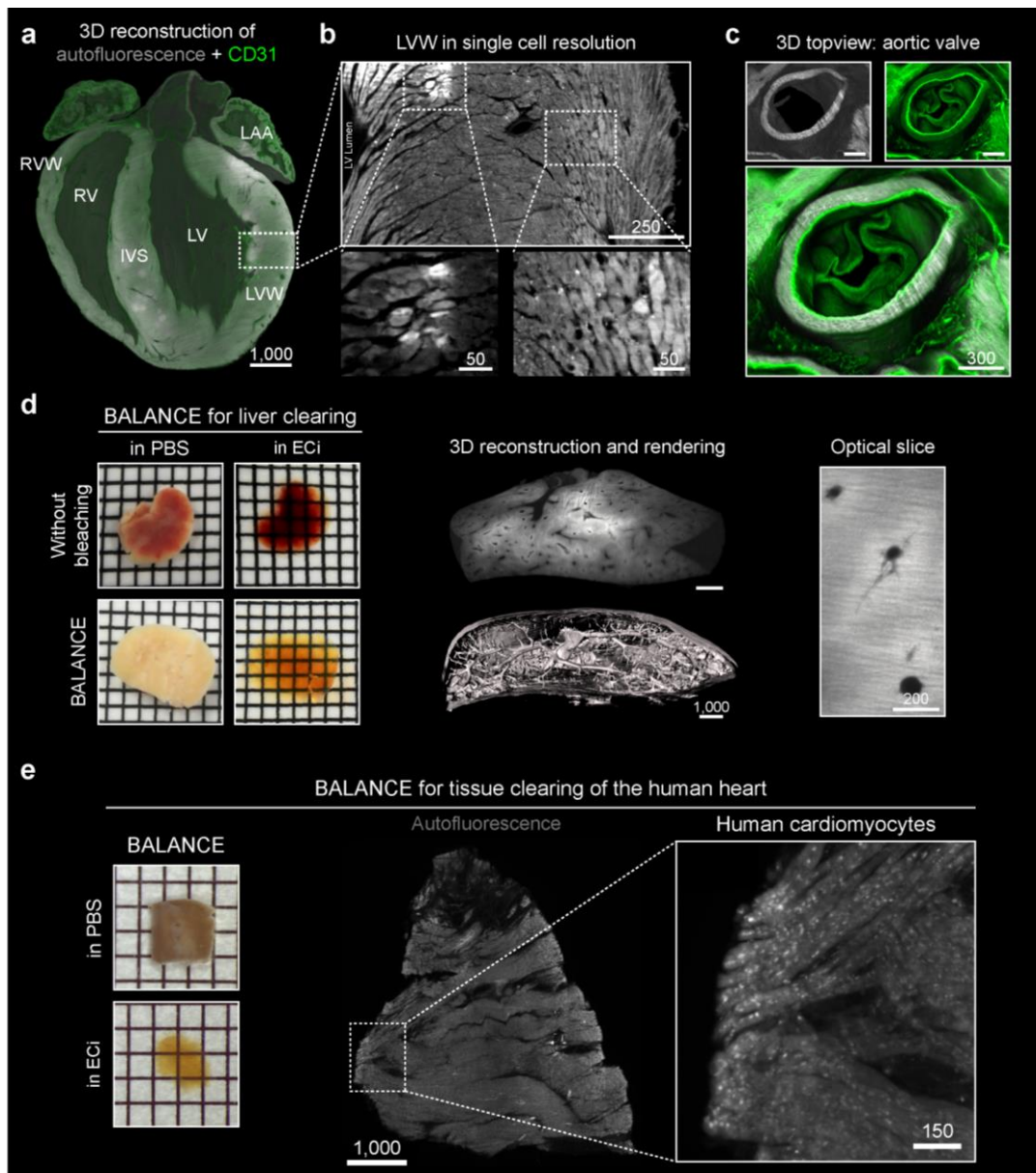


Figure 4-7: Fig. 2 High resolution light-sheet fluorescence microscopy (LSFM) of murine and human tissue. (a) 3D reconstruction of the inferior (dorsal) half of an ECI-cleared murine heart depicting both CD31 (blood vessels; green) and autofluorescence (total heart tissue; grey) showing distinct heart structures such as right ventricular wall (RVW), right ventricle (RV), intraventricular septum (IVS), left ventricle (LV), left ventricular wall (LVW) and left atrial appendage (LAA). (b) Single optical slice obtained by LSFM showing a cross-section of the LVW (enlarged ROI highlighted in (a)) with cellular detail using autofluorescence (grey) only. Enlargements show that high autofluorescence in restricted regions is of cellular origin (ROI left, different contrast settings) and that the directionality of visualized cardiac cells depends on their respective localization within the muscle (ROI right). Magnification: 8x. (c) 3D reconstruction of the aortic valve in a top-view visualized by autofluorescence (grey) and CD31 (green). Magnification: 4x. (d) BALANCE applied to murine liver enhances sample transparency (left) and enables imaging of large tissue samples for quantitative purposes (mid and right). High contrast between vessel lumen and surrounding tissue allows direct rendering of the portal vein system from autofluorescence raw data (mid). (e) Left: BALANCE also enables clearing of a human left atrial appendage (LAA) biopsy and enhances sample transparency. Mid: The autofluorescence signal alone gives a structural overview and single cellular resolution (right). Scale bar values in μm . One square on the macroscopic images equals $2 \times 2 \text{ mm}$. (ECi - ethyl cinnamate)

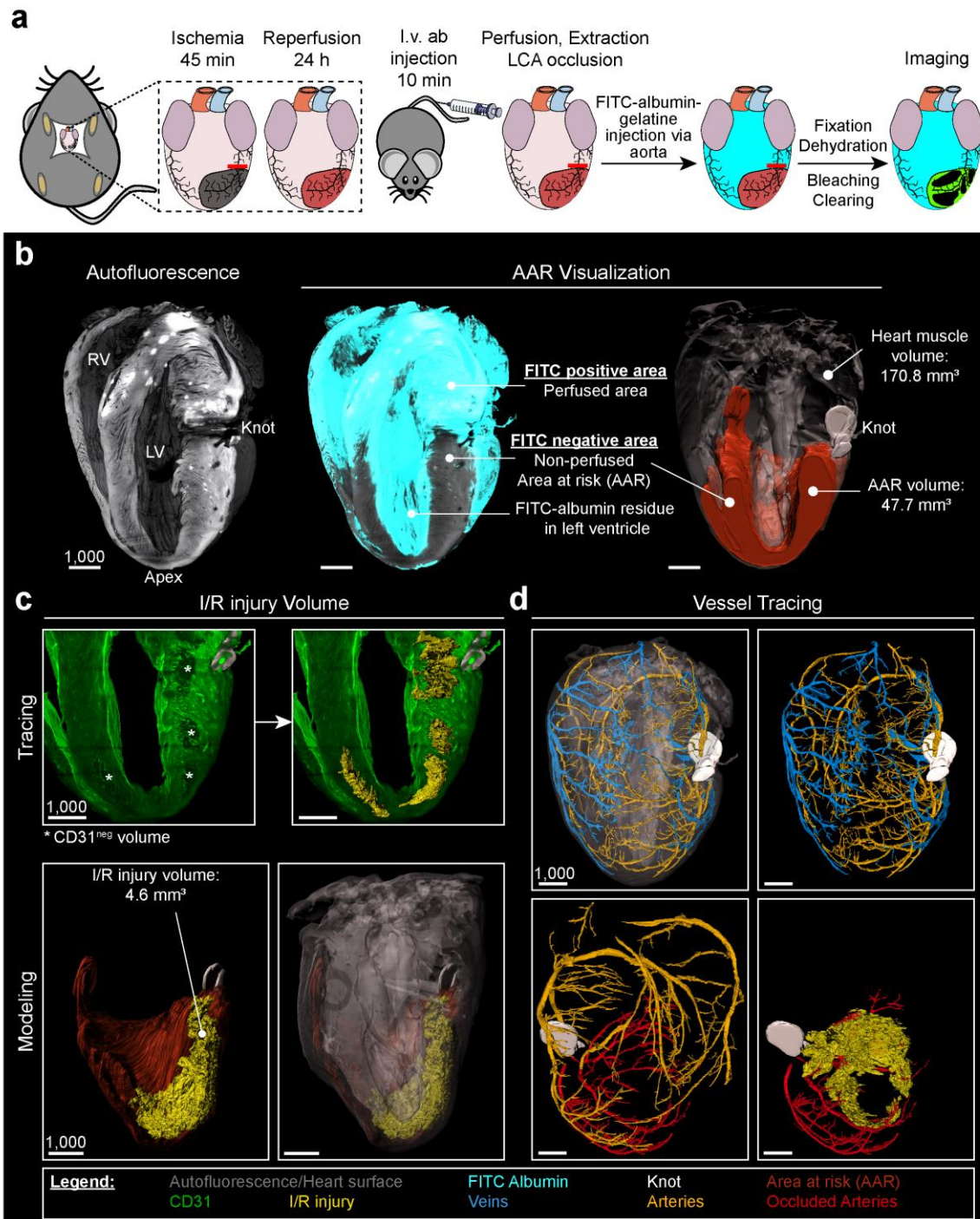


Figure 4-8: Fig. 3 3D quantification and characterization of ischemia/reperfusion (I/R) injury size using light sheet fluorescence microscopy (LSFM). (a) Workflow for LSFM-guided 3D analysis of I/R injury. (b) Quantification in 3D; Left: heart model based on autofluorescence (grey) for orientation. Middle: an overlay with the fluorescein isothiocyanate (FITC)-albumin filling (turquoise), all perfused areas are FITC positive (FITC^{pos}), whereas non-perfused areas show no FITC signal (FITC^{neg}) and autofluorescence only. Right: traced FITC^{neg} area, building up a volume model for the area at risk (AAR, orange). The traced shape of the knot (white) together with the heart surface (translucent grey) give detailed spatial information and enable volume measurements. (c) I/R injury quantification; Top: based on slice by slice tracing of areas negative for CD31 (CD31^{neg}) (white stars, left) a volume model of I/R injury (right) is reconstructed (bright yellow). Bottom: combined 3D models of I/R injury (yellow), AAR (orange), knot (white; left) and heart surface (right). (d) In vivo CD31 labeling and spatial information allow tracing of major arteries (dark yellow) and veins (blue). Together with the visualization of the knot, occlusion of the left coronary artery (LCA) can be confirmed and occluded arteries can be identified (red). Scale bar values in μm .

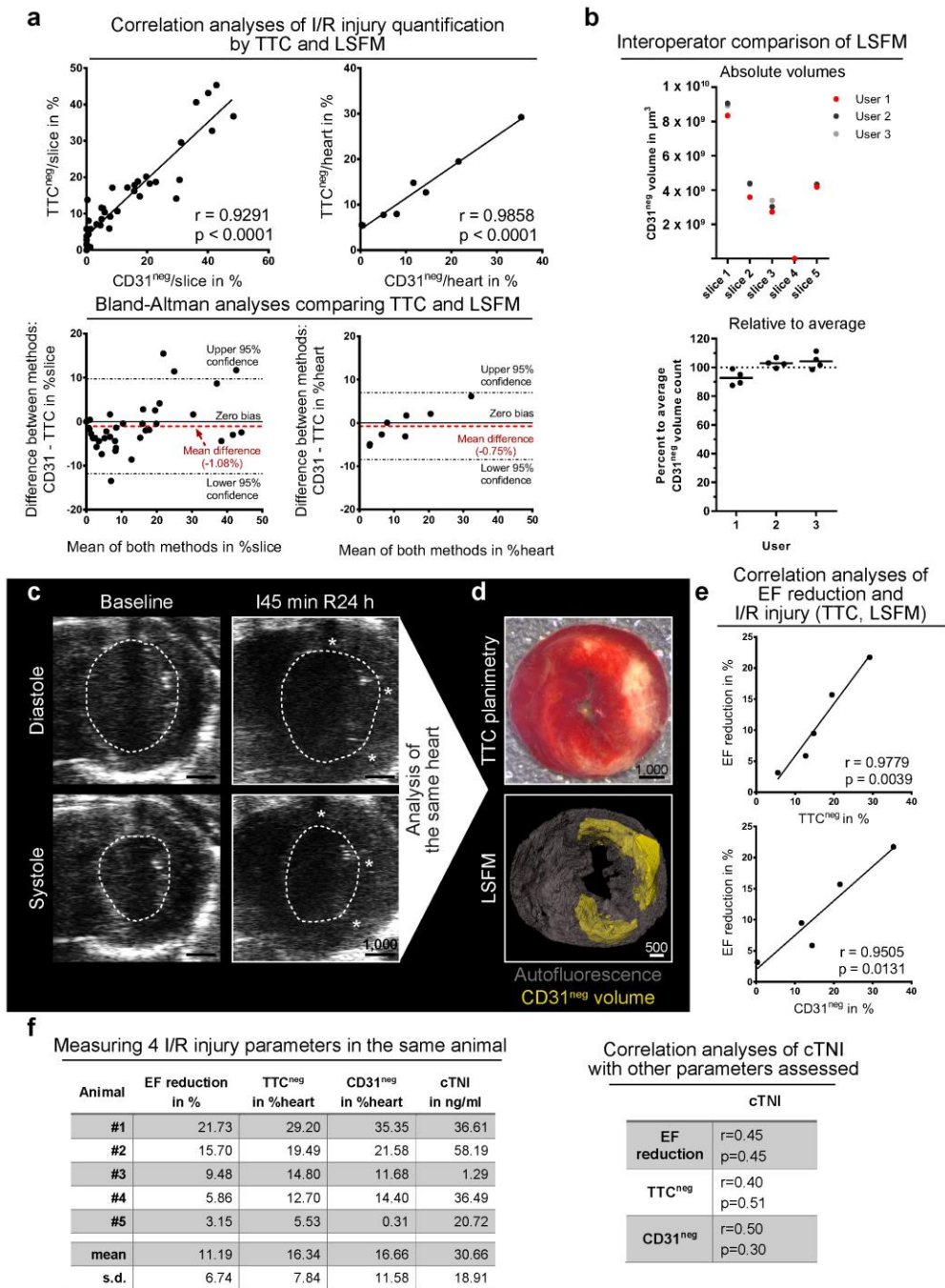


Figure 4-9: Fig. 4 Correlation of echocardiography, cardiac troponin I (cTNI) plasma levels, triphenyl tetrazolium chloride negative (TTC^{neg}) areas and CD31 negative (CD31^{neg}) volumes after 24 h of reperfusion in the same 5 mice. (a) Top panel: Correlation of CD31^{neg} volumes and TTC^{neg} areas per slice (left) and heart (right) of various infarct sizes (left: n=40 slices from 8 hearts; right: n=8 hearts; r- and p-values depicted). Bottom panel: Associated Bland-Altman analyses of CD31^{neg} volumes and TTC^{neg} areas per slice (left, -1.08% mean difference) and per heart (right, -0.75% mean difference) of correlations depicted above (dashed black lines mark 95% confidence intervals, solid black line marks zero bias, red dashed line marks mean difference). (b) Inter-operator CD31^{neg} volume quantification variances. (Top) Absolute quantified volume of 3 users in 5 randomly selected slices of different hearts subject to 45 min of ischemia and 24 h of reperfusion. (Bottom) The quantification results per user relative to the average (100%, dashed line) quantified volume (in comparison to left, slice #4 was excluded as no CD31^{neg} volume was measurable). (c) Original micrographs of echocardiographic imaging. Dashed lines indicate left ventricular lumen. White stars indicate zones of abnormal left ventricular wall movement. (d) Same I/R injury heart as in (c): exemplary TTC staining and subsequent light sheet fluorescence microscopy (LSFM)-based 3D reconstruction of the same slice. (e) Correlation of ejection fraction (EF) reduction with TTC^{neg} areas and CD31^{neg} volumes, respectively, per heart (n=5 hearts; r- and p-values depicted). (f) Left: raw data used for correlation of EF reduction, TTC^{neg} and CD31^{neg} with plasma cTNI levels (value for each animal given, n=5). Right: correlation of

3D vascular ultrastructure during I/R injury recovery

The CD31 label allowed to reconstruct the 3D appearance of the cardiac vasculature in detail. We observed a highly organized capillary network (Fig. 5a). 2D quantification of vessel densities revealed no significantly different values within the heart muscle, but high variances concerning the field of view in the same heart region (Supplementary Figure 6a). We observed a variability in directionality of vessels, which seemed to be linked to localization within the muscle (Supplementary Figure 6b). In addition, 3D analysis of the left ventricular wall displayed continuous tracts of capillaries surfacing multiple times in one image, which might explain counting errors in 2D immuno-histology (Supplementary Figure 6c). We next employed a filament tracing pipeline¹⁸ to quantify length and complexity of the vasculature in 3D. In the left ventricular wall we found a vessel length density (VLD) of 2,946 mm per mm³ and an interbranch distance (IBD) of 67 μm (median; n=3) reflecting a >2x higher VLD compared to brain (Fig. 5d, e and Supplementary Figure 6d)¹⁸. Hence, the blood vessel architecture is a characteristic hallmark of intact cardiac tissue.

Following I/R injury, the heart muscle undergoes a complex and dynamic healing process²⁶. To investigate whether such structural alterations were detectable by changes in the expression pattern of CD31, we investigated hearts 24 hours and 5 days following I/R by LSM (Fig. 5b, c). At day 5 post-I/R, we only found small CD31^{neg} areas throughout the damaged heart when compared with cardiac samples after 24 hours. With special regard to injured regions, we observed shorter, less oriented and more branched vessels within the damaged area at day 5 post-I/R. We termed this zone curly (CD31^{curly}) to describe its distinctive morphological features. Compared to healthy myocardium, filament tracing in curly areas revealed a trend for lower VLD (1,771 mm/mm³, median, n=3) and smaller IBD (51 μm , n=3, median) values, which principally confirms the initial observation of a shorter and more complex vascular network at sites of injury (Fig. 5d, e).

To better localize the I/R injury-zones, CD31^{neg} areas were overlaid to a well-known 17-segment heart muscle scheme²⁷ (Fig. 6a and Supplementary Figure 7). Apical and lateral heart segments were primarily affected (Fig. 6b). After 5d of reperfusion, the detectable I/R injury was largely resolved, with only residual peri-apical CD31^{neg} segments remaining. The analysis also suggested that CD31^{curly} zones on day 5 co-localized with previous CD31^{neg} I/R regions. Hence, curly zones might serve as a proxy

to delineate previous areas of I/R injury, even days after their revascularization (Fig. 5b, c and 6b).

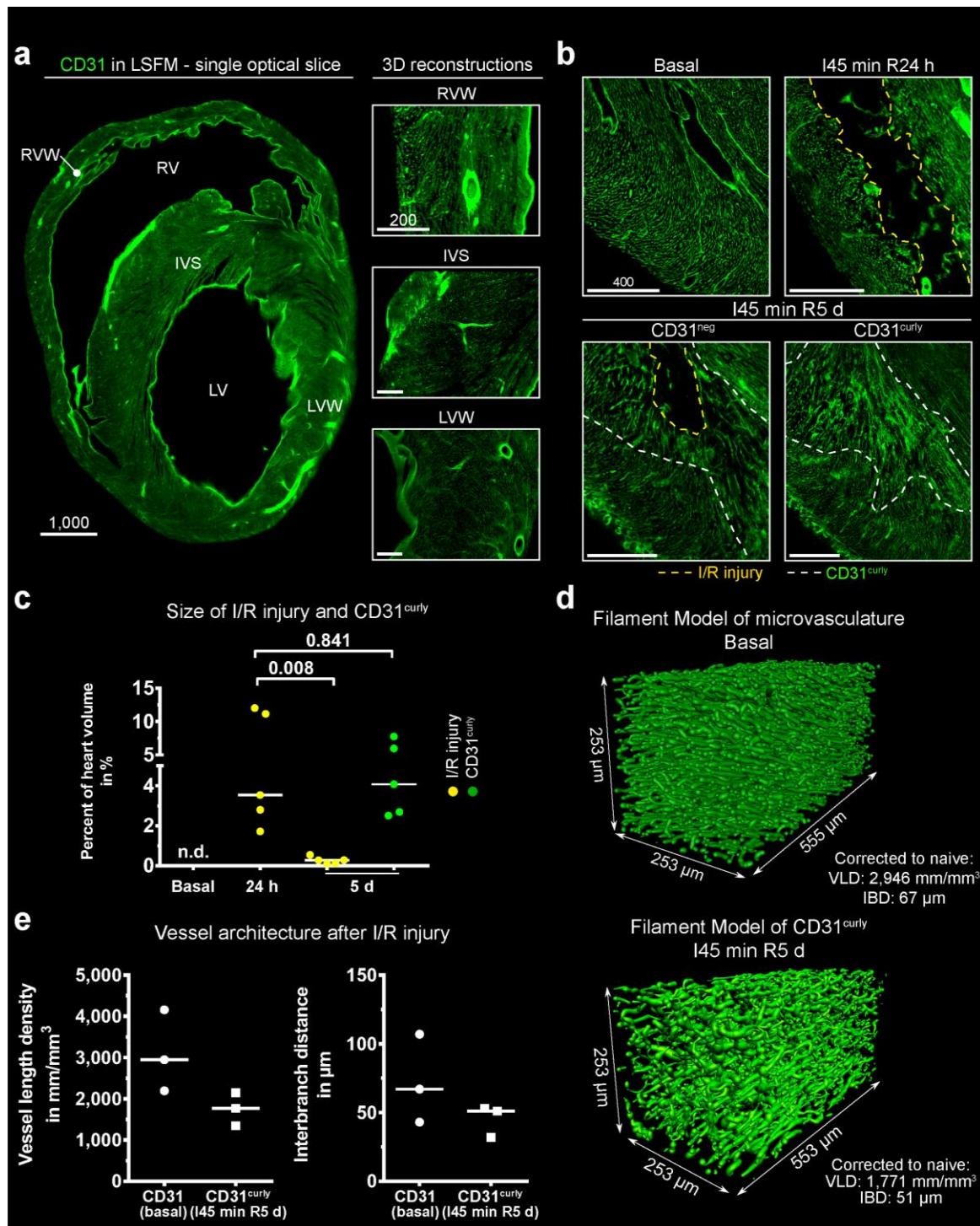


Figure 4-10: Fig. 5 4D analysis of vascular meshwork in basal and infarcted hearts (a) Left: single optical slice through a cleared murine heart depicting CD31 (green). Right: 3D reconstructions of enlargements, visualizing the microvasculature and its respective directionality. Magnification: 10x. (b) Maximum intensity projections (MIPs) comparing CD31 staining in basal, 24 h and 5 d murine hearts. I/R injury is highlighted with yellow dashed line, CD31 curly (CD31^{curly}) region with white dashed lines. Magnification: 6.4 x (basal), 3.2x (24 h), 4x (5 d). (c) Quantification of I/R injury and CD31^{curly} volume normalized to heart muscle volume (including appendages and right ventricle (RV)) over time (n=5 hearts; median; two-sided Mann-Whitney test, p-value depicted). (d) Filament model of CD31 baseline expression (top) and CD31^{curly} region (bottom). Magnification: 6.4x. (e) Vessel length density (VLD, left) and interbranch distance (IBD, right) in baseline and CD31^{curly} regions (ROIs from 3 hearts; median). Scale bar values in μ m. Source data are provided as a Source Data file.

3D mapping of immune cells to zones of infarction

To investigate the impact of cardiac tissue injury on inflammatory response mechanisms, we next assessed immune cell infiltration of I/R-affected zones. To this end we localized and quantified neutrophils and macrophages in the infarcted heart after 24 hours and 5 days of reperfusion. In line with previous studies and flow cytometric analyses of injured hearts, we found that Ly-6G positive (Ly-6G^{pos}) neutrophils were most prominent after 24 hours (Fig. 7a-c and Supplementary Movies 5-8). Intriguingly, the localization of neutrophils matched with CD31^{neg} areas, but did partly not overlap with TTC^{neg} zones (Supplementary Figure 8). Neutrophil numbers strongly decreased after 5 days, whereas F4/80 positive (F4/80^{pos}) macrophages increased. At 24 hours we found neutrophils to be highly enriched within the AAR and at the rim of infarct bodies (Supplementary Movie 5) indicating neutrophil presence at the border of infarction rather than within the damaged tissue itself (Fig. 7d and Supplementary Movies 7 and 8). Interestingly, at d5, the majority of neutrophils was no longer associated with the border of the residual infarct-body but localized in the CD31^{curly} volume (Fig. 7d, n=5, and Supplementary Movie 6). At this time, we could also detect F4/80^{pos} macrophages throughout this area (Fig. 7e, n=5). Such a timing of arrival might reflect the ongoing tissue repair mediated by macrophages²⁶.

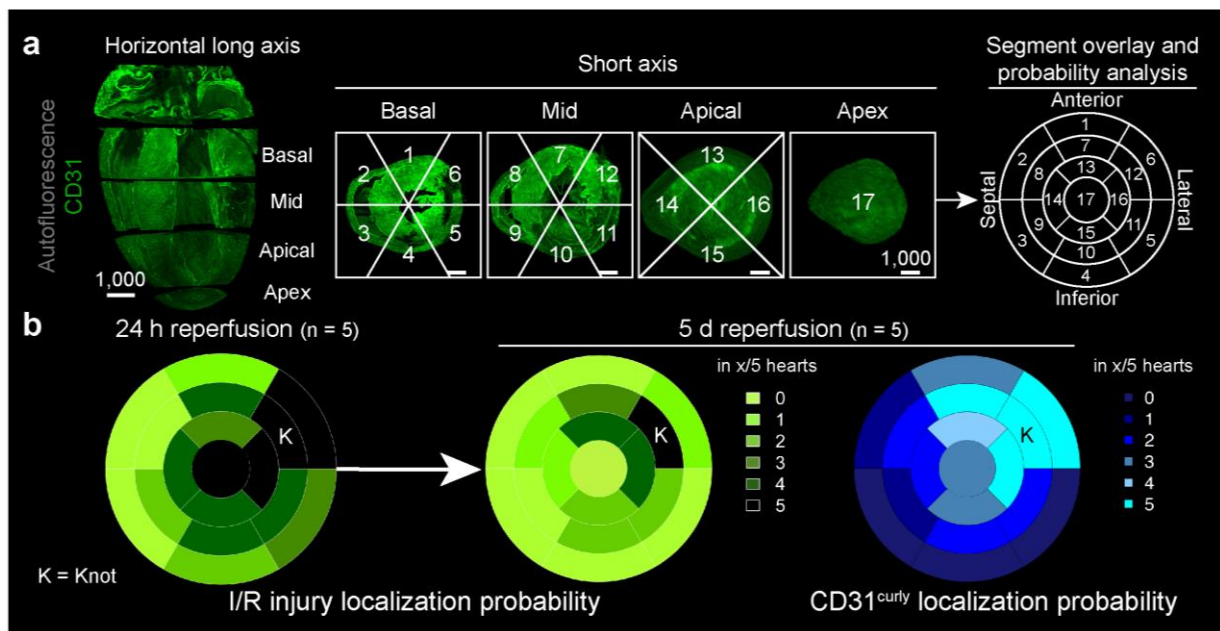


Figure 4-11: Fig. 6 Quantifying I/R injury, AAR and CD31^{curly} localization in mice with the left ventricular 17 segment model. (a) Left: 3D model of inferior heart half, cut along the horizontal long axis, based on CD31 labelling (green). Four slices are defined: Apex (1), not containing left ventricle (LV) lumen, Apical, Mid and Basal, which are equally spaced with LV lumen. Middle: These slices, viewed from the apex perspective, can be further segmented. The segments do not include the right ventricle. Right: Overlay of the segments viewed from the apex gives a backbone for probability heat-maps. (b) The localization probability of I/R injury after 24 h (left) and 5 d (middle) together with CD31^{curly} (right) given in the total amount of hearts affected, represented in heat-maps. K = position of knot in mid anterolateral (segment 12). Scale bar values in μm. Source data are provided as a Source Data file.

4.2.4 Discussion

We developed BALANCE for the fast 3D characterization of damage- and response-mechanisms in whole heart specimens. The ability to reconstruct the 3D shape of affected zones might require to re-define the current 2D-concept of myocardial infarction parameters into Volumes At Risk (VAR)/infarct-bodies to give credit to their real 3D nature.

The established protocol combines the use of non-toxic reagents, short handling and protocol times, less complexity and superior signal homogenization, required for myocardial I/R analysis and not available from other published clearing methods (Supplementary Table 2). In contrast to iDISCO clearing, ethanol was used for sample dehydration to avoid high methanol toxicity and reduce possible incompatibilities with following histological antibody stainings¹⁰. Also, long clearing times, e.g. in CUBIC²⁸ or passive CLARITY²⁹, were circumvented by the use of non-toxic ECI. BALANCE uses a minimum of hands-on time and procedure steps to circumvent initial adaption difficulties as compared to SWITCH³⁰. Most importantly, it homogenizes tissue autofluorescence throughout highly autofluorescent organs such as the heart, which is not the case in the original ECI protocol⁹ (Supplementary Table 1 and 2). With the advent of robotics and artificial intelligence (AI) to automate clearing procedures and data analyses⁹, the usability and reliability of clearing methods and staining results will be further improved.

Regarding time and expense of experiments, we compared the conventionally applied methods in the field of I/R injury in the murine heart with our current LSFM-based approach (Supplementary Table 3). The hands-on time of our proposed LSFM procedure is comparable to each of the classical methods¹⁴. However, none of the currently available approaches, including TTC staining, histology, immuno-histology and flow cytometry provides LSFM-comparable data. LSFM combines spatially resolved I/R injury parameter assessment with cellular quantification and 3D localization in the same heart. Furthermore, LSFM-based analysis offers, inherent from its 3D nature, the possibility to reconstruct the fine ultrastructure of the inspected feature such as the blood capillary network. We therefore believe that with our proposed method, the robustness over experiments can be increased. At the same time, combined experimental times needed to carry out all other individual methods in different animals can be significantly reduced by our multiplexing approach. In the near future, computer-based algorithms will further reduce analysis time.

Since our technique can be translated to any I/R injury model, this work opens multiple possibilities for identifying new therapeutic targets. Of note, clinical data on cardioprotection have been largely disappointing³¹ and morbidity and mortality for patients with an acute myocardial infarction remain considerably high³². Novel approaches are therefore desired to improve the outcome of patients. The underlying pathomechanisms in I/R injury are very complex and include e.g. the interaction of heart cells (cardiomyocytes, endothelium, fibroblasts) with platelets and immune cells finally producing heart cell death. It has recently been concluded that an ideal drug/approach for cardioprotection would target the cardiac vasculature, immune cells and cardiomyocytes^{14,31}. Several promising strategies have been forwarded recently including beta-blocking metoprolol³³⁻³⁵ and immune modulatory drugs^{36,37}. A common feature of these approaches is that they target not a single but multiple pathways involved in I/R injury. Metoprolol, e.g., interacts with beta-receptors on cardiomyocytes to reduce myocardial energy consumption while also inhibiting neutrophil-platelet interaction involved in microvascular obstruction³³⁻³⁵. With our proposed workflow, we provide a tool for the analysis of conventional I/R injury in conjunction with the characterization of the vascular injury several days after the initial I/R event. Another problem of previously forwarded potentially cardioprotective therapies appears to be the lack of rigor in experimental studies¹⁴. To establish rigor in our model, we performed benchmarking. Hence we have conducted correlation analyses of our proposed analysis tool for the CD31^{neg} I/R injury against recently recommended standard approaches for experimental animal studies¹⁴ and show a very good correlation (Fig. 4)^{7,8,14,23,38}. Of note, instead of using CD31 antibody labelling to stain the vasculature, a lectin-based approach would obtain comparable results, depending on the investigator's choice³⁹⁻⁴¹.

Remarkably, the vasculature has been largely affected as shown by our study and the vascular injury correlates with tissue damage as assessed by classical methods. It is therefore tempting to speculate that the vasculature could become a primary target for future cardioprotective strategies. Hence, we believe that BALANCE/LSFM might also help to identify additional potential novel therapeutic options for the treatment of I/R injury in the future.

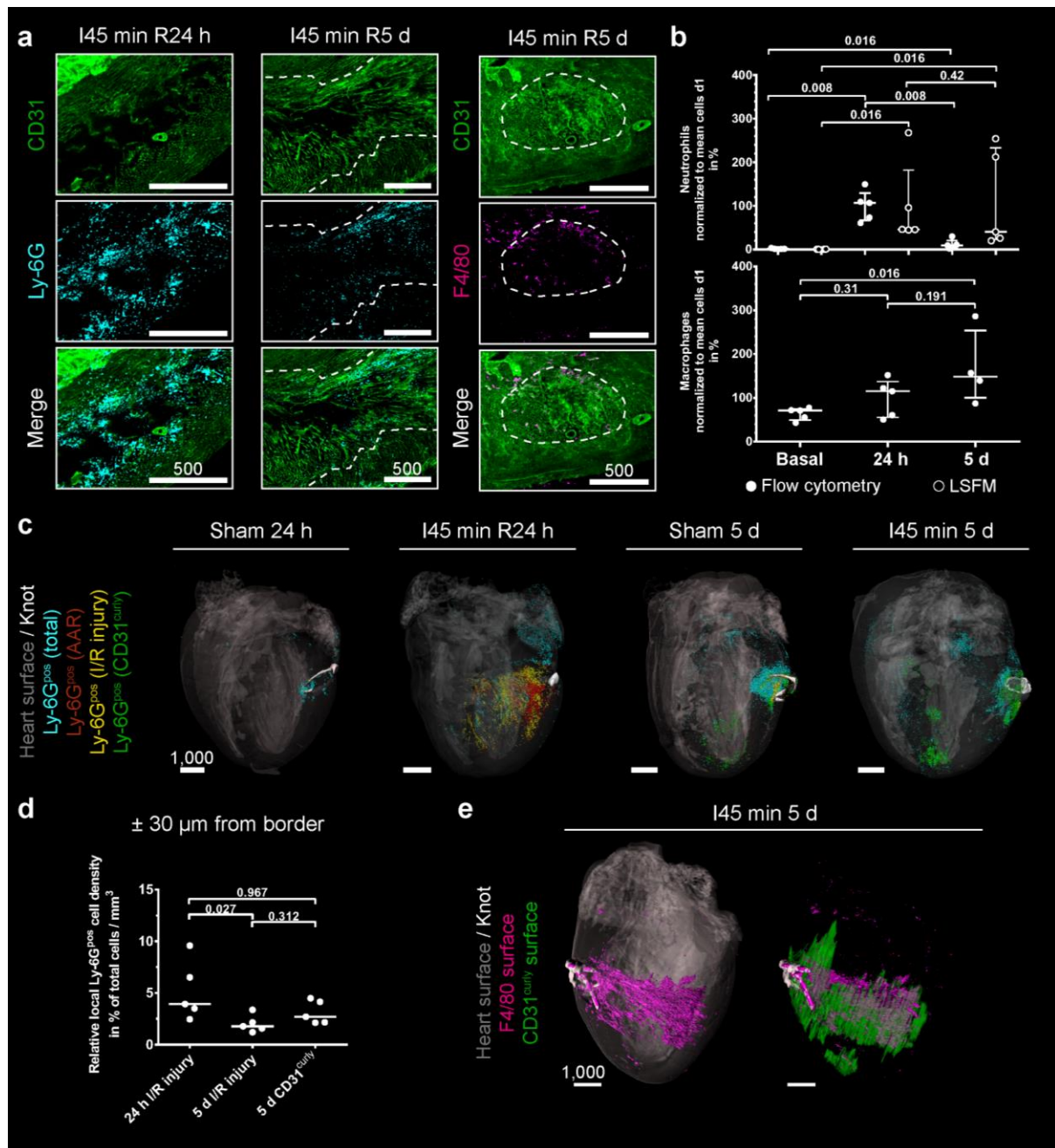


Figure 4-12: Fig. 7 Characterization of immune cell infiltrates into I/R injury. (a) Example maximum intensity projections (MIPs) of Ly-6G positive (Ly-6G^{pos}) neutrophils after 24 h (left) as well as Ly-6G^{pos} neutrophils and F4/80 positive (F4/80^{pos}) macrophages after 5 d (middle; right). Depicted are CD31 (green, top row) and Ly-6G (turquoise) or F4/80 (purple) signals (middle row) together with a merge (bottom). Dashed white line marks the border of the CD31^{curly} region. Magnification: 3.2x (24 h), 4x (5 d). (b) Immune cell quantities (top neutrophils, bottom macrophages) determined by flow cytometry (white, filled dots) or based on LSM analysis after 24 h and 5 d of reperfusion, as well as under baseline condition (n=4-5; median ± interquartile range; Kruskal-Wallis test with Dunn's correction). (c) Representative 3D visualization of Ly-6G^{pos} cell distribution across whole murine hearts. Heart structure (grey,) and knot (white) are shown for orientation. Ly-6G^{pos} cell populations are colored in respect to their localization in either AAR (red), I/R injury (yellow), CD31^{curly} (green) or outside the above-mentioned structures (turquoise). (d) Relative cell density ± 30 µm from the respective volume border (n=5; median; Kruskal-Wallis test with Dunn's correction). (e) 3D visualization of F4/80^{pos} signals depicted as a surface rendering (purple) in relation to heart surface (left; heart volume in grey) or CD31^{curly} surface (right; CD31^{curly} in green) after 5 d of reperfusion. The knot (white) is visualized for orientation. Scale bar values in µm. This finding was verified in 5 mice. Source data are provided as a Source Data file.

4.2.5 Methods

Animals

All experimental animal procedures were approved by the responsible governmental agency, the Ministry for Environment, Agriculture, Conservation and Consumer Protection of the State of North Rhine-Westphalia (MULNV) and complied with all relevant ethical regulations for animal testing and research. Male C57BL/6JRJ (12±3 weeks of age; Janvier) and Catchup (C57BL/6-Ly6g(tm2621(Cre-tdTomato)Arte); 12±3 weeks of age)⁴² mice were held at the local animal house on 12 h/12 h day and night cycle with water and food ad libitum.

Human studies

All human studies were approved by the local ethics committee of the Medical Faculty, University of Duisburg-Essen, Germany (Ethics Approval Nr. 18-8527-BO). The whole procedure was in accordance to the World Medical Association Declaration of Helsinki and conducted in accordance with the relevant ethical regulations. Written informed consent was obtained from all participants. The patients underwent coronary bypass surgery, during which human left atrial appendage (LAA) biopsies were routinely excised. This presented no further harm for the patient.

Ischemia/Reperfusion (I/R) heart injury

Male C57BL/6JRJ and Catchup mice (12±3 weeks of age) were subjected to a published myocardial I/R *in vivo* protocol³⁸. Briefly, mice were anesthetized by intraperitoneal (i.p.) injection of ketamine (100 mg/kg, CatNo. 9089.01.00, belapharma) and xylazin (Rompun 10 mg/kg, CatNo. 6324464.00.00, Ceva Tiergesundheit). They were orally intubated and ventilated throughout the operation procedure, with 0.8 l/min air and 0.2 l/min O₂ at a tidal volume of 250 µl/stroke and a breathing frequency of 140 strokes/min. Anesthesia was maintained during the operation by supplementing 2% isoflurane (Forene, CatNo. 2594.00.00, abbvie). The chest was opened through a left lateral thoracotomy and the left coronary artery (LCA) was ligated. After 45 min of ischemia, reperfusion was allowed for indicated time points. As previously described, different infarct sizes may be created by this method due to differences in mouse physiology^{43,44}. Mice were treated with 0.1 mg/kg buprenorphine (Temgesic, CatNo. 997.00.00, Indivior) subcutaneously every 8 h after operation for a total of 72 h. Mice received 1000 IE heparin (CatNo. 27586.00.00, LEO Pharma) i.p.

10 min before the end of the experimental protocol and were killed by cervical dislocation.

For light sheet experiments, mice received intravenous (i.v.) tail vein injections 10 min before sacrifice with 5 µg of each antibody in PBS in a total volume of 150 µl per animal of anti-mouse CD31 (clone: Mec13.3; purified: CatNo. 553369, BD; conjugated with AlexaFluor (AF) 647: CatNo. 102516 BioLegend), Ly-6G (clone: 1A8; purified: CatNo. 127602, BioLegend; conjugated with AF647: CatNo. 127610, BioLegend) and/or F4/80 antibody (clone: BM8; purified: CatNo. 123102, BioLegend; conjugated with AF594: CatNo. 123140, BioLegend). In other experiments, respective IgG control antibodies were used (rat IgG2a-AF647, CatNo. 400526, BioLegend; rat IgG2a-AF594, CatNo. 400555, BioLegend) (Supplementary Figure 9). Purified antibodies were conjugated with AF790 using an IgG coupling kit (CatNo. A20189, Thermo Fisher). After sacrifice, mice were perfused blood-free with phosphate-buffered saline (PBS), hearts were excised and subjected to following tissue processing.

To visualize the area at risk (AAR) for light sheet experiments, the heart was placed in ice-cold PBS after perfusion, the aorta was cannulated, the LCA re-occluded and 2% gelatin / 0.2% fluorescein isothiocyanate (FITC)-albumin in PBS (gelatin CatNo. G9391, Sigma Aldrich; FITC-albumin, CatNo. A9771, Sigma Aldrich) was injected via the aorta. After 10 min incubation in ice-cold PBS, hearts were subjected to tissue processing.

For hearts to be analyzed by both light sheet fluorescence microscopy (LSFM) and triphenyl tetrazolium chloride (TTC) staining, freshly excised hearts were cut transversely along the longitudinal axis in 2 mm slices and stained for 5 min at 37 °C with a 1% (w/v) TTC in 0.0774 M Na₂HPO₄ / 0.0226 M NaH₂PO₄ in ddH₂O solution (Na₂HPO₄, CatNo. 4984.2, Roth; NaH₂PO₄, CatNo. S5011, Sigma Aldrich). Subsequently, macroscopic images of the TTC-stained slices were taken with a M80 microscope with an IC80 HD camera at 1.6x – 2.5x magnifications (both Leica) before being subjected to tissue processing. Computer-assisted planimetry was performed in a double blinded fashion using ImageJ software⁴⁵.

Mouse plasma was prepared from whole blood taken from inferior vena cava shortly before heart extraction, mixed with 25 IE heparin (CatNo. 27586.00.00, LEO Pharma) and centrifuged 10 min at 3000 x g, 4 °C. Supernatant (plasma) was collected, snap-frozen in liquid N₂ and stored at -80 °C until analysis.

Quantification of I/R injury size using TTC staining

I/R injury size was quantified as described before³⁸. Briefly, after PBS perfusion and extraction, the LCA was re-occluded and 1 ml 1% Evans blue dye (CatNo E2129, Sigma Aldrich) in 0.9% NaCl was injected via the aorta to visualize the AAR. The heart is wrapped in clear food wrap and stored at -20 °C for 1 h. The heart is then cut in 2 mm slices orthogonal to the long axis and incubated in a 1% (w/v) TTC solution as described above. Areas of TTC^{neg}, AAR and non-ischemic myocardium were measured using ImageJ⁴⁵ by two blinded, independent operators. I/R injury size was expressed as percentage of AAR.

BALANCE protocol for tissue clearing

Perfused hearts were immersed in 4% paraformaldehyde (w/v, PFA, CatNo. 10195, Morphisto) in PBS for chemical fixation while standing for 4 h at 4 °C in 15 ml tubes. For all following steps, hearts were kept at 4 °C, always agitated, transferred only to pre-cooled solutions in 15 ml tubes and kept protected from light. Following fixation, hearts were dehydrated in an ascending ethanol series in ddH₂O (v/v) of 50%, 70% and 100% (CatNo. 9065.2, Roth) for at least 4 h while shaking. Samples can also be stored longer at each step without loss of staining quality.

Subsequently, samples were bleached for 4 h in freshly prepared 5% (v/v) hydrogen peroxide (CatNo. 349887; Sigma Aldrich) and 5% (v/v) dimethyl sulfoxide (CatNo. 4720.3, Roth) in 100% ethanol. Please beware of building pressure during this step. Bleaching was carried out to enhance sample clarity, enabling homogenous imaging in lower wavelength channels while preserving artificial fluorophore fluorescence (Fig. 1). After a washing step of at least 4 h in 100% ethanol, samples were warmed to room temperature (RT) for 5 min before transfer into 7 ml pure (99%) ethyl cinnamate (ECi, CatNo. 112372, Sigma Aldrich) in a glass vial for at least 4 h prior to imaging. Samples were kept at RT in the dark until and after imaging.

Additional bleaching protocols tested

Further tested bleaching protocols were performed after fixation and washing. Therefore, perfused hearts were immersed in 4% PFA in PBS for chemical fixation while standing for 4 h at 4 °C in 15 ml tubes, as mentioned above. Hearts were washed in 5 ml PBS + 0.01% sodium azide (w/v, Cat. No. K305.1, Roth) over night at room

temperature (RT), shaking. Afterwards, hearts were washed again another change of 5 ml PBS + 0.01% sodium azide for 1 h at RT, shaking.

Sudan Black bleaching was performed according to the original publication¹⁵. After fixation and washing, hearts were incubated in 0.5% (w/v) Sudan Black B (w/v, Cat. No. 199664, Sigma-Aldrich) in 70% ethanol in ddH₂O for 3 h at RT, shaking. After washing 3x in 5ml PBS + 0.01% sodium azide (w/v, Cat. No. K305.1, Roth) for 30 min at RT, shaking, hearts were dehydrated in ascending ethanol series in ddH₂O (v/v) of 50%, 70% and 100% for at least 4 h at 4 °C while shaking. Afterwards, hearts were warmed to RT for 5 min before transfer into 7 ml pure (99%) ECI in a glass vial for at least 4 h prior to imaging. Samples were kept at RT in the dark until and after imaging. Bleaching using heme elution was accomplished as published beforehand¹⁵. After fixation and washing, hearts were immersed in 50% CUBIC-1 reagent (v/v) in dH₂O for 3 h at 37 °C, shaking. CUBIC-1 reagent was prepared according to published protocols²⁸ and was comprised of 25% Urea (w/w, Cat. No. U5378, Sigma-Aldrich), 25% Quadrol (w/w, Cat. No. 122262, Sigma-Aldrich) and 15% Triton X-100 (w/w, Cat. No. X100, Sigma-Aldrich) in dH₂O. Afterwards, hearts were incubated in pure CUBIC-1 reagent over night at 37 °C, shaking and further in another change of CUBIC-1 reagent for 2 d at 37°C, shaking. Following, hearts were dehydrated in ascending ethanol series in ddH₂O (v/v) of 50%, 70% and 100% for at least 4 h at 4 °C while shaking. Afterwards, hearts were warmed to RT for 5 min before transfer into 7 ml pure (99%) ECI in a glass vial for at least 4 h prior to imaging. Samples were kept at RT in the dark until and after imaging.

CUBIC clearing protocol

CUBIC clearing protocol was performed as previously described²⁸. All following incubation steps were carried out in the dark. After perfusion, hearts were immersed in 4% PFA in PBS for chemical fixation while standing for 4 h at 4 °C in 15 ml tubes, as mentioned above. Hearts were washed in 5 ml PBS + 0.01% sodium azide (w/v, Cat. No. K305.1, Roth) over night at room temperature (RT), shaking. Afterwards, hearts were washed again another change of 5 ml PBS + 0.01% sodium azide for 1 h at RT, shaking. Afterwards, hearts were immersed in 50% CUBIC-1 reagent (v/v) in dH₂O for 3 h at 37 °C, shaking. CUBIC-1 reagent was prepared according to published protocols²⁸ and was comprised of 25% Urea (w/w, Cat. No. U5378, Sigma-Aldrich), 25% Quadrol (w/w, Cat. No. 122262, Sigma-Aldrich) and 15% Triton X-100 (w/w, Cat.

No. X100, Sigma-Aldrich) in dH₂O. Following, hearts were incubated in pure CUBIC-1 reagent over night at 37 °C, shaking and further in other changes of CUBIC-1 reagent for 2 d each for a total of 4 d at 37 °C, shaking. Hearts were then washed in three changes of PBS + 0.01% sodium azide for 2 h each at RT, shaking. Next, hearts were immersed in 50% CUBIC-2 reagent (v/v) in PBS for 6 h at 37 °C, shaking. CUBIC-2 reagent was comprised of 25% Urea (w/w), 50% Sucrose (w/w, Cat. No. S7903, Sigma-Aldrich) and 10% Triethanolamine (w/w, Cat. No. 90279, Sigma-Aldrich) in dH₂O following establish protocols²⁸. Afterwards, hearts were incubated in pure CUBIC-2 reagent over night at 37 °C, shaking and another change of CUBIC-2 reagent for 24h at 37 °C, shaking. Hearts were imaged in a 50%/50% silicon oil (Cat. No. 175633, Sigma-Aldrich) and mineral oil (Cat. No. M5904, Sigma-Aldrich) mixture.

Light sheet fluorescence microscopy and image processing

Samples were imaged using an Ultramicroscope II and ImSpector software (both LaVision BioTec). The microscope is based on a MVX10 zoom body (Olympus) with a 2x objective and equipped with a Neo sCMOS camera (Andor). For image acquisition, cleared samples were immersed in ECI in a quartz cuvette and excited with light sheets of different wavelengths (488 nm, 561 nm, 639 nm and 785 nm). Following band-pass emission filters (mean nm / spread) were used, depending on the excited fluorophores: 525/50 for FITC; 595/40 for AF594 or autofluorescence; 680/30 for AF647 and 835/70 for AF790. For quantitative imaging, whole hearts were imaged along the longitudinal axis. For image acquisition, hearts were trapped, with the apex and the aorta horizontally aligned, in a commercially available sample holder (LaVision BioTec). To avoid damage or deformation of the sample, ECI-cleared 1% phytigel/ H₂O (CatNo: P8169-100G, Sigma Aldrich) blocks were used as buffers between tissue and plastic holder. Hearts were also rotated along the longitudinal axis, so that the knot, which remains *in situ*, faced downwards. This reduced blockage of excitation or emission light to a minimum. Whole-heart data sets were obtained with 2x total magnification (pixel size of 3.25 µm / pixel x,y, lateral resolution: 6.5 µm in x and y) with 10 µm z spacing between optical planes. Since the camera's chip has 2560 x 2160 pixels, the field of view with this magnification amounts to 8.32 mm x 7.02 mm. It was thereby possible to image a whole mouse heart without multi-positioning, thus avoiding stitching algorithms while simultaneously reducing acquisition times. Sheet width was set to 4200 and numeric aperture to 0.148, resulting in an approximate light sheet thickness

of 4 μm in the horizontal focus. Illumination time was 350 ms, with enabled 8x dynamic focus in both left and right laser lines. Total acquisition time of one plane was thus, theoretically, 5.6 s. The vertical thickness of the hearts was generally smaller than 6 mm. This is the limiting factor due to the objective's working distance. Assuming a z stack as deep as 6 mm, this would have resulted in acquisition of 600 images x 4 channels = 2400 images, which would theoretically have taken 3.73 h. However, in our practical experience one murine heart takes 4 - 6 h of acquisition time. For regions of interest (ROIs), magnifications are indicated in the figure legends.

See <https://www.lavisionbiotec.com/products/UltraMicroscope/specification.html> for zoom factors, corresponding numerical apertures and resolutions. To avoid photobleaching during imaging, the longest wavelength was imaged first.

16bit OME.TIF stacks were converted (ImarisFileConverterx64, Version 9.2.0, BitPlane) into Imaris files (.ims). 3D reconstruction and subsequent analysis was done using Imaris software (BitPlane). Heart surface (25 μm grain size) and volume was determined using surface creation algorithms. All surface tracings (AAR, CD31^{neg}, CD31^{curly}, vessels) are based on the contour tracing tool and are carried out manually/semi-automatically. For surface creation, each (vessels), every 5th (CD31 tracings) or 10th (AAR) image was traced. Surfaces were created with maximum resolution (2160 x 2560 pixel) and preserved features, to ensure matching of the traced lines with the surface border. Discrimination of arteries and veins was done by their respective location within the heart muscle and the signal intensity of the CD31 staining (CD31^{high} for arteries, CD31^{low} for veins).

For 2D vessel counting, 8 slices of the right ventricular wall (RVW), the intraventricular septum (IVS) and the left ventricular wall (LVW) (n=3 mice) were analyzed. For this, capillaries in 8 fields of view of 251.49 μm x 251.49 μm size (not shrinkage corrected) were manually counted and extrapolated to capillaries per mm^2 .

Vessel quantification was performed as previously described¹⁸. Image data were first preprocessed, as a necessary step to reduce noise and improve vessel contrast, before applying a filament tracer model for vessel quantification in the 3D software package Imaris (BitPlane).

Briefly, image stacks were first preprocessed in the open source software ImageJ⁴⁵ by applying a Gaussian smoothing, where a Gaussian sigma of 2 μm was chosen to be less than half the diameter of the smallest vessels. This was followed by a rolling ball background subtraction. In order not to affect the intensity distribution within the

vessels themselves, a rolling ball radius of 20 μm was chosen, which was more than twice the diameter of the largest vessel. Any resulting edge artifacts from background variations could be removed during a later thresholding step in Imaris. The contrast of vessels was further enhanced using a python script (`vmtkimagevesselenhancement`) from the open source Vascular Modelling Toolkit project (VMTK: www.vmtk.org), which performed a multiscale Hessian-based Frangi vesselness filter⁴⁶. The feature-based enhancement filter of Frangi is now a well-established tool for vessel segmentation⁴⁷. In addition to the improved vessel contrast and non-vessel suppression, the Frangi filter also improved the continuity of the vessels by smoothing out inconsistencies in the vessel labeling along the length of the vessels. These preprocessing steps were found to be necessary for the fidelity of tracing smaller vessels when applying the filament-tracing algorithm in Imaris. In particular since, for the tracing of vessels, it was necessary to apply the ‘with loops’ filament tracing method, which uses an initial simple thresholding for segmenting the vessels. Without smoothing, background subtraction and contrast enhancement, small vessels that were less intense were either inconsistently segmented, due to variations in the background signal, not distinctly segmented when close to larger much brighter vessels, or were not segmented as an integral vessel, but were broken up due to inconsistencies in the labelling efficiency. It should also be noted that one known artifact of the Frangi filter is that it can lead to discontinuities at branching points. In particular, for branching that occurs in a direction orthogonal to the main branch. Although we observed a reduction in the vessel intensity at these points, this effect occurred at a range very close to the branch point, and for our data did not result in any discontinuities in the Imaris tracing. Furthermore, we also observed that the Frangi vessel filter can affect the relative intensities of the vessel branches. Indeed, the intensity of smaller vessels was seen to be enhanced relative to larger vessels. In the Imaris filament tracer, this could influence the evaluation of their relative diameters, due to the use of the simple intensity threshold method for segmentation. Indeed, in general, the application of a simple thresholding segmentation resulted in a relative mismatch in the filament diameters between small low intensity vessels and the larger brighter vessels, and also resulted in a mismatch for the filament path, calculated from the center lines of the segmented vessels. Therefore, following the construction of the initial filament model, this mismatch was corrected in Imaris with two further processing steps. Firstly, a ‘re-alignment’ of the filament model was performed against the channel corresponding to the Gaussian

smoothed and background subtracted vessel data. The same channel was then used to adjust the filament diameters, using an approach based on the relative contrast change across the diameter of the vessels. From the resulting filament model, parameters for the vascular length and branching points could be extracted.

For quantification of CD31 signal intensities over different specimens, single optical planes and MIPs of whole hearts were manually analyzed.

In order to determine the tissue shrinkage occurring during the BALANCE protocol we measured heart slice thickness after heart extraction (naïve, $1.9 \text{ mm} \pm 0.17$; mean \pm s.d.) and shortly before light sheet imaging (cleared, $1.555 \text{ mm} \pm 0.12$; mean \pm s.d.) in 3 mice. The slice height was reduced to $82\% \pm 2\%$ (mean \pm s.d.) of their original size. The factor used to correct all displayed volumes throughout the manuscript was therefore 1.22 (1 divided by 0.82) for every spatial dimension. Please note that displayed scale bars are not corrected, since they relate to the real size of the samples imaged within ECi.

Immune cell counts were determined using the spot detection algorithm with an assumed diameter of neutrophils of $7 \text{ } \mu\text{m}$ ($14 \text{ } \mu\text{m}$ z). After assessment of signal distributions in non-stained, basal, I45min R24h and I45min R5d hearts, a threshold was applied for all hearts (4500 - 35000 grey values, Supplementary Figure 9a and b). Localization of detected spots respective to surface borders was measured using the distance transformation extension on desired surfaces. As a result, spot intensity values are replaced by the minimum distance to the border of the transformed surface. The sum of all detected spots within $\pm 30 \text{ } \mu\text{m}$ of the surface borders of infarct bodies and CD31^{curly} regions were normalized to the respective volume and the total amount of cells present in the heart. We used a transgenic mouse line with endogenously labeled neutrophils (Catchup mice⁴²) to show that all neutrophils invading the myocardium are labeled using our i.v.-mediated staining approach (Supplementary Figure 2).

For the 17 segment model, clipping planes were introduced in the required locations of the left ventricle (see Cerqueira et al²⁷), images of 3D content per slice were taken and overlaid with a segment grid in Illustrator CC (Adobe). If a segment showed I/R injury/AAR/CD31^{curly}, it was digitally rated as positive. The sum of the counts per segment over all hearts was depicted as heat maps, generated using R software⁴⁸.

Due to the diffuse staining pattern of the F4/80 AF790 antibody, spot detection was not feasible, and we rendered the volume of the immune cell localization instead.

Enlargements and other displayed content was processed using ImageJ software⁴⁵.

Echocardiographic assessment

Mouse echocardiography was conducted using Visualsonics Vevo 2100 Imaging system. After initial anesthesia with 4% isoflurane in 1 L/min O₂, mice were placed on a heated plate and anesthesia was maintained with 1.5% isoflurane. A rectal probe was introduced and heart rate, respiratory rate and body temperature were monitored continuously. After hair removal, images of long and short parasternal axis were acquired in M-mode and B-mode. Ejection fraction was calculated using Simpson's method⁴⁹.

Cardiac troponin I ELISA

Cardiac troponin I levels were determined from heparin plasma using ultra-sensitive mouse cardiac troponin-I ELISA (CatNo CTNI-1-US, Life Diagnostics) following manufacturer's instructions. To obtain quantifiable results, samples were diluted 1:100 in diluent YD25-1, according to supplier's suggestions. Absorbance values were recorded using a FLUOStar Omega (BMG Labtech).

Flow cytometry procedure and analysis

PBS-perfused hearts of mice after 24 h and 5 d of reperfusion as well as under basal conditions, were mechanically minced and incubated in an enzyme solution comprised of 450 U/ml collagenase I (CatNo C0130, Sigma Aldrich), 125 U/ml collagenase XI (CatNo C7657, Sigma Aldrich), 60 U/ml hyaluronidase (CatNo H3506, Sigma Aldrich), 20mM HEPES (CatNo H3375, Sigma Aldrich), 60 U/ml DNase (CatNo D5319, Sigma Aldrich) in PBS for 40 min in a ThermoMixer C (Eppendorf) at 37 °C and 300 rpm. After enzymatic digestion, the solution was filtered through a 40 µm filter and flow-through was centrifuged for 5 min at 4 °C and 350 x g. Supernatant was discarded and cell pellet resuspended in 1.5 ml PBS. 100 µl of this solution per sample was used for staining, while one solution was chosen for fluorescence minus one (FMO) controls. Blocking of FC-receptors was done by adding 2 µl of TruStain fcX (CatNo 101319, BioLegend) and incubating for 20 min on ice in the dark. Samples were washed by adding 100 µl PBS, centrifuging for 5 min at 4 °C and 350 x g, discarding supernatant, and resuspending the cell pellet in 50 µl PBS. Samples were stained by adding 50 µl PBS containing antibodies CD45-AF700 (CatNo 103127, BioLegend), Ly-6G-

PerCP/Cy5.5 (CatNo 127615, BioLegend), CD11b-BV605 (CatNo 101257, BioLegend) and F4/80-BV421 (CatNo 123137, BioLegend), all at a dilution of 1:200. Incubation was done for 30 min at RT in the dark, with simultaneous dead and alive staining by addition of Zombie NIR dye (1:2000, CatNo 423105, BioLegend). After antibody incubation, samples were washed as before, supernatant was discarded and cell pellet was resuspended in 150 µl FACS-Buffer, comprised of 1% (v/v) fetal bovine serum (CatNo P30-3302, PAN Biotech) and 0.5% bovine serum albumin (CatNo 8076.3, Roth) in PBS. Data was acquired on a BD FACS Aria III (BD Biosciences) and analysis was performed using FlowJo software (Ashland, USA). Gating strategy is shown in Supplementary Figure 9c.

Statistical analysis

Statistical analysis was performed using GraphPad Prism 6.0 for Windows (GraphPad Software). Data are given as indicated in the figure legends. Student's t-test or Mann-Whitney U test were performed for comparison of two groups. Kruskal-Wallis or one-way / two-way ANOVA (with or without repeated measures) followed by Dunn's multiple comparisons test or Bonferroni's correction were performed for multiple group comparisons, as indicated. Correlation was performed using lineary regression best-fit and calculating Pearson's correlation coefficient r . Comparison of two methods was done by Bland-Altman analysis. P-values are depicted and a value of $p < 0.05$ was considered significant.

Data availability

The datasets generated during and/or analyzed during the current study are available from the corresponding authors upon request.

4.2.6 References

- 1 Yellon, D. M. & Hausenloy, D. J. Myocardial reperfusion injury. *N Engl J Med* 357, 1121-1135, doi:10.1056/NEJMr071667 (2007).
- 2 Robbers, L. F. et al. Magnetic resonance imaging-defined areas of microvascular obstruction after acute myocardial infarction represent microvascular destruction and haemorrhage. *Eur Heart J* 34, 2346-2353, doi:10.1093/eurheartj/ehs100 (2013).

- 3 Eltzschig, H. K. & Eckle, T. Ischemia and reperfusion--from mechanism to translation. *Nat Med* 17, 1391-1401, doi:10.1038/nm.2507 (2011).
- 4 Wang, J. et al. Visualizing the function and fate of neutrophils in sterile injury and repair. *Science* 358, 111-116, doi:10.1126/science.aam9690 (2017).
- 5 Neumann, J. et al. Very-late-antigen-4 (VLA-4)-mediated brain invasion by neutrophils leads to interactions with microglia, increased ischemic injury and impaired behavior in experimental stroke. *Acta Neuropathol* 129, 259-277 (2015).
- 6 Hulsmans, M. et al. Macrophages Facilitate Electrical Conduction in the Heart. *Cell* 169, 510-522 e520, doi:10.1016/j.cell.2017.03.050 (2017).
- 7 Luedike, P. et al. Cardioprotection through S-nitros(yl)ation of macrophage migration inhibitory factor. *Circulation* 125, 1880-1889, doi:10.1161/CIRCULATIONAHA.111.069104 (2012).
- 8 Rassaf, T. et al. Circulating nitrite contributes to cardioprotection by remote ischemic preconditioning. *Circ Res* 114, 1601-1610, doi:10.1161/CIRCRESAHA.114.303822 (2014).
- 9 Klingberg, A. et al. Fully Automated Evaluation of Total Glomerular Number and Capillary Tuft Size in Nephritic Kidneys Using Lightsheet Microscopy. *J Am Soc Nephrol* 28, 452-459, doi:10.1681/ASN.2016020232 (2017).
- 10 Belle, M. et al. Tridimensional Visualization and Analysis of Early Human Development. *Cell* 169, 161-173 e112, doi:10.1016/j.cell.2017.03.008 (2017).
- 11 Ding, Y. et al. Light-Sheet Imaging to Elucidate Cardiovascular Injury and Repair. *Curr Cardiol Rep* 20, 35, doi:10.1007/s11886-018-0979-6 (2018).
- 12 Richardson, D. S. & Lichtman, J. W. Clarifying tissue clearing. *Cell* 162, 246-257 (2015).
- 13 Erturk, A. et al. Three-dimensional imaging of solvent-cleared organs using 3DISCO. *Nat Protoc* 7, 1983-1995 (2012).
- 14 Botker, H. E. et al. Practical guidelines for rigor and reproducibility in preclinical and clinical studies on cardioprotection. *Basic Res Cardiol* 113, 39, doi:10.1007/s00395-018-0696-8 (2018).
- 15 Treweek, J. B. et al. Whole-body tissue stabilization and selective extractions via tissue-hydrogel hybrids for high-resolution intact circuit mapping and phenotyping. *Nat Protoc* 10, 1860-1896, doi:10.1038/nprot.2015.122 (2015).

- 16 Lee, S. E. et al. Three-dimensional Cardiomyocytes Structure Revealed By Diffusion Tensor Imaging and Its Validation Using a Tissue-Clearing Technique. *Sci Rep* 8, 6640, doi:10.1038/s41598-018-24622-6 (2018).
- 17 Fei, P. et al. Cardiac Light-Sheet Fluorescent Microscopy for Multi-Scale and Rapid Imaging of Architecture and Function. *Sci Rep* 6, 22489, doi:10.1038/srep22489 (2016).
- 18 Lugo-Hernandez, E. et al. 3D visualization and quantification of microvessels in the whole ischemic mouse brain using solvent-based clearing and light sheet microscopy. *J Cereb Blood Flow Metab* 37, 3355-3367, doi:10.1177/0271678X17698970 (2017).
- 19 Männ, L. et al. CD11c.DTR mice develop a fatal fulminant myocarditis after local or systemic treatment with diphtheria toxin. *Eur J Immunol* 46, 2028-2042, doi:10.1002/eji.201546245 (2016).
- 20 Nehrhoff, I., Ripoll, J., Samaniego, R., Desco, M. & Gomez-Gaviro, M. V. Looking inside the heart: a see-through view of the vascular tree. *Biomed Opt Express* 8, 3110-3118, doi:10.1364/BOE.8.003110 (2017).
- 21 Zundler, S. et al. Three-Dimensional Cross-Sectional Light-Sheet Microscopy Imaging of the Inflamed Mouse Gut. *Gastroenterology* 153, 898-900, doi:10.1053/j.gastro.2017.07.022 (2017).
- 22 Grüneboom, A. et al. A network of trans-cortical capillaries as mainstay for blood circulation in long bones. *Nature Metabolism*, doi:10.1038/s42255-018-0016-5 (2019).
- 23 Hendgen-Cotta, U. B. et al. Nitrite reductase activity of myoglobin regulates respiration and cellular viability in myocardial ischemia-reperfusion injury. *Proc Natl Acad Sci U S A* 105, 10256-10261, doi:10.1073/pnas.0801336105 (2008).
- 24 Fishbein, M. C. et al. Early phase acute myocardial infarct size quantification: validation of the triphenyl tetrazolium chloride tissue enzyme staining technique. *Am Heart J* 101, 593-600 (1981).
- 25 Thygesen, K. et al. Fourth universal definition of myocardial infarction (2018). *Eur Heart J* 40, 237-269, doi:10.1093/eurheartj/ehy462 (2019).
- 26 Nahrendorf, M. Myeloid cell contributions to cardiovascular health and disease. *Nat Med* 24, 711-720, doi:10.1038/s41591-018-0064-0 (2018).
- 27 Cerqueira, M. D. et al. Standardized myocardial segmentation and nomenclature for tomographic imaging of the heart. A statement for healthcare

- professionals from the Cardiac Imaging Committee of the Council on Clinical Cardiology of the American Heart Association. *Circulation* 105, 539-542 (2002).
- 28 Susaki, E. A. et al. Advanced CUBIC protocols for whole-brain and whole-body clearing and imaging. *Nat Protoc* 10, 1709-1727, doi:10.1038/nprot.2015.085 (2015).
 - 29 Tomer, R., Ye, L., Hsueh, B. & Deisseroth, K. Advanced CLARITY for rapid and high-resolution imaging of intact tissues. *Nat Protoc* 9, 1682-1697, doi:10.1038/nprot.2014.123 (2014).
 - 30 Yu, T., Qi, Y., Gong, H., Luo, Q. & Zhu, D. Optical clearing for multiscale biological tissues. *J Biophotonics* 11, doi:10.1002/jbio.201700187 (2018).
 - 31 Davidson, S. M. et al. Multitarget Strategies to Reduce Myocardial Ischemia/Reperfusion Injury: JACC Review Topic of the Week. *J Am Coll Cardiol* 73, 89-99, doi:10.1016/j.jacc.2018.09.086 (2019).
 - 32 Szummer, K. et al. Relations between implementation of new treatments and improved outcomes in patients with non-ST-elevation myocardial infarction during the last 20 years: experiences from SWEDEHEART registry 1995 to 2014. *Eur Heart J* 39, 3766-3776, doi:10.1093/eurheartj/ehy554 (2018).
 - 33 Ibanez, B. et al. Effect of early metoprolol on infarct size in ST-segment-elevation myocardial infarction patients undergoing primary percutaneous coronary intervention: the Effect of Metoprolol in Cardioprotection During an Acute Myocardial Infarction (METOCARD-CNIC) trial. *Circulation* 128, 1495-1503, doi:10.1161/CIRCULATIONAHA.113.003653 (2013).
 - 34 Garcia-Ruiz, J. M. et al. Impact of the Timing of Metoprolol Administration During STEMI on Infarct Size and Ventricular Function. *J Am Coll Cardiol* 67, 2093-2104, doi:10.1016/j.jacc.2016.02.050 (2016).
 - 35 Garcia-Prieto, J. et al. Neutrophil stunning by metoprolol reduces infarct size. *Nat Commun* 8, 14780, doi:10.1038/ncomms14780 (2017).
 - 36 Liberale, L. et al. Post-ischaemic administration of the murine Canakinumab-surrogate antibody improves outcome in experimental stroke. *Eur Heart J* 39, 3511-3517, doi:10.1093/eurheartj/ehy286 (2018).
 - 37 Gomez, D. et al. Interleukin-1beta has atheroprotective effects in advanced atherosclerotic lesions of mice. *Nat Med* 24, 1418-1429, doi:10.1038/s41591-018-0124-5 (2018).

- 38 Totzeck, M., Hendgen-Cotta, U. B., French, B. A. & Rassaf, T. A practical approach to remote ischemic preconditioning and ischemic preconditioning against myocardial ischemia/reperfusion injury. *J Biol Methods* 3, doi:10.14440/jbm.2016.149 (2016).
- 39 Nguyen, C. et al. Near-infrared fluorescence imaging of mouse myocardial microvascular endothelium using Cy5.5-lectin conjugate. *J Biophotonics* 5, 754-767, doi:10.1002/jbio.201100119 (2012).
- 40 Robertson, R. T. et al. Use of labeled tomato lectin for imaging vasculature structures. *Histochem Cell Biol* 143, 225-234, doi:10.1007/s00418-014-1301-3 (2015).
- 41 Laitinen, L. Griffonia simplicifolia lectins bind specifically to endothelial cells and some epithelial cells in mouse tissues. *Histochem J* 19, 225-234 (1987).
- 42 Hasenberg, A. et al. Catchup: a mouse model for imaging-based tracking and modulation of neutrophil granulocytes. *Nat Methods* 12, 445-452, doi:10.1038/nmeth.3322 (2015).
- 43 Chen, J., Ceholski, D. K., Liang, L., Fish, K. & Hajjar, R. J. Variability in coronary artery anatomy affects consistency of cardiac damage after myocardial infarction in mice. *Am J Physiol Heart Circ Physiol* 313, H275-H282, doi:10.1152/ajpheart.00127.2017 (2017).
- 44 Yang, Z., Berr, S. S., Gilson, W. D., Toufektsian, M. C. & French, B. A. Simultaneous evaluation of infarct size and cardiac function in intact mice by contrast-enhanced cardiac magnetic resonance imaging reveals contractile dysfunction in noninfarcted regions early after myocardial infarction. *Circulation* 109, 1161-1167, doi:10.1161/01.CIR.0000118495.88442.32 (2004).
- 45 Schneider, C. A., Rasband, W. S. & Eliceiri, K. W. NIH Image to ImageJ: 25 years of image analysis. *Nat Methods* 9, 671-675 (2012).
- 46 Frangi, A. F., Niessen, W. J., Vincken, K. L. & Viergever, M. A. Multiscale vessel enhancement filtering. *Medical Image Computing and Computer-Assisted Intervention - Miccai'98* 1496, 130-137 (1998).
- 47 Lesage, D., Angelini, E. D., Bloch, I. & Funka-Lea, G. A review of 3D vessel lumen segmentation techniques: models, features and extraction schemes. *Med Image Anal* 13, 819-845, doi:10.1016/j.media.2009.07.011 (2009).
- 48 R Core Team. R: A Language and Environment for Statistical Computing. (2014).

- 49 Heinen, A. et al. Echocardiographic Analysis of Cardiac Function after Infarction in Mice: Validation of Single-Plane Long-Axis View Measurements and the Bi-Plane Simpson Method. *Ultrasound Med Biol* 44, 1544-1555, doi:10.1016/j.ultrasmedbio.2018.03.020 (2018).

Acknowledgements

We thank the imaging center Essen (IMCES, <https://imces.uk-essen.de>) for continuous support of our imaging experiments.

Author Contributions

SFM, SK developed the BALANCE protocol and performed the LSM experiments together with JD. SFM, SK, LB analyzed the data, generated all illustrations as well as schematics and prepared the figures. PS, SK and LM performed mouse surgeries, TTC planimetry, cardiac troponin I and echocardiographic measurements. AS supervised modeling of the vessel system and CS translated results in R software. HL, MK, JK, DRE, DMH, TR, UHC, MT and MG provided supervision. MT and MG conceived of the study and wrote the manuscript together with TR, UHC, SFM, SK and LB.

Competing Interest

M. Gunzer and J. Klode received general research funding from LaVision BioTec GmbH. Beyond that, the authors declare no competing interests.

4.2.7 Supplementary material

Supplementary Note 1

Alternative bleaching protocols

We tested the efficiency of BALANCE against Sudan Black bleaching and heme elution, both established protocols for reducing tissue autofluorescence¹. Sudan Black bleaching was conducted before dehydration of the sample. However, incubation with Sudan Black left the heart tissue stained black, preventing laser penetration into the tissue for more than a few micrometers (Supplementary Figure 1 b). For heme elution, we incorporated CUBIC-1 reagent² incubation steps before the original ethyl cinnamate (ECi) protocol's³ dehydration. This extended the time needed until the imaging process by 2 d (compared to the BALANCE protocol). We achieved

autofluorescence homogenization of some parts of the heart, while we still found several spots of high background signal (Supplementary Figure 1 c).

Supplementary Note 2

Endogenous fluorophores

We used the Catchup mouse model⁴ expressing tdTomato in neutrophils to benchmark our i.v.-mediated Ly-6G staining in terms of cellular labeling efficiency. Clearing an infarcted murine Catchup heart with ethyl cinnamate (without peroxide treatment) allowed for visualization of both, i.v.-mediated Ly-6G labeling and tdTomato signal (Supplementary Figure 2 c and d)³. Here, we found that all tdTomato positive cells in the tissue were also positive for Ly 6G labeling, strengthening the applicability of this antibody delivery route for immune cells and surface markers. However, the signal-to-noise ratio of tdTomato was low, with signal intensities matching muscle autofluorescence. Using BALANCE, we lowered the tissue autofluorescence in order to enhance sample clarity and signal homogeneity of synthetic dyes. However, hereby endogenously expressed tdTomato was quenched as well (Supplementary Figure 2 b). Additionally, when using the CUBIC protocol², we were able to visualize the endogenous fluorescence, but observed less sample clarity and lost the artificial Ly-6G staining completely (Supplementary Figure 2 a; this caveat is described in the original paper and can be potentially circumvented by further establishment).

Table 4-1: Supplementary Table 1 Comparison of alternative bleaching approaches with the BALANCE protocol. No bleaching³, Sudan Black bleaching¹ and heme elution^{1,2} were conducted as previously published.

| | Autofluorescence homogenization | Sample clarity | Endogenous fluorophore bleaching | Fluorescent labeling |
|-----------------------------------|---|-----------------------------------|-------------------------------------|----------------------|
| No bleaching³ | no homogenization in 488 and 561 | grid lines hardly visible | no | preserved |
| Sudan Black¹ | no homogenization in 488, 561 and 647 | grid lines not visible | N.A. | preserved |
| Heme elution^{1,2} | homogenous in all channels; autofluorescent spots | grid lines visible; brown color | no | reduced |
| BALANCE | homogenous in all channels | grid lines visible; reduced color | yes | preserved |

Table 4-2: Supplementary Table 2 Comparison of established clearing methods with the BALANCE protocol (shrinkage is mean \pm s.d.). Evaluation of CUBIC⁵, CLARITY⁵, iDISCO⁶ and SWITCH⁶ as previously published.

| | Macroscopic sample clarity | Autofluorescence homogenization | Endogenous fluorophores preserved | Tissue alteration | Sample integrity | Incubation time | Characteristics |
|----------------------------|----------------------------------|------------------------------------|---|--------------------------------|---------------------|--------------------|-----------------|
| ECi | Moderate - brown | No | Yes | Slight shrinkage (~20%) | Stiff | 1 d | Non-toxic |
| BALANCE | Clear - light yellow | Yes | No | Slight shrinkage (18% \pm 2) | Stiff | 1.5 d | Non-toxic |
| | | | | | | | |
| CUBIC⁵ | Moderate – light brown | Not tested | Yes | Expansion | Spongy | 14 d | Non-toxic |
| CLARITY⁵ | Moderate – light brown | Not tested | Yes | Expansion | Spongy | 10 d | Toxic |
| iDISCO⁶ | Clear – light brown | Yes | Yes | Shrinkage | Stiff | Hours – days | Toxic |
| SWITCH⁶ | Clear – light yellow | Yes | No | Slight expansion | Not tested | Days | Toxic |

Table 4-3: Supplementary Table 3 Comparison of assessed parameters, shortcomings, time-expense and difficulty of available techniques to evaluate myocardial ischemia/reperfusion (I/R) injury and associated parameters. (2D – two-dimensional, AAR – area at risk, d – days, h – hours, LSFM – light sheet fluorescence microscopy, TTC – triphenyl tetrazolium chloride; asterisk - protocol time depends on automation processes)

| Methods | Parameters assessed | Shortcomings | Total time until results | Hands-on time | Analysis time | Difficulty |
|----------------------------|--|--|--------------------------|---------------|---|---|
| TTC-planimetry | Myocardial infarction parameters: Infarct size, AAR, remote zone (with blue dye), In pseudo-3D | No single cell resolution | 2.5 h | 1 h | 0.25 h | Simple, parameters vary depending e.g. on operator and camera settings |
| Flow cytometry | Immune cell quantification and subset analysis | No precise assessment of I/R areas, no cell localization context | 3.5 h | 1.5 h | 0.5 h | Simple to advanced analysis, depending on staining panel |
| (Immuno-) Histology | Infarct size, immune cell localization and quantification | Limited 3D spatial information due to thin 2D slices (<10µm); 3D information in sequential slices possible, but high time and cost expense and computational power involved | 3-7 d | 4 h | 1-2 h, depending on level of analysis | Simple (H&E) to advanced (multicolor sequential immunohistochemistry) |
| BALANCE/ LSFM | Multiplexed infarction parameters (vascular damage, AAR and remote zone) with target cells in 3D; Identification of regions of interest for further processing (e.g. immuno-histology) | Need for bleaching, due to whole organ imaging; target cell detection restricted to surface markers (i.v.-mediated staining), limited multiplexing. 3D rendering software and computational power required | 1.5–4 d* | 2.5 h | 1.5 h for basic I/R injury parameters and cell segmentation; segment model or distance analysis more time consuming | Simple (infarction parameters and 3D immune cell localization) to advanced, depending on staining panel and post-processing |

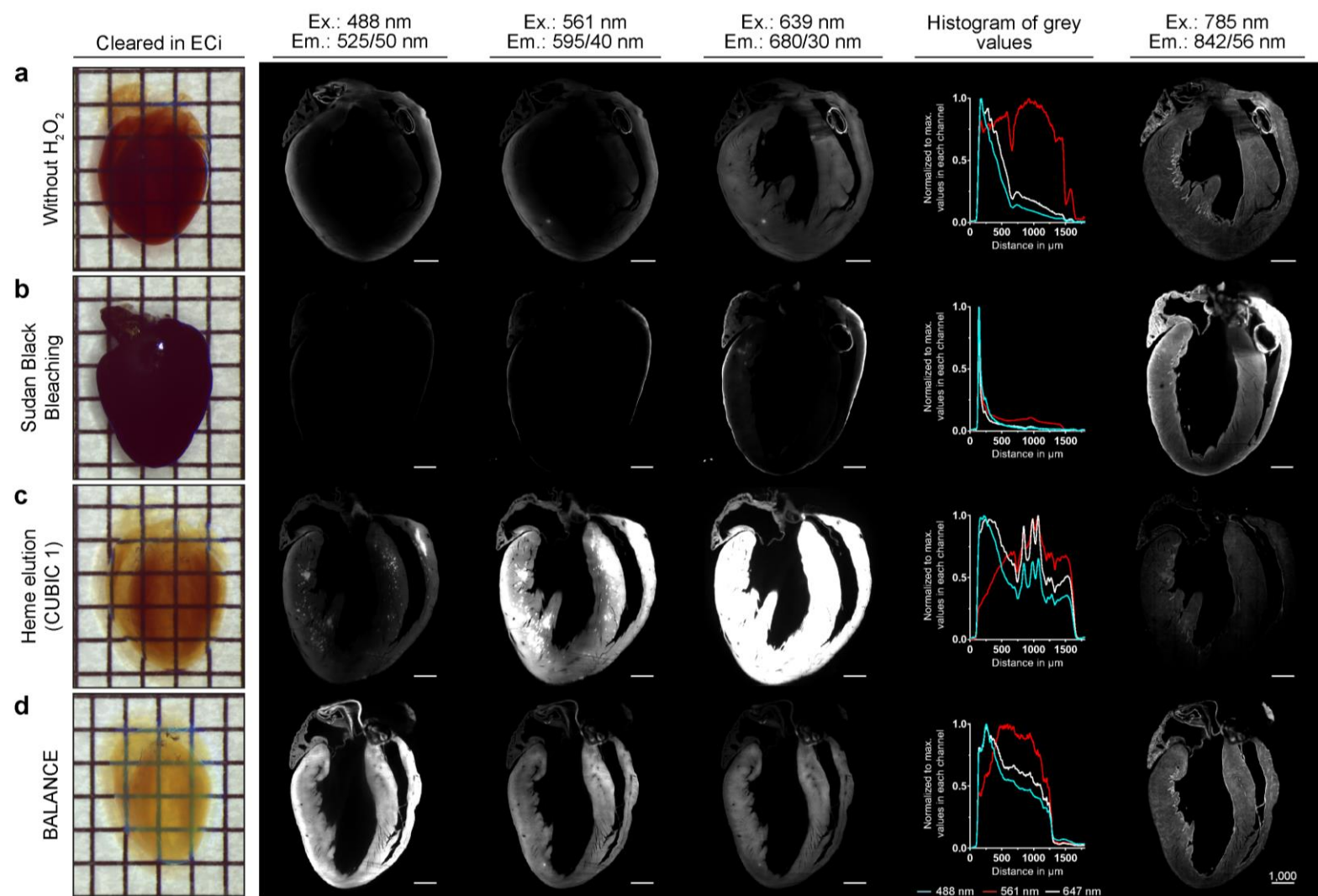


Figure 4-13: Supplementary Figure 1 Tissue autofluorescence homogenization using different bleaching protocols. Evaluation of ECI clearing combined with (a) no bleaching³, (b) Sudan Black bleaching¹, (c) heme elution (CUBIC 1)^{1,2} and (d) peroxide (H₂O₂)-based bleaching (BALANCE) with regard to signal tissue penetration in indicated fluorescent channels. Scale bar values in μm . One square in the macroscopic images is 2x2 mm. Source data are provided as a Source Data file. (ECi – ethyl cinnamate, Ex. – excitation, Em. – emission)

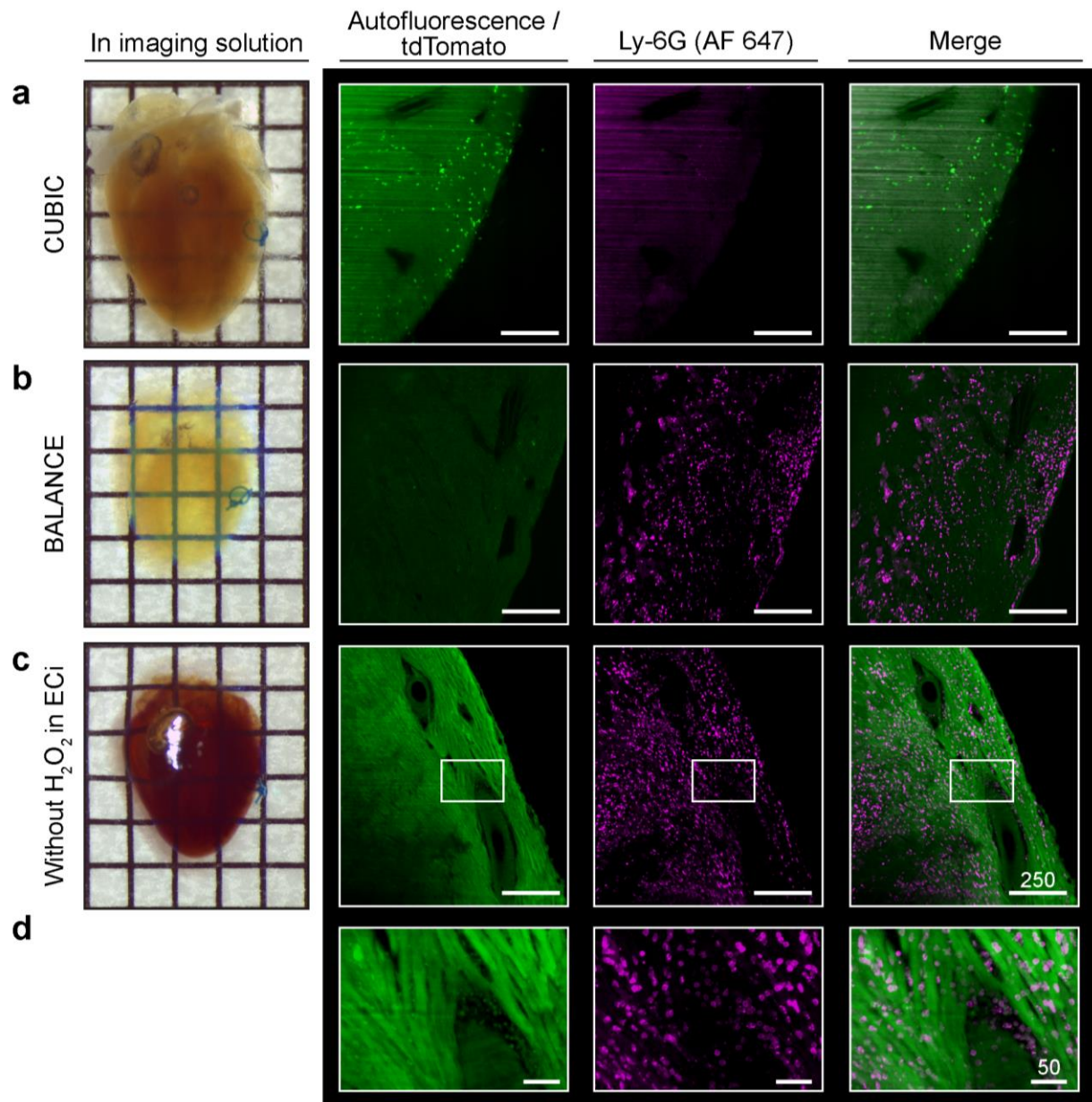


Figure 4-14: Supplementary Figure 2 Endogenous fluorescence and i.v.-mediated staining in organic- and water-based clearing. Comparison of (a) CUBIC⁵, (b) BALANCE and (c) ECI-only³ clearing in their capabilities of preserving endogenous (tdTomato, green) and artificial fluorophore (anti-mLy-6G AF647, magenta) fluorescence in Catchup mouse⁴ hearts (neutrophils tdTomato positive) after myocardial ischemia/reperfusion (I/R) injury. (d) Magnification of ROIs depicted in (c, white rectangles). Scale bar values in μm . One square on the macroscopic images (left) equals 2x2 mm.

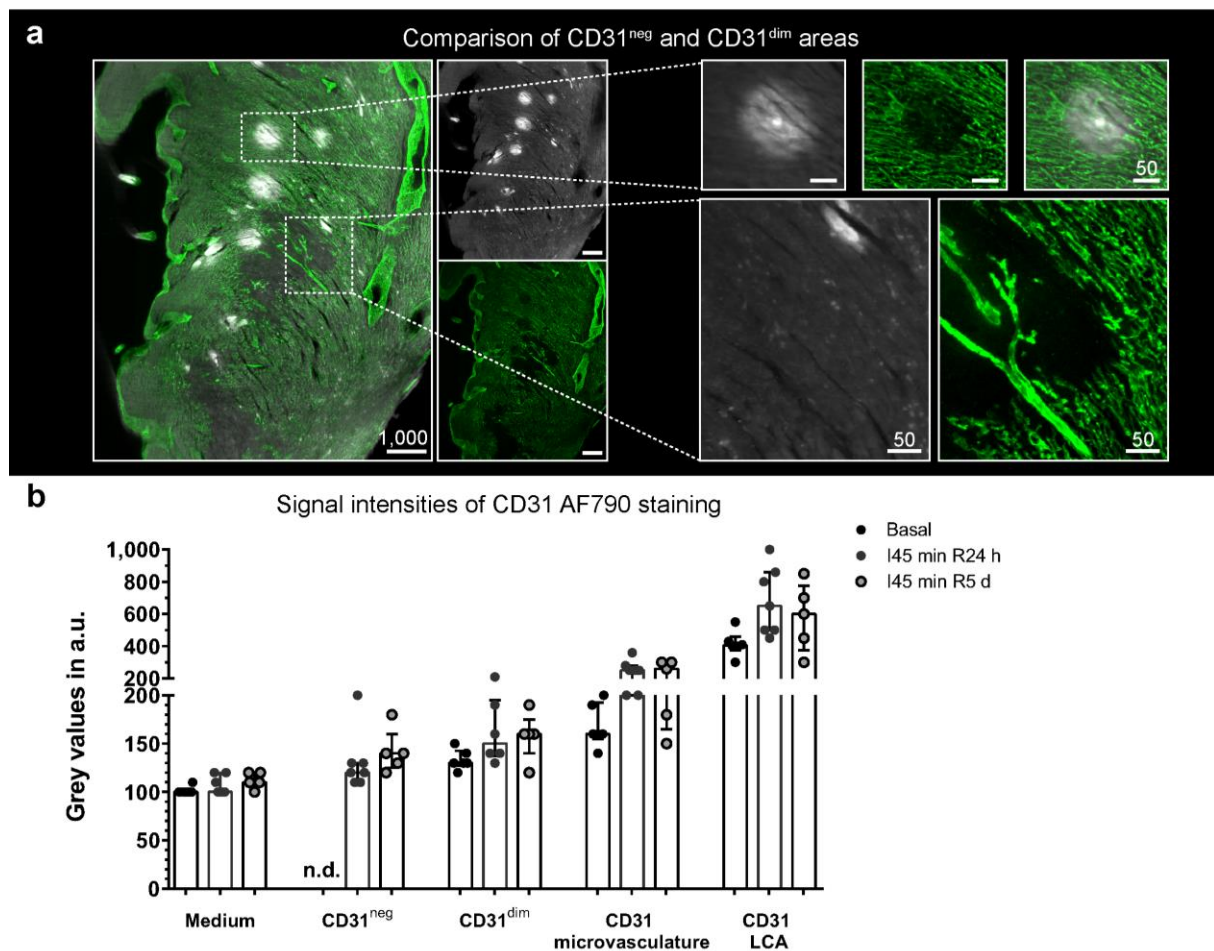


Figure 4-15: Supplementary Figure 3 CD31 imaging in the heart. (a) Left: ROI of an exemplary infarcted heart at 8x magnification showing CD31 (green) and autofluorescence (grey). Right: ROIs depicted on the left side in digital magnification. On the top, co-localization of a CD31 dim (CD31^{dim}) area (green) and high autofluorescence (grey to white) is shown. At the bottom, CD31 negative (CD31^{neg}) does not co-localize with increased autofluorescence. (b) CD31-AlexaFluor 790 raw values from various experimental end points and heart structures as indicated (median \pm interquartile range; $n=5$). Scale bar values in μm . Source data are provided as a Source Data file.

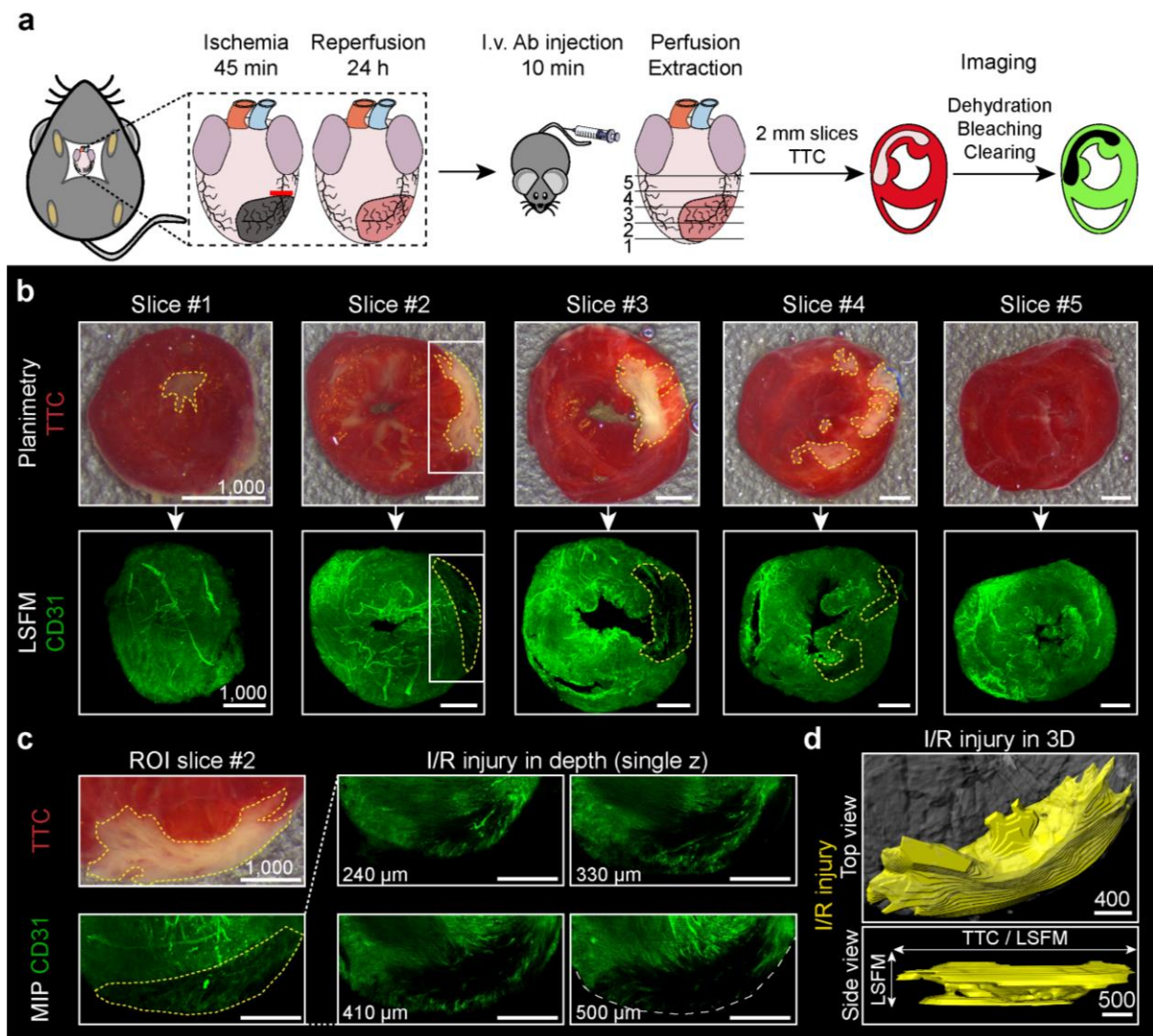


Figure 4-16: Supplementary Figure 4 TTC-planimetry and subsequent LSFM of murine hearts in a myocardial ischemia/reperfusion (I/R) model. (a) Workflow for comparison of triphenyl tetrazolium chloride (TTC)- and LSFM-based analysis in single heart slices. (b) Slice by slice comparison of an exemplary heart analyzed first by TTC-planimetry (upper row), followed by LSFM (maximum intensity projections (MIP), lower row) of the same slice (white = TTC negative / metabolically inactive, red = TTC positive / metabolically active). TTC negative / CD31 negative areas (dashed yellow lines) are largely overlapping. (c) Left: Comparison of TTC and LSFM-MIP from slice #2 in (b). Right: single optical slices in z depth, indicating complete loss of CD31 signal in a 3D structure. (d) 3D volume visualization of CD31 negative signal from the slice depicted in (c). (e) Correlation of TTC negative and CD31 negative area sizes in the same slice (r- and p-values from linear regression given, n=3 hearts, 5 slices per heart). Scale bar values in μm .

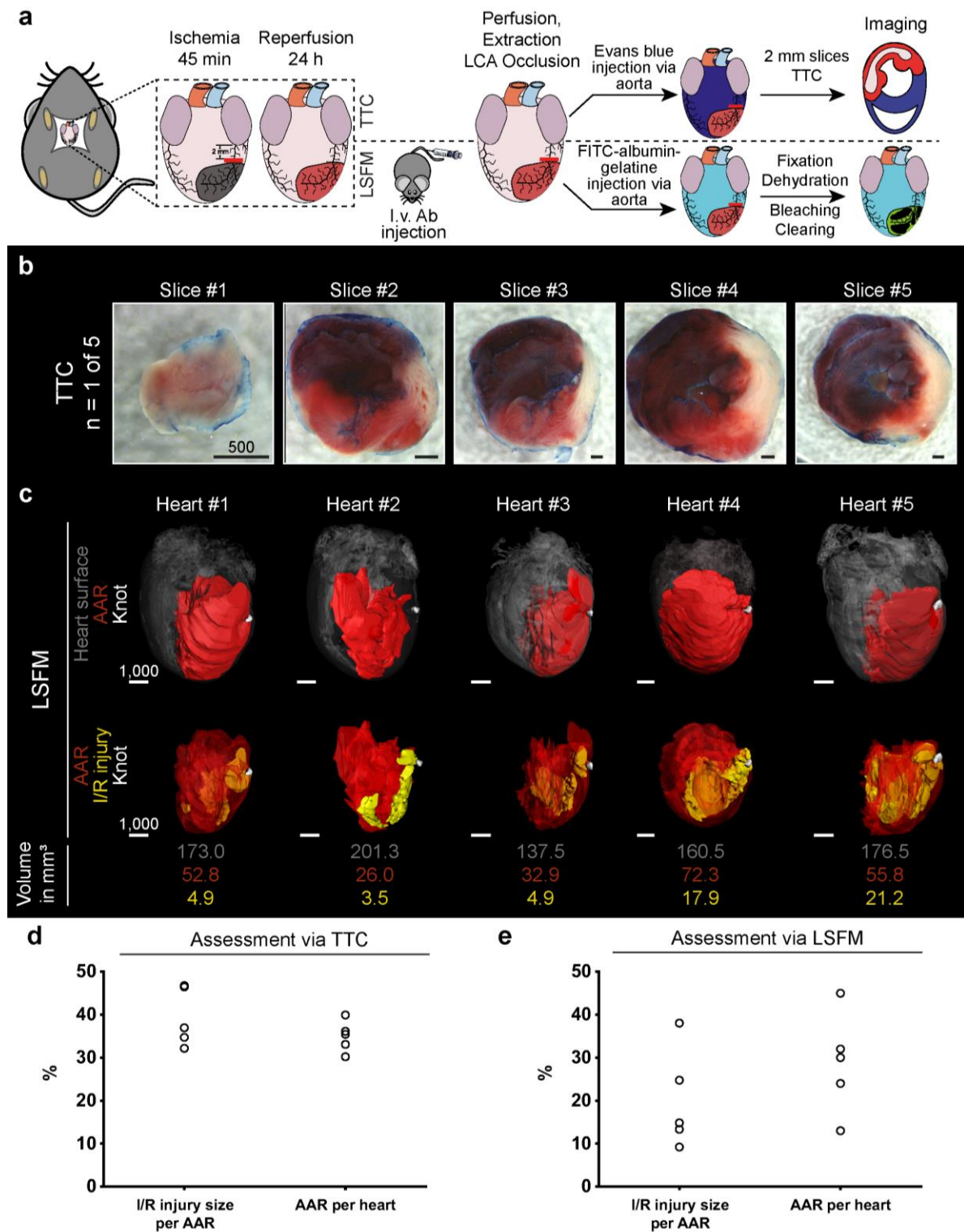


Figure 4-17: Supplementary Figure 5 Ischemia/reperfusion (I/R) injury parameters in 3D – triphenyl tetrazolium chloride (TTC)- and light sheet fluorescence microscopy (LSFM)-based analysis in comparison. (a) Workflow for 2D TTC- and 3D LSFM-based analysis of myocardial I/R injury. (b) Planimetry of 2 mm thick slices of one exemplary heart stained with TTC / Evans blue (EB; White = TTC negative / metabolically inactive, red = TTC positive / metabolically active, not blue = EB negative = area at risk (AAR)). (c) Five hearts were analyzed using LSFM and in silico post-processing. All hearts are shown with their anterior side to the front, the knot (white) being on the right side. Upper row: heart surface (translucent grey) together with AAR volume (red). Lower row: same hearts with traced I/R injury volume (yellow). Numbers at the bottom represent heart (grey), AAR (red) and I/R injury volume (yellow) for the respective heart. (d) I/R injury size per AAR and AAR per heart as assessed by TTC and EB staining (n=5). (e) I/R injury size per AAR and AAR per heart as assessed by CD31 and FITC staining (n=5). Hearts depicted in (d) and (e) stem from separate cohorts. Scale bar values in μm . Source data are provided as a Source Data file.

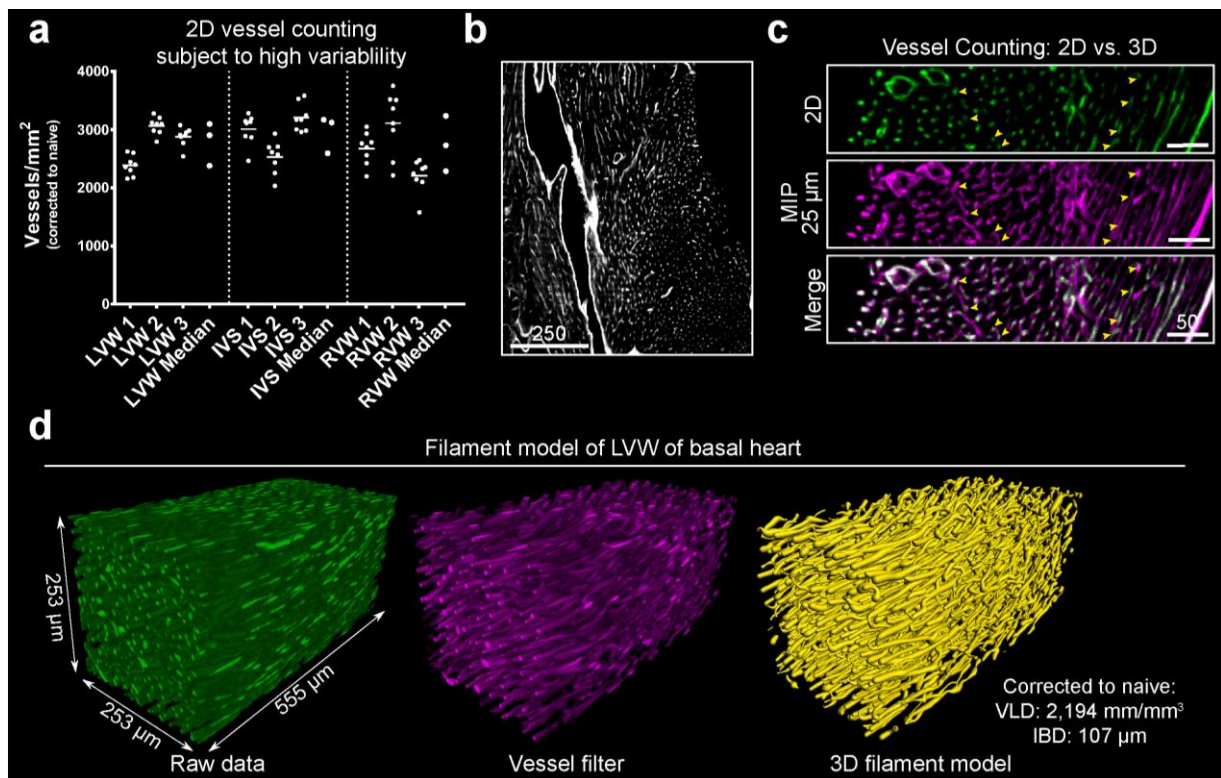


Figure 4-18: Supplementary Figure 6 2D and 3D cardiac vessel measurements. (a) Quantification of CD31 positive vessels in optical slices at different z positions of the right ventricular wall (RVW), intraventricular septum (IVS) and left ventricular wall (LVW) of the murine heart ($n=3$ mice, each dot represents one counted ROI; the respective median, as well as a median summary for each compartment is shown; values have been corrected for shrinkage). (b) Exemplary field of view showing diverse vessel directionality in LVW. (c) Images show that counting in 2D (e.g. optical slice) is difficult and results in repeated measures of the same vessel (yellow arrows) visualized by a maximum intensity projection (MIP) of 25 μ m z depth (magenta). Magnification: 6.4x. (d) Computing a 3D filament model: from a 3D reconstruction of the raw data (green) via a vessel-filtered data set (magenta) using the FRANGI algorithm to the 3D filament model (yellow) of the LVW microvasculature. This model allows in-depth analysis of the vascular network, including parameters like vessel length density (VLD) and measures of complexity e.g. interbranch distance (IBD). Based on a magnification of 6.4x. This represents one experiment ($n=1$). Scale bar values in μ m. Source data are provided as a Source Data file.

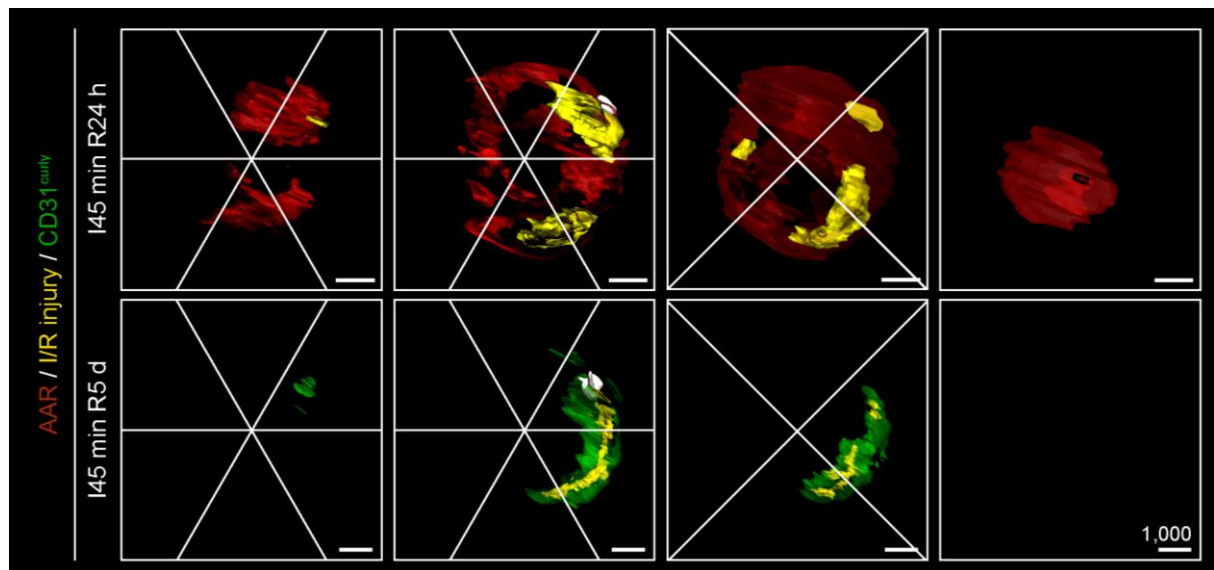


Figure 4-19: Supplementary Figure 7 Quantifying ischemia/reperfusion (I/R) injury, area at risk (AAR) and CD31 curly localization. To quantify the detailed localization of I/R injury, AAR and CD31 curly, we used the left ventricular 17 segment model⁷ in mice in combination with 3D LSFM data. Representative examples of scored hearts after 24 h (upper row) and 5 d (lower row) of reperfusion depicting AAR (red), CD31 negative (yellow) and newly vascularized CD31 curly (green) volumes are shown. Scale bar values in μm .

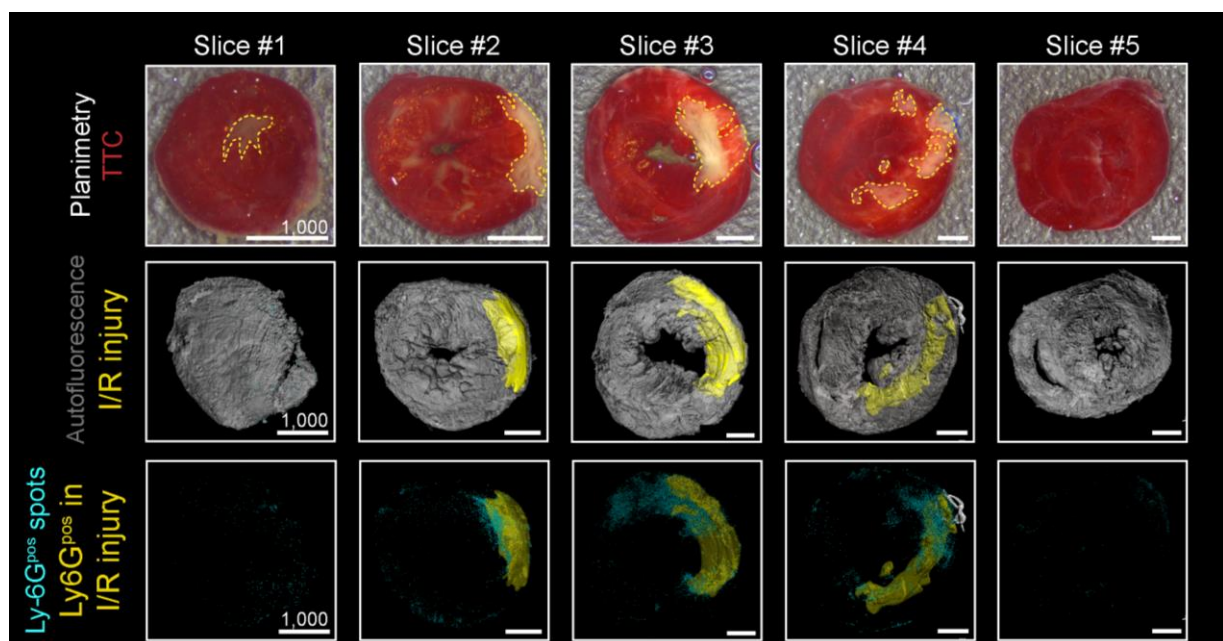


Figure 4-20: Supplementary Figure 8 Co-localization of ischemia/reperfusion (I/R) injury with Ly-6G positive (Ly-6G^{pos}) neutrophils. Top: 2 mm thick TTC slices as already shown in Supplementary Figure 4 for orientation. Middle: 3D reconstruction of slices showing autofluorescence (grey) and CD31 negative (CD31^{neg}) I/R injury volume (yellow). Bottom: Total Ly-6G^{pos} neutrophils (turquoise) were detected using IMARIS spot function. Ly-6G^{pos} spots inside the I/R injury are colored in yellow. These findings were verified in 3 mice. Scale bar values in μm .

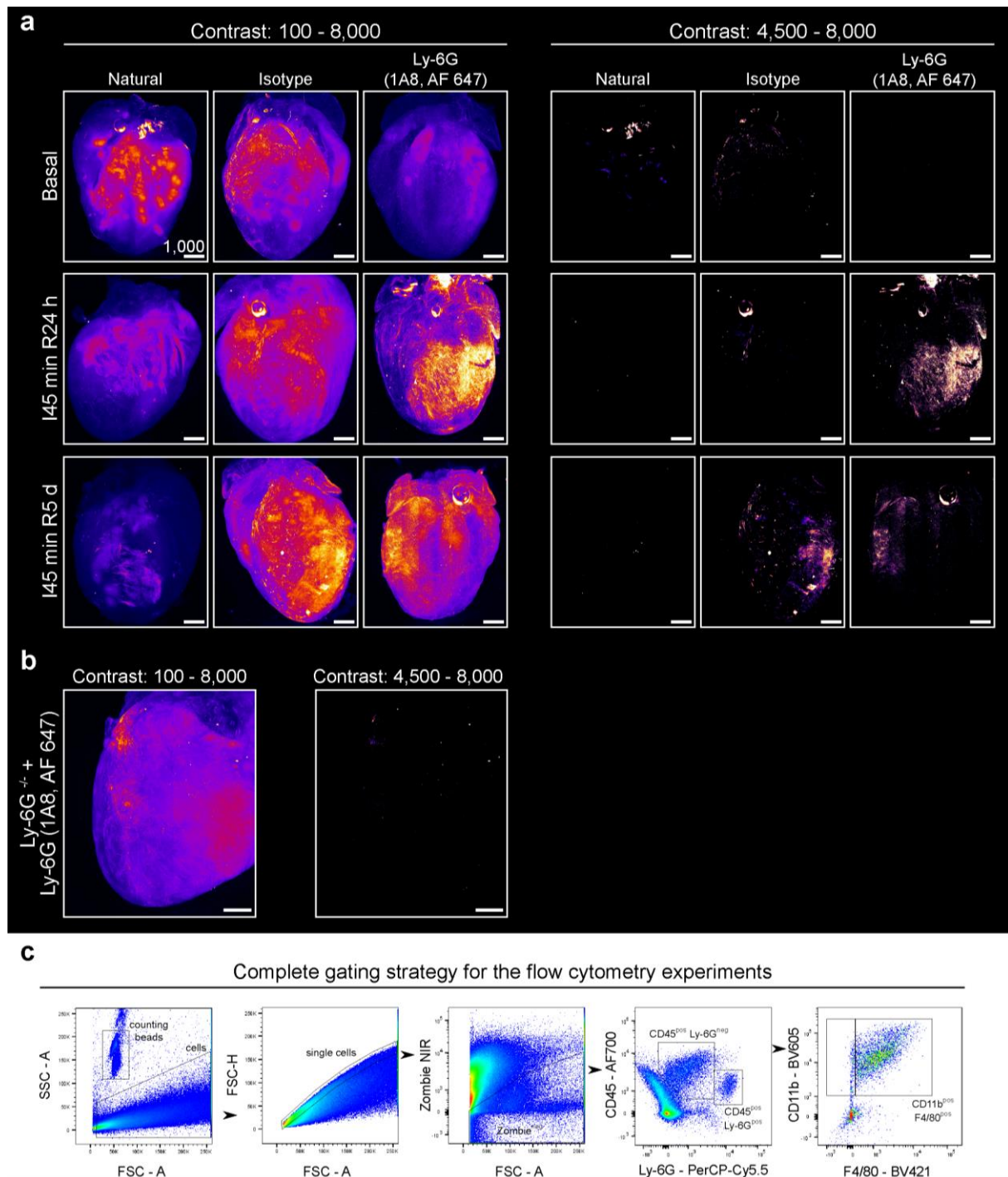


Figure 4-21: Supplementary Figure 9 Immune cell identification in LSFM and flow cytometry analysis. (a) Left: Ly-6G AlexaFluor 647 signal obtained from various, exemplary hearts displayed as a heat map of greyscale values ranging from 100 to 8000 counts. Right: same hearts as depicted on the left, with a narrower greyscale value (4500 – 8000 counts), adjusted to minimize signal in the baseline heart with Ly-6G AlexaFluor 647 antibody (right top image). (b) As a control, Ly-6G^{-/-} knockout mice were injected with Ly-6G AlexaFluor 647 antibody 24 h after ischemia and processed and imaged as before. Ly-6G positive (Ly-6G^{pos}) signals inside the heart could be obtained with a wide threshold (100 – 8000 counts greyscale value), but were no longer detectable with the narrow threshold applied above (4500 – 8000 counts greyscale value). (c) Flow cytometry gating strategy. Pseudo color density plots of an exemplary heart analyzed by flow cytometry are shown. After gating for forward and side scatter, doublet cells and dead/alive staining, cells are gated for CD45 and Ly-6G expression and further analyzed as displayed. CD45^{pos} / Ly-6G^{pos} cells are considered neutrophils. CD45^{pos} / Ly-6G^{neg} cells are gated for CD11b and F4/80 expression. CD11b^{pos} / F4/80^{pos} cells are considered macrophages. Total cell numbers per heart are obtained using counting beads.

Supplementary References

- 1 Treweek, J. B. et al. Whole-body tissue stabilization and selective extractions via tissue-hydrogel hybrids for high-resolution intact circuit mapping and phenotyping. *Nat Protoc* 10, 1860-1896, doi:10.1038/nprot.2015.122 (2015).
- 2 Susaki, E. A. et al. Advanced CUBIC protocols for whole-brain and whole-body clearing and imaging. *Nat Protoc* 10, 1709-1727, doi:10.1038/nprot.2015.085 (2015).
- 3 Klingberg, A. et al. Fully Automated Evaluation of Total Glomerular Number and Capillary Tuft Size in Nephritic Kidneys Using Lightsheet Microscopy. *J Am Soc Nephrol* 28, 452-459, doi:10.1681/ASN.2016020232 (2017).
- 4 Hasenberg, A. et al. Catchup: a mouse model for imaging-based tracking and modulation of neutrophil granulocytes. *Nat Methods* 12, 445-452, doi:10.1038/nmeth.3322 (2015).
- 5 Orlich, M. & Kiefer, F. A qualitative comparison of ten tissue clearing techniques. *Histol Histopathol* 33, 181-199, doi:10.14670/HH-11-903 (2018).
- 6 Yu, T., Qi, Y., Gong, H., Luo, Q. & Zhu, D. Optical clearing for multiscale biological tissues. *J Biophotonics* 11, doi:10.1002/jbio.201700187 (2018).
- 7 Cerqueira, M. D. et al. Standardized myocardial segmentation and nomenclature for tomographic imaging of the heart. A statement for healthcare professionals from the Cardiac Imaging Committee of the Council on Clinical Cardiology of the American Heart Association. *Circulation* 105, 539-542 (2002).

5 Discussion

Cardiovascular diseases remain the leading cause of death worldwide. Atherosclerosis occurs in people exposed to risk factors over long periods of time and can lead to acute coronary syndromes including AMI. In the course of ischemia and reperfusion, CMs in the area at risk are damaged and undergo either necrosis or apoptosis. Loss of CMs reduces cardiac pump function and the salvage of damaged/dying CMs is a desirable target.⁹ Small capillaries can stay occluded after I/R by various mechanisms and result in microinfarctions and no-reflow areas, which leads to cardiac tissue death.⁶⁵ Dead cells inside the myocardium release DAMP signals and trigger an immune cell response. Inflammation after AMI is a delicately orchestrated process, that requires a precise balance between the clearance of dead cells and debris on the one hand and the rebuilding of connective tissue via myofibroblasts and scar formation on the other.¹¹² Ultimately, the inability of the heart to compensate for reduced functional capacities results in further remodeling of cardiac tissue with an increase in the ventricular volume without an increase in muscular mass. When the heart reaches its enlargement limit, heart failure is imminent.⁹⁸

The therapy of choice is a timely reperfusion regime to reduce infarct size and prevent heart failure. Additional strategies to preserve cardiac function have not translated from experimental studies to clinical practice in recent years, which may be due to the fact that the research was narrowly focused on strategies targeting either CM survival, vascular integrity, or immune modulation. Recently, multi-target approaches have been proposed to overcome this limitation and are seen as highly promising for reducing the health burden due to AMI in the coming years.¹⁰²

In this work the influence of NO-modulated calpain function on infarct size reduction has been investigated.¹¹³ Supplemented nitrite is transformed into NO as the biologically active molecule, and it has been shown that NO not only impacts vascular tone but also the immune response and CM intracellular pathways.¹¹⁴ Therefore nitrite may represent a multi-target strategy. This work will add to the existing evidence of the positive influence of nitrite its modulation of calpains as an important factor in CM cell death. Whether such modulation by either NO or specific inhibitors is beneficial in a clinical context, should to be the focus of future studies and is beyond the scope of this work.

Given that the simultaneous measurement of I/R injury size and response is not possible with the currently established gold standard methods, this work introduces a

novel intravenous vascular staining approach combined with staining for immune cells to capture the 3D nature of both the injury size and response using LSM.

5.1 Calpains as mediators of nitric oxide derived cardioprotection

Cardioprotection itself has been described as “a fairly vague term” summarizing all measures taken to reduce the burden of myocardial I/R¹¹⁵, and clinical applications are still rare after three decades of research. In 1986 it was already shown that short periods of I/R before an AMI reduced infarct size in an experimental setup, which was termed ischemic pre-conditioning (IPC).¹¹⁶ Arguably, therapy prior to illness is hardly feasible. Later, conditioning was found to be effective even after ischemic events (ischemic post-conditioning [IPost])¹¹⁷ and also when applied not to the heart itself, but non-invasively to a limb (remote ischemic conditioning [RIC])¹¹⁸, though in experimental setups only. Clinical studies on IPost and RIC have been disappointing.¹¹⁹ The targeted modulation of molecular pathways discovered during the investigation of conditioning strategies has since been a mainstay of cardioprotection research, with a particular focus in recent years on preserving mitochondrial integrity. Among them mitochondrial permeability transition pore (MPTP) opening inhibition via cyclosporin-A has been widely discussed with mixed results in experimental^{120,121} and clinical studies.^{122–124} Impacting the PKC by direct inhibition using PKC inhibitor Delcasertib¹²⁵ or its related pathway were likewise not successful in clinical practice. Innovation in cardioprotective interventions is therefore needed. Supplementation with nitrite has been discussed for a few years, with mixed results from clinical studies.¹²⁶ In animal experiments it was shown multiple times to reduce I/R injury size^{35,127,128} and partly owing to posttranslational S-nitrosation of proteins.³⁶ Calpains are likely a formidable target to study, as they have been described to reduce infarct size when inhibited¹²⁹ as well as being modified via NO.¹³⁰ Furthermore, the pharmacological inhibition of calpains proved to be rather unspecific and to involve the co-inhibition of other proteases such as cathepsin.¹³¹ Notably, prolonged blockage of calpain activity may result in deleterious effects.³⁰

In this work, the effect of calpain inhibition via nitrite was shown both *in vitro* and *in vivo*. For the *in vitro* approach, the established HL-1 cell line was used and the cell culture media was supplemented with a final concentration of 300 μ M sodium nitrite, which has been previously shown to exert beneficial effects.¹³² The amount of surviving cells after 22 h of hypoxia and 1 h of reoxygenation was doubled when supplementing

with nitrite. There was a concomitant increase in S-nitrosation for calpain 1 and 2 ($124.7\% \pm 45.3$ and $107.3\% \pm 28.9$, respectively), but not calpain 10 and an overall decrease in calpain activity of about 25% (see Figure 4-1). A variation in intracellular calcium levels during these experiments, which could explain calpain activity differences, was not found (see Figure 4-5). In addition, calpain activity was also decreased after the *in vitro* incubation of purified, activated calpain 1 with S-Nitroso-N-acetyl- DL-penicillamine (SNAP), a potent NO donor, adding further evidence of the inhibition of calpain activity by NO (see Figure 4-4). Nevertheless the question remains whether NO also modulates typical calpain activation, i.e., dissociation from endogenous inhibitor calpastatin. Recent and previous studies in this field suggest that S-nitrosation inhibits activity rather than activation, as both NO and calpastatin have been shown to act synergistically¹³³ and pharmacological inhibition of calpain catalytic center (cysteine-histidine-asparagine) nullified NO mediated activity decrease.¹³⁴

In the *in vivo* approach, the results from the *in vitro* experiments were matched. C57BL/6J mice, aged 12 ± 3 weeks, were subjected to transient ligation of the left coronary artery (LCA) for 30 min followed by either 5 min of reperfusion for S-nitrosation and calpain activity assessment or 24 h of reperfusion for infarct size measurements and electron microscopy. At 5 min prior to reperfusion, $1.67 \mu\text{mol/kg}$ sodium nitrite was injected into the left ventricular cavity. As previously published, infarct size was decreased in the nitrite supplemented group.¹³⁵ This decrease was attended by increased S-nitrosation of calpain 1 and 2 ($57\% \pm 18$ and $45.7\% \pm 8.9$, respectively), but again no modification of calpain 10 was detectable. Calpain activity *in vivo* was decreased by about 50% after nitrite supplementation (see Figure 4-2). Additional analysis using electron microscopy revealed less calpain 1 and 10 located at the mitochondria after I/R and supplementation with nitrite (see Figure 4-3). Translocation of calpains to organelles such as the mitochondria was also previously shown. As this facilitates apoptotic pathways (e.g. cleavage of AIF), the blockage of translocation is desired.¹³⁶

Overall, the inhibition of calpain activity via nitrite supplementation seems beneficial. However, some studies on macrophages have shown detrimental effects on calpains, whereby NO led to increased intracellular calcium and increased calpain activation.¹³⁷ In the *in vitro* experiments herein, no difference in intracellular calcium concentrations (which were not studied in the *in vivo* experiments) was found, though calpain activity was still decreased. Whether modulation is dependent on calcium levels cannot be

stated. First, no variation in calcium levels or their effect on calpain activity was evaluated. Second, current available assays may not be suited to measuring the subtle differences needed to assess calpain activity *in vivo*.¹³⁸ Furthermore this work neglected to analyze specific calpain isoforms and their contribution to infarct size reduction after nitrite supplementation, which could be analyzed in respective knock-out animals. In addition, the proteolytic targets of calpains were not investigated to determine the exact pathway affected. In this regard, an analysis of calpain mutants varying in cysteine deletion could help to identify both the exact site required for NO - mediated modulation, as well as present a future target for the development of a more specific inhibition. As such further research on NO mediated modulation of calpains is warranted.

Besides S-nitrosation of proteins inside CMs, the beneficial effects of NO have been found in various other processes. NO has been described to reduce the adhesion of platelets and leukocytes to both themselves and ECs.¹³⁹ Furthermore, NO suppresses the production of TNF α and interleukin-1 (IL-1), two potent pro-inflammatory cytokines.^{140,141} Therefore, the decreased NO levels observed after I/R may promote inflammation and adhesion-based MVO. In addition, NO acts as a vasodilator via modulation of cGMP levels.¹⁴² Taken together, NO may represent a highly viable multi-target strategy for the treatment of AMI.

5.2 Simultaneous measurement of I/R injury and response for multi-target strategies

Tissue injury, vascular dysfunction and inflammation are inseparably linked during I/R, as one begets the other two.⁶⁵ Tools for the simultaneous analysis of all three targets are currently not available and the established gold standard methods are time consuming and/or require the use of separate specimens, which precludes correlation. The present work delineates a novel light sheet-guided workflow to overcome these limitations. LSFM combines the detection of fluorescent or fluorescently-labeled markers (e.g. antibodies for immune cell identification) with the 3D scanning of entire organs or even organisms. In addition, the technology leaves the specimen intact, thereby enabling further analysis.¹⁴³ The main challenge of whole organ imaging techniques is their common feature of opacity yielding an imaging depth of no more than a few micrometers. Consequently, clearing techniques have been developed to achieve light refractory index matching between the specimen, imaging solution and

detector. Many of them have been developed with a focus on the sample or marker physique.¹⁴⁴

In this work, a version of organic solvent based ethyl cinnamate (ECi)⁶⁶ clearing adapted to the specific configuration of the myocardium was used, termed BALANCE (Bleaching-Augmented soLvent-bAsed Non-toxic CLEaring). This protocol has several advantages over other clearing techniques. First and foremost, despite making the organ transparent, no processing step contains toxic substances as is the case with most other clearing protocols (e.g. iDISCO [immunolabeling-enabled three-dimensional imaging of solvent-cleared organs]).¹⁴⁵ The entire procedure from sample harvesting to computational analysis takes no longer than 4 days for investigation of morphological features, which is much faster than classic histology and other non-toxic clearing protocols such as CUBIC (Clear, Unobstructed Brain/Body Imaging Cocktails and Computational analysis; see Table 4-2 and Table 4-3).¹⁴⁶ Although, both triphenyl tetrazolium chloride (TTC) staining for viable myocardium and flow cytometry for immune cell infiltration are faster, they require separate specimens (see Table 4-3). The adapted protocol presented contains a bleaching step (5% H₂O₂ in ethanol [EtOH]), which quenches fluorophores like dtTomato used here (see. Figure 4-14). As such endogenously expressed markers are not advised. The bleaching step was necessary to reduce heart tissue autofluorescence; without it, the laser penetration depth was only about 200 µm in the lower wavelength channels (see Figure 4-6).

LSFM in combination with the intravenous (i.v.) administered endothelial marker CD31 has been used previously to image the 3D blood vessel network in various organs, including the murine heart.^{66,67,147} It was also used in an analysis of I/R injury of the brain and was determined to be a promising marker for myocardial I/R injury.⁶⁸ Indeed it was possible to accurately image the heart vessel structure (see Figure 4-15), with distinct CD31 negative (CD31^{neg}) volumes in infarcted hearts after 24 h of reperfusion. Furthermore, 3D quantification was feasible and combined with delineation of the area at risk (AAR) using fluorescein isothiocyanate (FITC) injections via the aorta after permanent ligation of the LCA (see Figure 4-8, Figure 4-17). This is an exclusion staining, meaning that the AAR remains FITC negative and the remote myocardium (the area unaffected by ischemia) is FITC positive. In short, it was now possible to identify 2D structures indicated by TTC/Evans blue (the gold standard method for experimental infarct size measurement) in 3D volumes.

Arguably, CD31 staining labels ECs and a missing signal would suggest dysfunctional vessels rather than metabolically inactive cells as in TTC staining. To this end, a direct comparison of CD31 and TTC staining in the same hearts and heart slices (TTC is stained in slices of ~2mm thickness) was made. Areas that were TTC negative (TTC^{neg}) were also mostly CD31^{neg}, but imaging using LSM revealed even in these slices a more complex 3D structure in the CD31^{neg} areas than was apparent in the TTC^{neg} areas (see Figure 4-16). A more thorough analysis showed that the TTC^{neg} areas and CD31^{neg} volumes in relation to the whole slice or heart area/volume correlated well (Pearson's $r = 0.9291$ and $r = 0.9858$, respectively; see Figure 4-9). Both methods measured nearly the same I/R injury size (mean difference via Bland-Altman analysis -1.08% for slices and -0.75% for whole hearts), though the variance was high for small values. For comparison, similar values were obtained when magnetic resonance imaging (now a well-established method) was first used to measure infarct size in mice.¹⁰⁸ In comparison with other recommended I/R injury parameters¹⁰³, both TTC and CD31 staining correlated with decreased ejection fraction (EF) as a measure of reduced heart function ($r = 0.9779$ and $r = 0.9606$) but not with plasma cardiac troponin I (cTNI) levels (see Figure 4-9). The correlation between infarct size and cTNI concentration appears to be intricate and has produced mixed results in both experimental and clinical studies.^{4,103}

Healing myocardium is dependent on angiogenesis and revascularization to both sustain the tissue with nutrients and oxygen and to path a way for (myo-) fibroblasts to replace dead cells.⁷¹ The regeneration of blood vessels was analyzed at day 5 after reperfusion and compared to both baseline controls and the status after 24 h. As expected, CD31^{neg} areas at day 5 were smaller than those after 24 h. Surrounding tissue was CD31 positive, but abnormal in structure when compared to baseline controls. This abnormal structure (containing the still CD31^{neg} areas) was similar in size and localization to the CD31^{neg} areas after 24 h, possibly providing a proxy for the initial damage days after the ischemic incidence (see Figure 4-10, Figure 4-11 and Figure 4-19). A recently established imaging method, called the filament model, was used to investigate the state of vessel regeneration.⁶⁸ This model enables the 3D reconstruction of all blood vessels in a defined volume. In the hearts after 5 days, vessel length density (VLD), which describes the overall amount of blood vessels, was nearly half that in the baseline hearts. Additionally the interbranch distance (IBD) was shorter, reflecting smaller distances between vessel junctions and thus a healing

capillary network (see Figure 4-10 and Figure 4-18). Since the CD31 staining of this abnormal structure in both the raw data and the reconstructions from the filament model appeared frizzy, it was termed CD31^{curly} (see Figure 4-10).

The CD31 imaging using LSFM depicts the extent of I/R injury quite accurately. The addition of more markers is easily feasible and was tested for immune cells invading the myocardium after I/R, namely neutrophils (using Ly-6G antibody) and macrophages (using F4/80 antibody). These markers are well established for the particular cells.⁹⁰ In the hearts at 24 h of reperfusion, Ly-6G positive cells co-localized with areas both TTC^{neg} and CD31^{neg} (see Figure 4-20), which makes sense because neutrophils migrate along a DAMP and cytokine gradient.⁷¹ In combination with the beforehand CD31/FITC staining for I/R injury and AAR localization, it was possible to map every neutrophil inside the heart to either the remote myocardium, AAR or I/R injury zone. Neutrophils were mostly localized inside the AAR encircling the I/R injury zone and were rarely within the damaged area (see Figure 4-12). Localization at 5 days of reperfusion (where a distinction between the remote myocardium and AAR is not possible) was done in relation to CD31^{curly} areas, as they were most likely formerly CD31^{neg} areas. Here, neutrophils resided within CD31^{curly} but were not in contact with the remaining still CD31^{neg} area, which indicates the halted invasion of neutrophils deeper into infarcted tissue. On the other hand, F4/80 positive signals (for macrophages) on the other hand could be found throughout the CD31^{curly} area (see Figure 4-12).

However, some limitations remain. First, it is not certain that CD31^{neg} staining represents dead ECs, ECs that have shed CD31, or the inaccessibility of CD31 due to occluded vessels or blood cells covering the vessel wall. The occlusion or covering of vessels could be tested by using a filling with labeled gelatin as done for the FITC staining presented here or by using lectins.^{148,149} If no filling occurs, the vessels are occluded, if it does occur the vessel wall is likely covered. As organs processed by the presented protocol are essentially histological samples after the wash-out of ECi (thus making them opaque again), the status of ECs can be checked by subsequent immunohistology staining for CD31 using another label. If this new CD31 staining is also negative, CD31 was shed. H&E staining can be used to determine damaged cells. Apart from whatever it is that CD31^{neg} really illustrates, it is a vascular staining and therefore cannot directly show tissue/CM damage, for which novel markers are necessary that can be imaged using LSFM. Simultaneous injections of thioflavin S

could be used to separate no-reflow areas from CD31^{neg} areas.⁶⁵ Redox sensors that react to active dehydrogenases in a similar way as TTC and are stable during LSFM processing could possibly enable the same staining as that currently used. Nevertheless, the workflow presented here is capable of imaging at least two targets that are of interest in a multi-target cardioprotection strategy (the endothelium and immune cell reaction). Hence, further investigation of the remaining target is warranted.

5.3 Conclusion and outlook

Cardioprotection remains a desirable therapeutic target after the initial resolution of ischemia by reperfusion. Past endeavors did not stand the test of clinical trials, which was attributed to two major flaws. First, basic science studies on substances associated with cardioprotection have produced mixed results lacking reproducibility.¹⁵⁰ Exemplary of the disastrous situation of the research conducted in this field is the fact that two reviews on guidelines for basic science in cardiovascular research have been recently published.^{103,151} Second, clinical trials for cardioprotective agents have often neglected fundamental principles in favor of primary endpoint criteria and patient cohort selection.¹⁵² In addition, since the clinical reality involves patients with various co-morbidities that cannot be accounted for in experimental setups, a major infarct size reduction in the lab may only translate to minor benefits in humans. Experimental studies on multi-target strategies are scarce, though they have mostly demonstrated the additive potential of the cardioprotective agents used.¹⁰² The data presented in this work suggests NO as a possible multi-target approach; indeed, some studies have combined NO-donors with other agents that show a synergistic effect.^{153,154} Although the investigation relies on a single endpoint (infarct size), assessment of the contribution of investigated substances to reducing tissue injury, vascular damage and inflammation still requires up to three different specimens. Accordingly, the light sheet-guided analysis presented herein can provide simultaneous data on all three targets in question.

Ultimately, cardioprotection remains an achievable therapeutic target that can enable maximum infarct size reduction in combination with reperfusion therapy.

6 References

1. European Heart Network. European Cardiovascular Disease Statistics 2017 edition. (2017).
2. Statistisches Bundesamt. Gesundheit - Todesursachen in Deutschland 2015. **Fachserie 12**, (2017).
3. Szummer, K. *et al.* Relations between implementation of new treatments and improved outcomes in patients with non-ST-elevation myocardial infarction during the last 20 years: experiences from SWEDHEART registry 1995 to 2014. *Eur. Heart J.* **39**, 3766–3776 (2018).
4. Thygesen, K. *et al.* Fourth Universal Definition of Myocardial Infarction (2018). *J. Am. Coll. Cardiol.* **72**, 2231–2264 (2018).
5. Flynn, M. C., Pernes, G., Lee, M. K. S., Nagareddy, P. R. & Murphy, A. J. Monocytes, Macrophages, and Metabolic Disease in Atherosclerosis. *Front. Pharmacol.* **10**, (2019).
6. Hausenloy, D. J. & Yellon, D. M. Myocardial ischemia-reperfusion injury: a neglected therapeutic target. *J. Clin. Invest.* **123**, 92–100 (2013).
7. Ibanez, B. *et al.* 2017 ESC Guidelines for the management of acute myocardial infarction in patients presenting with ST-segment elevation: The Task Force for the management of acute myocardial infarction in patients presenting with ST-segment elevation of the European Society of Cardiology (ESC). *Eur. Heart J.* **39**, 119–177 (2018).
8. Yellon, D. M. & Hausenloy, D. J. Myocardial Reperfusion Injury. *N. Engl. J. Med.* **357**, 1121–1135 (2007).
9. Hausenloy, D. J. *et al.* Novel targets and future strategies for acute cardioprotection: Position Paper of the European Society of Cardiology Working Group on Cellular Biology of the Heart. *Cardiovasc. Res.* **113**, 564–585 (2017).
10. Benzing, H., Lösse, B., Schuchhardt, S. & Niederle, N. Simultaneous measurement of regional blood flow and oxygen pressure in the dog myocardium during coronary occlusion or hypoxic hypoxia. *Adv. Exp. Med. Biol.* **37A**, 541–546 (1973).
11. Lemasters, J. J. *et al.* The pH paradox in ischemia-reperfusion injury to cardiac myocytes. in *Myocardial Ischemia: Mechanisms, Reperfusion, Protection* (ed. Karmazyn, M.) 99–114 (Birkhäuser Basel, 1996).
12. Avkiran, M. & Marber, M. S. Na⁺/H⁺ exchange inhibitors for cardioprotective therapy: progress, problems and prospects. *J. Am. Coll. Cardiol.* **39**, 747–753 (2002).
13. Murphy, M. P. & Hartley, R. C. Mitochondria as a therapeutic target for common pathologies. *Nat. Rev. Drug Discov.* **17**, 865–886 (2018).

14. Shahzad, S. *et al.* Elevated DNA Damage, Oxidative Stress, and Impaired Response Defense System Inflicted in Patients With Myocardial Infarction. *Clin. Appl. Thromb. Off. J. Int. Acad. Clin. Appl. Thromb.* **24**, 780–789 (2018).
15. Marchi, S. & Pinton, P. The mitochondrial calcium uniporter complex: molecular components, structure and physiopathological implications. *J. Physiol.* **592**, 829–839 (2014).
16. Honda, H. M., Korge, P. & Weiss, J. N. Mitochondria and ischemia/reperfusion injury. *Ann. N. Y. Acad. Sci.* **1047**, 248–258 (2005).
17. Suzuki, K., Hata, S., Kawabata, Y. & Sorimachi, H. Structure, Activation, and Biology of Calpain. *Diabetes* **53**, S12–S18 (2004).
18. Huang, Y. & Wang, K. K. W. The calpain family and human disease. *Trends Mol. Med.* **7**, 355–362 (2001).
19. Hood, J. L., Brooks, W. H. & Roszman, T. L. Subcellular mobility of the calpain/calpastatin network: an organelle transient. *BioEssays News Rev. Mol. Cell. Dev. Biol.* **28**, 850–859 (2006).
20. Molinari, M. & Carafoli, E. Calpain: a cytosolic proteinase active at the membranes. *J. Membr. Biol.* **156**, 1–8 (1997).
21. Shore, A. C. *et al.* Association of calpain-10 gene with microvascular function. *Diabetologia* **45**, 899–904 (2002).
22. Arrington, D. D., Van Vleet, T. R. & Schnellmann, R. G. Calpain 10: a mitochondrial calpain and its role in calcium-induced mitochondrial dysfunction. *Am J Physiol Cell Physiol* **291**, C1159–71 (2006).
23. Chen, Q. *et al.* Activation of mitochondrial mu-calpain increases AIF cleavage in cardiac mitochondria during ischemia-reperfusion. *Biochem Biophys Res Commun* **415**, 533–8 (2011).
24. Chen, M. *et al.* Bid is cleaved by calpain to an active fragment in vitro and during myocardial ischemia/reperfusion. *J Biol Chem* **276**, 30724–8 (2001).
25. Singh, R. B., Chohan, P. K., Dhalla, N. S. & Netticadan, T. The sarcoplasmic reticulum proteins are targets for calpain action in the ischemic-reperfused heart. *J Mol Cell Cardiol* **37**, 101–10 (2004).
26. Iizuka, K., Kawaguchi, H. & Kitabatake, A. Effects of thiol protease inhibitors on fodrin degradation during hypoxia in cultured myocytes. *J. Mol. Cell. Cardiol.* **25**, 1101–1109 (1993).
27. Barta, J. *et al.* Calpain-1-sensitive myofibrillar proteins of the human myocardium. *Mol Cell Biochem* **278**, 1–8 (2005).
28. Kang, M. Y. *et al.* Receptor-independent cardiac protein kinase Calpha activation by calpain-mediated truncation of regulatory domains. *Circ Res* **107**, 903–12 (2010).

29. Kishimoto, A. *et al.* Limited proteolysis of protein kinase C subspecies by calcium-dependent neutral protease (calpain). *J. Biol. Chem.* **264**, 4088–4092 (1989).
30. Inserte, J., Hernando, V. & Garcia-Dorado, D. Contribution of calpains to myocardial ischaemia/reperfusion injury. *Cardiovasc Res* **96**, 23–31 (2012).
31. Ohno, S. *et al.* Evolutionary origin of a calcium-dependent protease by fusion of genes for a thiol protease and a calcium-binding protein? *Nature* **312**, 566–70 (1984).
32. Heusch, G., Boengler, K. & Schulz, R. Cardioprotection Nitric Oxide, Protein Kinases, and Mitochondria. *Circulation* **118**, 1915–1919 (2008).
33. Cosby, K. *et al.* Nitrite reduction to nitric oxide by deoxyhemoglobin vasodilates the human circulation. *Nat. Med.* **9**, 1498–1505 (2003).
34. Rassaf, T. *et al.* Nitrite Reductase Function of Deoxymyoglobin Oxygen Sensor and Regulator of Cardiac Energetics and Function. *Circ. Res.* **100**, 1749–1754 (2007).
35. Hendgen-Cotta, U. B. *et al.* Nitrite reductase activity of myoglobin regulates respiration and cellular viability in myocardial ischemia-reperfusion injury. *Proc. Natl. Acad. Sci.* **105**, 10256–10261 (2008).
36. Luedike, P. *et al.* Cardioprotection Through S-Nitros(yl)ation of Macrophage Migration Inhibitory Factor Clinical Perspective. *Circulation* **125**, 1880–1889 (2012).
37. Boyd, C. S. & Cadenas, E. Nitric oxide and cell signaling pathways in mitochondrial-dependent apoptosis. *Biol. Chem.* **383**, 411–423 (2002).
38. Yun, H. Y., Gonzalez-Zulueta, M., Dawson, V. L. & Dawson, T. M. Nitric oxide mediates N-methyl-D-aspartate receptor-induced activation of p21ras. *Proc. Natl. Acad. Sci. U. S. A.* **95**, 5773–5778 (1998).
39. Michetti, M., Salamino, F., Melloni, E. & Pontremoli, S. Reversible inactivation of calpain isoforms by nitric oxide. *Biochem Biophys Res Commun* **207**, 1009–14 (1995).
40. Chohan, P. K., Singh, R. B., Dhalla, N. S. & Netticadan, T. L-arginine administration recovers sarcoplasmic reticulum function in ischemic reperfused hearts by preventing calpain activation. *Cardiovasc Res* **69**, 152–63 (2006).
41. Stempien-Otero, A. *et al.* Mechanisms of hypoxia-induced endothelial cell death. Role of p53 in apoptosis. *J. Biol. Chem.* **274**, 8039–8045 (1999).
42. Maxwell, L. & Gavin, J. B. The role of post-ischaemic reperfusion in the development of microvascular incompetence and ultrastructural damage in the myocardium. *Basic Res. Cardiol.* **86**, 544–553 (1991).
43. Noll, T., Muhs, A., Besselmann, M., Watanabe, H. & Piper, H. M. Initiation of hyperpermeability in energy-depleted coronary endothelial monolayers. *Am. J. Physiol.* **268**, H1462–1470 (1995).
44. Becker, B. F., Chappell, D. & Jacob, M. Endothelial glycocalyx and coronary vascular permeability: the fringe benefit. *Basic Res. Cardiol.* **105**, 687–701 (2010).

45. Chappell, D. *et al.* TNF-alpha induced shedding of the endothelial glycocalyx is prevented by hydrocortisone and antithrombin. *Basic Res. Cardiol.* **104**, 78–89 (2009).
46. van den Berg, B. M., Vink Hans & Spaan Jos A.E. The Endothelial Glycocalyx Protects Against Myocardial Edema. *Circ. Res.* **92**, 592–594 (2003).
47. Chappell, D. *et al.* Glycocalyx protection reduces leukocyte adhesion after ischemia/reperfusion. *Shock Augusta Ga* **34**, 133–139 (2010).
48. Chappell, D. *et al.* Protection of glycocalyx decreases platelet adhesion after ischaemia/reperfusion: an animal study. *Eur. J. Anaesthesiol.* **31**, 474–481 (2014).
49. Aslam, S. N. *et al.* Bacterial Polysaccharides Suppress Induced Innate Immunity by Calcium Chelation. *Curr. Biol.* **18**, 1078–1083 (2008).
50. Kuhne, W. *et al.* Disintegration of cytoskeletal structure of actin filaments in energy-depleted endothelial cells. *Am. J. Physiol.* **264**, H1599–1608 (1993).
51. Weis, S. M. & Cheresh, D. A. Pathophysiological consequences of VEGF-induced vascular permeability. *Nature* **437**, 497 (2005).
52. Niccoli, G., Scalone, G., Lerman, A. & Crea, F. Coronary microvascular obstruction in acute myocardial infarction. *Eur. Heart J.* **37**, 1024–1033 (2016).
53. Manciet, L. H., Poole, D. C., McDonagh, P. F., Copeland, J. G. & Mathieu-Costello, O. Microvascular compression during myocardial ischemia: mechanistic basis for no-reflow phenomenon. *Am. J. Physiol.-Heart Circ. Physiol.* **266**, H1541–H1550 (1994).
54. Heusch, G., Skyschally, A. & Kleinbongard, P. Coronary microembolization and microvascular dysfunction. *Int. J. Cardiol.* **258**, 17–23 (2018).
55. Dörge, H. *et al.* Perfusion-contraction mismatch with coronary microvascular obstruction: role of inflammation. *Am. J. Physiol. Heart Circ. Physiol.* **279**, H2587–2592 (2000).
56. Driesen, R. B. *et al.* Histological correlate of a cardiac magnetic resonance imaged microvascular obstruction in a porcine model of ischemia-reperfusion. *Cardiovasc. Pathol. Off. J. Soc. Cardiovasc. Pathol.* **21**, 129–131 (2012).
57. Sheridan, F. M., Dauber, I. M., McMurtry, I. F., Lesnefsky, E. J. & Horwitz, L. D. Role of leukocytes in coronary vascular endothelial injury due to ischemia and reperfusion. *Circ. Res.* **69**, 1566–1574 (1991).
58. Barrabés, J. A. *et al.* Platelet deposition in remote cardiac regions after coronary occlusion. *Eur. J. Clin. Invest.* **37**, 939–946 (2007).
59. Leineweber, K. *et al.* Intense vasoconstriction in response to aspirate from stented saphenous vein aortocoronary bypass grafts. *J. Am. Coll. Cardiol.* **47**, 981–986 (2006).
60. Kleinbongard, P. *et al.* Vasoconstrictor potential of coronary aspirate from patients undergoing stenting of saphenous vein aortocoronary bypass grafts and its pharmacological attenuation. *Circ. Res.* **108**, 344–352 (2011).

61. Kleinbongard, P. *et al.* Aspirate from human stented native coronary arteries vs. saphenous vein grafts: more endothelin but less particulate debris. *Am. J. Physiol. Heart Circ. Physiol.* **305**, H1222-1229 (2013).
62. Heusch, G. Cardioprotection: chances and challenges of its translation to the clinic. *The Lancet* **381**, 166–175 (2013).
63. Skyschally, A., Amanakis, G., Neuhäuser, M., Kleinbongard, P. & Heusch, G. Impact of electrical defibrillation on infarct size and no-reflow in pigs subjected to myocardial ischemia-reperfusion without and with ischemic conditioning. *Am. J. Physiol. Heart Circ. Physiol.* **313**, H871–H878 (2017).
64. Hale, S. L., Herring, M. J. & Kloner, R. A. Delayed treatment with hypothermia protects against the no-reflow phenomenon despite failure to reduce infarct size. *J. Am. Heart Assoc.* **2**, e004234 (2013).
65. Heusch, G. The Coronary Circulation as a Target of Cardioprotection. *Circ. Res.* **118**, 1643–1658 (2016).
66. Klingberg, A. *et al.* Fully Automated Evaluation of Total Glomerular Number and Capillary Tuft Size in Nephritic Kidneys Using Lightsheet Microscopy. *J. Am. Soc. Nephrol.* ASN.2016020232 (2016) doi:10.1681/ASN.2016020232.
67. Männ, L., Klingberg, A., Gunzer, M. & Hasenberg, M. Quantitative Visualization of Leukocyte Infiltrate in a Murine Model of Fulminant Myocarditis by Light Sheet Microscopy. *J. Vis. Exp. JoVE* (2017) doi:10.3791/55450.
68. Lugo-Hernandez, E. *et al.* 3D visualization and quantification of microvessels in the whole ischemic mouse brain using solvent-based clearing and light sheet microscopy. *J. Cereb. Blood Flow Metab.* 0271678X17698970 (2017) doi:10.1177/0271678X17698970.
69. Ambrosio, G., Weisman, H. F., Mannisi, J. A. & Becker, L. C. Progressive impairment of regional myocardial perfusion after initial restoration of postischemic blood flow. *Circulation* **80**, 1846–1861 (1989).
70. Timmers, L. *et al.* The innate immune response in reperfused myocardium. *Cardiovasc. Res.* **94**, 276–283 (2012).
71. Chen, B. & Frangogiannis, N. G. Immune cells in repair of the infarcted myocardium. *Microcirc. N. Y. N 1994* **24**, (2017).
72. Stephen, B. & Hajjar, J. Overview of Basic Immunology for Clinical Investigators. *Adv. Exp. Med. Biol.* **995**, 1–31 (2017).
73. Delves, P. J. & Roitt, I. M. The immune system. First of two parts. *N. Engl. J. Med.* **343**, 37–49 (2000).
74. Parkin, J. & Cohen, B. An overview of the immune system. *The Lancet* **357**, 1777–1789 (2001).

75. Mortensen, R. M. Immune Cell Modulation of Cardiac Remodeling. *Circulation* **125**, 1597–1600 (2012).
76. Arslan, F., de Kleijn, D. P. & Pasterkamp, G. Innate immune signaling in cardiac ischemia. *Nat. Rev. Cardiol.* **8**, 292–300 (2011).
77. Dobaczewski, M., Gonzalez-Quesada, C. & Frangogiannis, N. G. The extracellular matrix as a modulator of the inflammatory and reparative response following myocardial infarction. *J. Mol. Cell. Cardiol.* **48**, 504–511 (2010).
78. Chan, J. K. *et al.* Alarmins: awaiting a clinical response. *J. Clin. Invest.* **122**, 2711–2719 (2012).
79. Swirski, F. K. & Nahrendorf, M. Leukocyte Behavior in Atherosclerosis, Myocardial Infarction, and Heart Failure. *Science* **339**, 161–166 (2013).
80. Vinten-Johansen, J. Involvement of neutrophils in the pathogenesis of lethal myocardial reperfusion injury. *Cardiovasc. Res.* **61**, 481–497 (2004).
81. Savchenko, A. S. *et al.* VWF-mediated leukocyte recruitment with chromatin decondensation by PAD4 increases myocardial ischemia/reperfusion injury in mice. *Blood* **123**, 141–148 (2014).
82. Hayward, R., Campbell, B., Shin, Y. K., Scalia, R. & Lefer, A. M. Recombinant soluble P-selectin glycoprotein ligand-1 protects against myocardial ischemic reperfusion injury in cats. *Cardiovasc. Res.* **41**, 65–76 (1999).
83. Ma, X. L., Tsao, P. S. & Lefer, A. M. Antibody to CD-18 exerts endothelial and cardiac protective effects in myocardial ischemia and reperfusion. *J. Clin. Invest.* **88**, 1237–1243 (1991).
84. Nahrendorf, M. *et al.* The healing myocardium sequentially mobilizes two monocyte subsets with divergent and complementary functions. *J. Exp. Med.* **204**, 3037–3047 (2007).
85. Zouggar, Y. *et al.* B lymphocytes trigger monocyte mobilization and impair heart function after acute myocardial infarction. *Nat. Med.* **19**, 1273–1280 (2013).
86. Boag, S. E. *et al.* T lymphocytes and fractalkine contribute to myocardial ischemia/reperfusion injury in patients. *J. Clin. Invest.* **125**, 3063–3076 (2015).
87. Prabhu, S. D. & Frangogiannis, N. G. The Biological Basis for Cardiac Repair After Myocardial Infarction From Inflammation to Fibrosis. *Circ. Res.* **119**, 91–112 (2016).
88. Frangogiannis, N. G. Regulation of the Inflammatory Response in Cardiac Repair. *Circ. Res.* **110**, 159–173 (2012).
89. Crouch, S. P., Slater, K. J. & Fletcher, J. Regulation of cytokine release from mononuclear cells by the iron-binding protein lactoferrin. *Blood* **80**, 235–240 (1992).

90. Horckmans, M. *et al.* Neutrophils orchestrate post-myocardial infarction healing by polarizing macrophages towards a reparative phenotype. *Eur. Heart J.* (2016) doi:10.1093/eurheartj/ehw002.
91. Chen, W. *et al.* Endogenous IRAK-M attenuates postinfarction remodeling through effects on macrophages and fibroblasts. *Arterioscler. Thromb. Vasc. Biol.* **32**, 2598–2608 (2012).
92. Hilgendorf, I. *et al.* Ly-6Chigh monocytes depend on Nr4a1 to balance both inflammatory and reparative phases in the infarcted myocardium. *Circ. Res.* **114**, 1611–1622 (2014).
93. Saxena, A. *et al.* IL-1 induces proinflammatory leukocyte infiltration and regulates fibroblast phenotype in the infarcted myocardium. *J. Immunol. Baltim. Md 1950* **191**, 4838–4848 (2013).
94. Weirather, J. *et al.* Foxp3+ CD4+ T cells improve healing after myocardial infarction by modulating monocyte/macrophage differentiation. *Circ. Res.* **115**, 55–67 (2014).
95. Borg, N. *et al.* CD73 on T-Cells Orchestrates Cardiac Wound Healing After Myocardial Infarction by Purinergic Metabolic Reprogramming. *Circulation* CIRCULATIONAHA.116.023365 (2017) doi:10.1161/CIRCULATIONAHA.116.023365.
96. Frantz, S. *et al.* Monocytes/macrophages prevent healing defects and left ventricular thrombus formation after myocardial infarction. *FASEB J. Off. Publ. Fed. Am. Soc. Exp. Biol.* **27**, 871–881 (2013).
97. Ramos, G., Hofmann, U. & Frantz, S. Myocardial fibrosis seen through the lenses of T-cell biology. *J. Mol. Cell. Cardiol.* **92**, 41–45 (2016).
98. Knöll, R. *et al.* Towards a re-definition of ‘cardiac hypertrophy’ through a rational characterization of left ventricular phenotypes: a position paper of the Working Group ‘Myocardial Function’ of the ESC. *Eur. J. Heart Fail.* **13**, 811–819 (2011).
99. Jordan, J. E., Zhao, Z.-Q. & Vinten-Johansen, J. The role of neutrophils in myocardial ischemia–reperfusion injury. *Cardiovasc. Res.* **43**, 860–878 (1999).
100. Faxon, D. P. *et al.* The effect of blockade of the CD11/CD18 integrin receptor on infarct size in patients with acute myocardial infarction treated with direct angioplasty: the results of the HALT-MI study. *J. Am. Coll. Cardiol.* **40**, 1199–1204 (2002).
101. Heusch Gerd, Skyschally Andreas & Kleinbongard Petra. Translation, Translation, Translation. *Circ. Res.* **123**, 931–933 (2018).
102. Davidson, S. M. *et al.* Multitarget Strategies to Reduce Myocardial Ischemia/Reperfusion Injury: JACC Review Topic of the Week. *J. Am. Coll. Cardiol.* **73**, 89–99 (2019).
103. Bøtker, H. E. *et al.* Practical guidelines for rigor and reproducibility in preclinical and clinical studies on cardioprotection. *Basic Res. Cardiol.* **113**, (2018).

104. Reimer, K. A., Lowe, J. E., Rasmussen, M. M. & Jennings, R. B. The wavefront phenomenon of ischemic cell death. 1. Myocardial infarct size vs duration of coronary occlusion in dogs. *Circulation* **56**, 786–794 (1977).
105. Nachlas, M. M. & Shnitka, T. K. Macroscopic Identification of Early Myocardial Infarcts by Alterations in Dehydrogenase Activity. *Am. J. Pathol.* **42**, 379–405 (1963).
106. Fishbein, M. C. *et al.* Early phase acute myocardial infarct size quantification: validation of the triphenyl tetrazolium chloride tissue enzyme staining technique. *Am. Heart J.* **101**, 593–600 (1981).
107. Park, S. W. *et al.* Quantitative assessment of infarct size in vivo by myocardial contrast echocardiography in a murine acute myocardial infarction model. *Int. J. Cardiol.* **97**, 393–398 (2004).
108. Yang, Z., Berr Stuart S., Gilson Wesley D., Toufektsian Marie-Claire & French Brent A. Simultaneous Evaluation of Infarct Size and Cardiac Function in Intact Mice by Contrast-Enhanced Cardiac Magnetic Resonance Imaging Reveals Contractile Dysfunction in Noninfarcted Regions Early After Myocardial Infarction. *Circulation* **109**, 1161–1167 (2004).
109. Cullen, L. A., Mills, N. L., Mahler, S. & Body, R. Early Rule-Out and Rule-In Strategies for Myocardial Infarction. *Clin. Chem.* **63**, 129–139 (2017).
110. Hausenloy, D. J. *et al.* Targeting reperfusion injury in patients with ST-segment elevation myocardial infarction: trials and tribulations. *Eur. Heart J.* **38**, 935–941 (2017).
111. Heusch, G. Molecular basis of cardioprotection: signal transduction in ischemic pre-, post-, and remote conditioning. *Circ. Res.* **116**, 674–699 (2015).
112. Christia, P. *et al.* Systematic Characterization of Myocardial Inflammation, Repair, and Remodeling in a Mouse Model of Reperfused Myocardial Infarction. *J. Histochem. Cytochem.* **61**, 555–570 (2013).
113. Rassaf, T. *et al.* Positive effects of nitric oxide on left ventricular function in humans. *Eur. Heart J.* **27**, 1699–1705 (2006).
114. Zweier, J. L. & Talukder, M. A. H. The role of oxidants and free radicals in reperfusion injury. *Cardiovasc. Res.* **70**, 181–190 (2006).
115. Heusch, G., Boengler, K. & Schulz, R. Inhibition of mitochondrial permeability transition pore opening: the holy grail of cardioprotection. *Basic Res. Cardiol.* **105**, 151–154 (2010).
116. Murry, C. E., Jennings, R. B. & Reimer, K. A. Preconditioning with ischemia: a delay of lethal cell injury in ischemic myocardium. *Circulation* **74**, 1124–1136 (1986).
117. Zhao, Z.-Q. *et al.* Inhibition of myocardial injury by ischemic postconditioning during reperfusion: comparison with ischemic preconditioning. *Am. J. Physiol. Heart Circ. Physiol.* **285**, H579–588 (2003).

118. Przyklenk, K., Bauer, B., Ovize, M., Kloner, R. A. & Whittaker, P. Regional ischemic 'preconditioning' protects remote virgin myocardium from subsequent sustained coronary occlusion. *Circulation* **87**, 893–899 (1993).
119. Heusch, G. & Rassaf, T. Time to Give Up on Cardioprotection? A Critical Appraisal of Clinical Studies on Ischemic Pre-, Post-, and Remote Conditioning*. *Circ. Res.* **119**, 676–695 (2016).
120. Karlsson, L. O. *et al.* Cyclosporine does not reduce myocardial infarct size in a porcine ischemia-reperfusion model. *J. Cardiovasc. Pharmacol. Ther.* **15**, 182–189 (2010).
121. Lim, W. Y., Messow, C. M. & Berry, C. Cyclosporin variably and inconsistently reduces infarct size in experimental models of reperfused myocardial infarction: a systematic review and meta-analysis. *Br. J. Pharmacol.* **165**, 2034–2043 (2012).
122. Cung, T.-T. *et al.* Cyclosporine before PCI in Patients with Acute Myocardial Infarction. *N. Engl. J. Med.* **373**, 1021–1031 (2015).
123. Piot, C. *et al.* Effect of cyclosporine on reperfusion injury in acute myocardial infarction. *N. Engl. J. Med.* **359**, 473–481 (2008).
124. Ottani, F. *et al.* Cyclosporine A in Reperfused Myocardial Infarction: The Multicenter, Controlled, Open-Label CYCLE Trial. *J. Am. Coll. Cardiol.* **67**, 365–374 (2016).
125. Lincoff, A. M. *et al.* Inhibition of delta-protein kinase C by delcasertib as an adjunct to primary percutaneous coronary intervention for acute anterior ST-segment elevation myocardial infarction: results of the PROTECTION AMI Randomized Controlled Trial. *Eur. Heart J.* **35**, 2516–2523 (2014).
126. Siddiqi, N. *et al.* Intravenous sodium nitrite in acute ST-elevation myocardial infarction: a randomized controlled trial (NIAMI). *Eur. Heart J.* **35**, 1255–1262 (2014).
127. Duranski, M. R. *et al.* Cytoprotective effects of nitrite during in vivo ischemia-reperfusion of the heart and liver. *J. Clin. Invest.* **115**, 1232–1240 (2005).
128. Martin, C. *et al.* Microdialysis-based analysis of interstitial NO in situ: NO synthase-independent NO formation during myocardial ischemia. *Cardiovasc. Res.* **74**, 46–55 (2007).
129. Neuhof, C. *et al.* Reduction of myocardial infarction by calpain inhibitors A-705239 and A-705253 in isolated perfused rabbit hearts. *Biol Chem* **385**, 1077–82 (2004).
130. Liu, R., Li, Y., Wang, M., Zhou, G. & Zhang, W. Effect of protein S-nitrosylation on autolysis and catalytic ability of μ -calpain. *Food Chem.* **213**, 470–477 (2016).
131. Donkor, I. O. A survey of calpain inhibitors. *Curr. Med. Chem.* **7**, 1171–1188 (2000).
132. Totzeck, M. *et al.* Nitrite circumvents canonical cGMP signaling to enhance proliferation of myocyte precursor cells. *Mol. Cell. Biochem.* **401**, 175–183 (2014).
133. Liu, R. *et al.* Effect of nitric oxide and calpastatin on the inhibition of μ -calpain activity, autolysis and proteolysis of myofibrillar proteins. *Food Chem.* **275**, 77–84 (2019).

134. Koh, T. J. & Tidball, J. G. Nitric oxide inhibits calpain-mediated proteolysis of talin in skeletal muscle cells. *Am J Physiol Cell Physiol* **279**, C806-12 (2000).
135. Rassaf, T. *et al.* Circulating Nitrite Contributes to Cardioprotection by Remote Ischemic Preconditioning. *Circ. Res.* **114**, 1601–1610 (2014).
136. Smith, M. A. & Schnellmann, R. G. Calpains, mitochondria, and apoptosis. *Cardiovasc. Res.* **96**, 32–37 (2012).
137. Zhao, J.-F., Shyue, S.-K. & Lee, T.-S. Excess Nitric Oxide Activates TRPV1-Ca²⁺-Calpain Signaling and Promotes PEST-dependent Degradation of Liver X Receptor α . *Int. J. Biol. Sci.* **12**, 18–29 (2016).
138. Neuhof, C. & Neuhof, H. Calpain system and its involvement in myocardial ischemia and reperfusion injury. *World J Cardiol* **6**, 638–52 (2014).
139. Kubes, P., Suzuki, M. & Granger, D. N. Nitric oxide: an endogenous modulator of leukocyte adhesion. *Proc. Natl. Acad. Sci. U. S. A.* **88**, 4651–4655 (1991).
140. Anaya-Prado, R. *et al.* Exogenous nitric oxide donor and related compounds protect against lung inflammatory response after hemorrhagic shock and resuscitation. *J. Trauma* **57**, 980–988 (2004).
141. Franco-Gou, R. *et al.* How ischaemic preconditioning protects small liver grafts. *J. Pathol.* **208**, 62–73 (2006).
142. Garreffa, A. M., Woodman, O. L., Cao, A. H. & Ritchie, R. H. Sodium nitroprusside protects adult rat cardiac myocytes from cellular injury induced by simulated ischemia: role for a non-cGMP-dependent mechanism of nitric oxide protection. *J. Cardiovasc. Pharmacol.* **47**, 1–8 (2006).
143. Santi, P. A. Light sheet fluorescence microscopy: a review. *J. Histochem. Cytochem. Off. J. Histochem. Soc.* **59**, 129–138 (2011).
144. Orlich, M. & Kiefer, F. A qualitative comparison of ten tissue clearing techniques. *Histol. Histopathol.* **33**, 181–199 (2018).
145. Belle, M. *et al.* Tridimensional Visualization and Analysis of Early Human Development. *Cell* **169**, 161-173.e12 (2017).
146. Susaki, E. A. *et al.* Advanced CUBIC protocols for whole-brain and whole-body clearing and imaging. *Nat. Protoc.* **10**, 1709–1727 (2015).
147. Nehrhoff, I., Ripoll, J., Samaniego, R., Desco, M. & Gómez-Gaviro, M. V. Looking inside the heart: a see-through view of the vascular tree. *Biomed. Opt. Express* **8**, 3110–3118 (2017).
148. Nguyen, C. *et al.* Near-infrared fluorescence imaging of mouse myocardial microvascular endothelium using Cy5.5-lectin conjugate. *J. Biophotonics* **5**, 754–767 (2012).

149. Robertson, R. T. *et al.* Use of labeled tomato lectin for imaging vasculature structures. *Histochem. Cell Biol.* **143**, 225–234 (2015).
150. Bolli, R. New Initiatives to Improve the Rigor and Reproducibility of Articles Published in Circulation Research. *Circ. Res.* **121**, 472–479 (2017).
151. Lindsey, M. L. *et al.* Guidelines for experimental models of myocardial ischemia and infarction. *Am. J. Physiol.-Heart Circ. Physiol.* **314**, H812–H838 (2018).
152. Heusch, G. Critical Issues for the Translation of Cardioprotection. *Circ. Res.* **120**, 1477–1486 (2017).
153. Rastaldo, R. *et al.* A lipophilic nitric oxide donor and a lipophilic antioxidant compound protect rat heart against ischemia-reperfusion injury if given as hybrid molecule but not as a mixture. *J. Cardiovasc. Pharmacol.* **59**, 241–248 (2012).
154. Sun, J. *et al.* Additive cardioprotection by pharmacological postconditioning with hydrogen sulfide and nitric oxide donors in mouse heart: S-sulfhydration vs. S-nitrosylation. *Cardiovasc. Res.* **110**, 96–106 (2016).

7 Appendix

7.1 Author publication contributions

Author contributions for the paper

S-nitrosation of calpains is associated with cardioprotection in myocardial I/R injury

SK: Sebastian Korste

Experimental work

| | |
|---------------------------|---------|
| a. Mouse handling/surgery | SK 30% |
| b. Cell culture | SK 100% |
| c. Biochemical assays | SK 100% |
| d. Western blot | SK 100% |
| e. Electron microscopy | SK 0% |

Data analysis

| | |
|------------------------|---------|
| a. Western blot | SK 100% |
| b. Biochemical assays | SK 100% |
| c. Dead/alive staining | SK 100% |
| d. TTC planimetry | SK 50% |
| e. Electron microscopy | SK 50% |
| f. Statistics | SK 100% |

Manuscript

| | |
|---|---------|
| a. Figure preparation | SK 100% |
| b. Main Text | SK 50% |
| c. Supplement preparation (Figure legends etc.) | SK 100% |

| | |
|---|---|
|  |  |
| Sebastian Korste | Matthias Totzeck |

Author contributions for the paper

Contemporaneous 3D characterization of acute and chronic myocardial I/R injury and response

SK: Sebastian Korste; SFM: Simon Frederik Merz; LB: Lea Bornemann

Experimental work

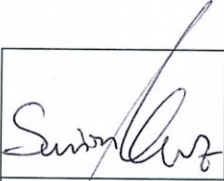

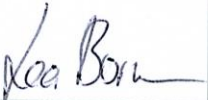
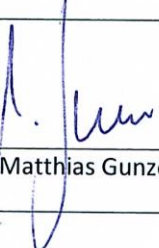
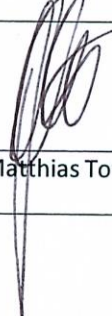
- | | |
|--|-----------------|
| a. Mouse handling/surgery | SK 30% |
| b. Development of protocol & staining strategy | SK 50%; SFM 50% |
| c. Sample processing until LSFM | SK 75%; SFM 25% |
| 2. Data acquisition | |
| i. LSFM | SK 50%; SFM 50% |
| ii. TTC planimetry | SK 100% |
| iii. Flow cytometry | SK 100% |

Data analysis

- | | |
|--------------------------------|-------------------------|
| 1. IMARIS | |
| i. Vessel tracing | SFM 10%; LB 90% |
| ii. Thresholdings | SK 10%; SFM 80%; LB 10% |
| iii. Cell counting | SK 25%; SFM 50%; LB 25% |
| iv. Volume tracing/measurement | SK 33%; SFM 33%; LB 33% |
| v. Filament Model | SK 20%; SFM 20% |
| 2. FlowJo | SK 100% |
| 3. ImageJ | SFM 75%; LB 25% |
| 4. Statistics | SK 45%; SFM 10%; LB 45% |

Manuscript

- | | |
|---|-------------------------|
| 1. Figure preparation | SK 15%; SFM 25%; LB 60% |
| 2. Main Text | SK 25%; SFM 25%; LB 25% |
| 3. Supplement preparation (Figure legends etc.) | SK 40%; SFM 40%; LB 20% |

| | | | | |
|---|---|---|--|---|
|  |  |  |  |  |
| Simon F. Merz | Sebastian Korste | Lea Bornemann | Matthias Gunzer | Matthias Totzeck |

7.2 Acknowledgement

At the end I'd like to express my gratitude to a few people that have helped greatly during the experimental process and writing of this work.

First and foremost, I say my thanks to Prof. Dr. Tienush Rassaf for giving me the opportunity to conduct the research presented here in his laboratories, for the scientific support and discussions we had over the years and for being an inspiring example of both commitment to and discipline for one's goals.

I would like to thank Prof. Dr. Peter Bayer for the scientific supervision and assessment of this thesis.

I am truly grateful that I could work together with PD Dr. Matthias Totzeck, whose impact on my scientific career and development cannot be accounted for enough. Thank you for always being the one to motivate me to give it all I got.

I give my thanks to PD. Dr. Ulrike Hendgen-Cotta for asking the problematic questions, for being understanding and ready to help when times were rough and for giving me the freedom and support I needed.

I'd like to thank Simon Merz and Lea Bornemann, as well as Prof. Dr. Matthias Gunzer for the joint venture of what might be the most defining project of my career up until now.

My thanks go to my colleagues from the CardioScienceLabs and the Totzeck group, namely Elisa Ankert, Anna-Lena Beerlage, Sonja Esfeld, Jacqueline Heinen-Weiler, Martin Heisler, Lena Hindrichs, Daniel Messiah, Lars Michel, Raluca Mincu, Simone Mrotzek, Andrea Odersky, Julia Pohl, Tobias Radecke, Anna Roth and Pia Stock, who made work in and outside the lab a lot more entertaining.

I thank my parents Isolde and Ludger Korste for enabling me to pursue my dreams and giving their all for making it possible. Also a huge thank you to my sister Alexandra, without whom my life so far would have been a lot less happy. Additionally I thank Nita for being herself. I would also like to thank my aunt Resi for myriads of things she did to support me.

To Natascha Hofer, my partner in crime, I will always be thankful for the times your smile lifted me up and your presence turned the good moments into great ones.

I'd like to thank my friends and family that undoubtedly have in some way or other helped me on my path here.

Lastly, I want to emphasize the sacrifice of the countless mice, which hopefully will one day lead to advancement of humankind.

7.3 Curriculum vitae

Der Lebenslauf ist in der Online-Version aus Gründen des Datenschutzes nicht enthalten.

7.4 Eidesstattliche Erklärung

Hiermit erkläre ich, gem. § 6 Abs. (2) g) der Promotionsordnung der Fakultät für Biologie zur Erlangung der Dr. rer. nat., dass ich das Arbeitsgebiet, dem das Thema „Development of a 3D myocardial damage analysis tool for the evaluation of multi-target cardioprotection strategies“ zuzuordnen ist, in Forschung und Lehre vertrete und den Antrag von Sebastian Korste befürworte und die Betreuung auch im Falle eines Weggangs, wenn nicht wichtige Gründe dem entgegenstehen, weiterführen werde.

Essen, den _____

Prof. Dr. Peter Bayer

Hiermit erkläre ich, gem. § 7 Abs. (2) d) + f) der Promotionsordnung der Fakultät für Biologie zur Erlangung des Dr. rer. nat., dass ich die vorliegende Dissertation selbständig verfasst und mich keiner anderen als der angegebenen Hilfsmittel bedient, bei der Abfassung der Dissertation nur die angegebenen Hilfsmittel benutzt und alle wörtlich oder inhaltlich übernommenen Stellen als solche gekennzeichnet habe.

Essen, den _____

Sebastian Korste

Hiermit erkläre ich, gem. § 7 Abs. (2) e) + g) der Promotionsordnung der Fakultät für Biologie zur Erlangung des Dr. rer. nat., dass ich keine anderen Promotionen bzw. Promotionsversuche in der Vergangenheit durchgeführt habe und dass diese Arbeit von keiner anderen Fakultät/Fachbereich abgelehnt worden ist.

Essen, den _____

Sebastian Korste